Developing low-cost remote sensing methods for multiscale habitat mapping of an intertidal seagrass-macroalgae environment

Eylem Elma

Thesis submitted to the

School of Natural and Environmental Sciences

In fulfilment of the requirements of the degree of

Doctor of Philosophy



Newcastle University

January 2024

Abstract

Seagrass ecosystems around the UK are in poor condition and continue to decline, in large part due to anthropogenic activities, such as nutrient pollution, which may also lead to macroalgae proliferation that is detrimental to seagrass growth. To better understand declines and support recovery efforts, accurate spatiotemporal monitoring of seagrass habitat health and macroalgae distributions are required. Remote sensing offers the potential to map large or inaccessible areas, cost-effectively, providing coastal managers with promising data for assessment. This PhD thesis evaluates the potential of using remote sensing technologies to map and monitor a complex intertidal seagrass-macroalgae environment in Lindisfarne, Northumberland, UK. A multiscale mapping approach was used to evaluate multiple platforms and sensors, with differing spatial and spectral resolution. Different classification approaches were tested, the monitoring and management implications of each considered. A Maximum Likelihood classifier and multispectral Unoccupied Aerial Vehicle (UAV) imagery successfully mapped seagrass-macroalgae distribution to species level, with an Overall Accuracy (OA) ranging between 84% and 91%. A random forest classifier with airborne hyperspectral imagery and high resolution PlanetScope satellite imagery was able to produce 6-class large-scale habitat maps with OA of over 90%, for each. This was repeatable across multiple images and may enable monitoring of seasonal and interannual changes in seagrass and macroalgae distribution. The benefit of red edge and near infrared bands was highlighted across multiple platforms. These are offered by the low-cost multispectral UAV that is then able to discriminate between vegetation classes, with similar map accuracies to those achieved when reducing hyperspectral imagery spectral bands (23) to 5-8 bands. Large-scale maps can be used to reveal distribution patterns of seagrass and macroalgae as snapshots and over time, elucidating seagrass-macroalgae dynamics, to support coastal managers' decisionmaking and management. Overall, this PhD provides a comprehensive critical evaluation of optical remote sensing methods for effective monitoring and its operationalisation for use for seagrass ecosystem conservation.

Acknowledgements

I would like to express my sincere gratitude to my supervisors Prof Clare Fitzsimmons, Dr Rachel Gaulton, Dr Catherine Scott, Dr Holly East and Dr Hannah Westoby for their invaluable guidance and support throughout the entirety of my PhD journey. Their mentorship, encouragement and expertise have shaped both my academic and personal development.

I thank Natural England for giving me the opportunity to pursue my research field work in Lindisfarne National Nature Reserve (LNNR). I thank the management team of LNNR for their invaluable knowledge, shared experiences, and logistical support during the field surveys of this study. I would like to express my thanks to Andrew Craggs, the manager of the site for his support and commitment to ensuring the safety of myself and my team in the field. I extend my appreciation to the Environment Agency for their collaborative engagement and their commitment to advancing my knowledge in this field of research. I also extend deep thanks to all the incredible participants and volunteers who generously dedicated their time, whether under rainy or sunny conditions in the field.

Finally, a heartfelt thanks and love to my family and friends. Their attentive ears, love, thoughtful acts of kindness and consistent motivation were invaluable support during challenging times.

Contents

| | | ii |
|--|---|----------------------------------|
| Ackno | wledgements | iii |
| List of | Figures | vii |
| List of | Tables | xi |
| Chapte | r 1: Introduction | 1 |
| 1.1. | Importance, threats and decline of seagrass | 1 |
| 1.2. | Seagrass biology and distribution | 3 |
| 1.2 | .1. Temperate seagrass species | 5 |
| 1.3. | Need for effective management and conservation methods | 5 |
| 1.3 | .1. Habitat maps | 7 |
| 1.4. | Study site | 9 |
| 1.5. | Thesis aim and structure | 12 |
| Chapte | r 2: Remote Sensing Review | 14 |
| 2.1. | Optical remote sensing | 14 |
| 2.2. | Applications of optical remote sensing in seagrass habitats | 22 |
| 2.3. | Application of optical remote sensing in temperate seagrass habitats | 23 |
| Chapte | er 3: Evaluating multispectral UAV imagery for mapping a multispe | cies |
| :-44:- | | |
| mentic | al seagrass environment | 29 |
| 3.1. | lal seagrass environment Introduction | |
| | | 29 |
| 3.1. 3.2. | Introduction | 29 |
| 3.1. 3.2. | Introduction | 29 31 31 |
| 3.1. 3.2. 3.2 | Introduction | 29 31 31 |
| 3.1. 3.2. 3.2 3.2 | Introduction Methods and Materials .1. Study site .2. Equipment specifications .3. UAV and ground-truth survey | 29 31 31 32 |
| 3.1. 3.2. 3.2 3.2 3.2 | Introduction | 29 31 32 33 |
| 3.1. 3.2. 3.2 3.2 3.2 3.2 | Introduction Methods and Materials .1. Study site .2. Equipment specifications .3. UAV and ground-truth survey .4. Image pre-processing .5. Training data and image classification | 29 31 32 33 34 |
| 3.1. 3.2. 3.2 3.2 3.2 3.2 3.2 3.2 | Introduction Methods and Materials .1. Study site .2. Equipment specifications .3. UAV and ground-truth survey .4. Image pre-processing .5. Training data and image classification | 29 31 32 33 34 35 |
| 3.1. 3.2. 3.2 3.2 3.2 3.2 3.2 3.2 | Introduction Methods and Materials .1. Study site .2. Equipment specifications .3. UAV and ground-truth survey .4. Image pre-processing .5. Training data and image classification .6. Accuracy assessment Results | 29 31 32 33 35 37 |
| 3.1. 3.2. 3.2 3.2 3.2 3.2 3.2 3.3.3 | Introduction Methods and Materials 1. Study site 2. Equipment specifications 3. UAV and ground-truth survey 4. Image pre-processing 5. Training data and image classification 6. Accuracy assessment Results 1. Training data separability | 29 31 32 34 35 37 |
| 3.1. 3.2. 3.2 3.2 3.2 3.2 3.3. 3.3. | Introduction Methods and Materials 1. Study site 2. Equipment specifications 3. UAV and ground-truth survey 4. Image pre-processing 5. Training data and image classification 6. Accuracy assessment Results 1. Training data separability | 29 31 32 33 35 37 37 40 |

| | 3.4.2. | Limitations, challenges, and recommendations | 45 |
|----|-------------|---|----|
| | 3.4.3. | Benefits for management | 46 |
| | 3.4.4. | Conclusion | 46 |
| C | hapter 4: | Mapping intertidal seagrass and macroalgae using Hyperspectra | al |
| C | ASI image | ery | 48 |
| | 4.1. Intr | oduction | 48 |
| | 4.2. Mat | terials and Methods | 51 |
| | 4.2.1. | Ground truth sampling | 51 |
| | 4.2.2. | Benthic Classes | 52 |
| | 4.2.3. | CASI information and Image acquisition | 53 |
| | 4.2.4. | Pre-processing of imagery | 54 |
| | 4.2.5. | Classification method and accuracy assessment | 55 |
| | 4.3. Res | sults | 58 |
| | 4.3.1. | Spectral signatures | 58 |
| | 4.3.2. | Accuracy assessment | 60 |
| | 4.4. Dis | cussion | 69 |
| | 4.4.1. | Habitat classification | 70 |
| | 4.4.2. | Ecology and implications for management | 72 |
| | 4.4.3. | Limitations, challenges, and recommendations | 75 |
| | 4.4.4. | Conclusion | 76 |
| C | hapter 5: | Using PlanetScope imagery to map and assess spatiotemporal | |
| ir | ntertidal s | eagrass-macroalgae dynamics | 78 |
| | 5.1. Intr | oduction | 78 |
| | 5.2. Met | thods and Materials | 81 |
| | 5.2.1. | Ground-truth data | 81 |
| | 5.2.2. | Image data acquisition | 83 |
| | 5.2.3. | PlanetScope pre-processing | 86 |
| | 5.2.4. | Classifier and accuracy assessment | 87 |
| | 5.3. Res | sults | 88 |
| | 5.3.1. | Spectral reflectance | 88 |
| | 5.3.2. | Accuracy assessment and habitat classification | 90 |
| | 5.3.3. | Habitat change detection | 92 |
| | 5.4. Dis | cussion | 99 |
| | 5.4.1. | Habitat classification | 99 |

| 5.4 | .2. | Change detection, ecology, and implications for management | 101 |
|--------|-------|---|-----|
| 5.4.3. | | Limitations, challenges, and recommendations | 105 |
| 5.4 | .4. | Conclusion | 106 |
| Chapte | er 6: | Thesis overview, limitations, and future directions | 108 |
| 6.1. | Key | / findings | 108 |
| 6.2. | Imp | lications for management | 113 |
| | | Applications of multiscale mapping for management and cost- | 113 |
| 6.3. | Wic | der implications | 115 |
| 6.4. | Lim | itations and future directions | 118 |
| 6.5. | Cor | ncluding remarks | 119 |
| Appen | dix A | \ · | 121 |
| Refere | nces | 3 | 122 |

List of Figures

| Figure 1.1. Diagram showing morphological differences between algae (left) and |
|--|
| seagrass (right). (Source: https://ocean.si.edu/holding-tank/images-hide/algae-vs- |
| seagrass) |
| Figure 1.2. Variations in density of seagrass habitats at low tide: a) dense Zostera |
| noltii patch; b) sparse Zostera marina patch4 |
| Figure 1.3. Images of the two common temperate intertidal seagrass species: |
| Zostera noltii and Zostera marina5 |
| Figure 1.4. National Seagrass Layers of current spatial extent of Zostera spp. (dark |
| blue polygon area) in Lindisfarne and Plymouth Tamar that provide |
| presence/absence data (Source: Natural England, 2024: Contains public sector |
| information licensed under the Open Government Licence v3.0.)9 |
| Figure 1.5. Map showing field site located in the North East of the UK (bottom left). |
| Extent of Lindisfarne National Nature Reserve (red boundary) and different regions |
| of studied field sites, including Causeway area, Fenham Flats and Budle Bay 11 |
| Figure 2.1. Varying spatial resolution (from high to low) of an intertidal seagrass |
| environment taken with different platforms and sensors including an Unoccupied |
| Aerial Vehicle (UAV), airborne and satellite imagery15 |
| Figure 2.2. Schematic illustration of the evolution of classification methods used for |
| remote sensing image classification18 |
| Figure 3.1. a) Map showing LNNR (red boundary outline) indicating the field survey |
| area (white square) in the Causeway area and b) the flight transects surveyed in this |
| study32 |
| Figure 3.2. a) Flight transect showing the pre-defined regular points for photo |
| quadrats (n=20) across a flight transect. b) Image showing the quadrat and a Trimble |
| receiver to record the northern corner of the quadrat sample. c) Photographs of a |
| Zostera noltii, Zostera marina and Macroalgae dominated quadrats |
| Figure 3.3. Images of benthic substrates initially identified in quadrat photographs |
| before aggregation benthic classes in further analysis. a) Zostera noltii, b) Zostera |
| marina, c) macroalgae, d) bare ground, e) lugwormcasts, f) shells, g) anoxic |
| sediment h) decomposing vegetation. Arrows highlight examples of categories |
| including dark material/shadow and sunglint/shells |

| Figure 3.4. Spectral signatures of generated training data including all benthic |
|--|
| classes across the multispectral bands for a) Zostera noltii transect b) Zostera |
| marina transect, and c) Macroalgae transect. Boxplots show the median value |
| (horizontal line), the interquartile range representing the dispersion of the data (size |
| of the box), the upper and lower quartiles, and outliers |
| Figure 3.5. a) Raw UAV orthomosaic are displayed using the red, green, and blue |
| colour composite, b) classified map and, c) a close-up example for each transect |
| survey (Zostera noltii, Zostera marina and Macroalgae) |
| Figure 4.1. Map showing the ground-truth sampling points where quadrat |
| photographs were taken in the Causeway area (red boundary)51 |
| Figure 4.2. a) Quadrat photographs of identified benthic classes. b) Diagram of the |
| three different investigated Scenarios with differing numbers of benthic classes |
| including the number of training sample data for each benthic class. Sparse SG = |
| sparse seagrass, moderate SG = moderate seagrass, dense SG = dense seagrass, |
| SG/MA mixed = seagrass/macroalgae mixed, bare ground = bare ground, water = |
| water53 |
| Figure 4.3. The Mosaic of the hyperspectral imagery scene and the investigated |
| intertidal area in Lindisfarne National Nature Reserve (LNNR) (red boundary) |
| (Source: Geomatics, 2024: Contains public sector information licensed under the |
| Open Government Licence v3.0.) |
| Figure 4.4. Spectral reflectance curves of benthic class training data across all |
| hyperspectral bands for Scenario 1, Scenario 2, and Scenario 3. The shaded area |
| represents ± standard deviation |
| Figure 4.5. Confusion matrix outputs of the Random Forest classification method |
| showing misclassification between true labels and predicted labels. Values represent |
| the percent (%) numbers of misclassified pixels |
| Figure 4.6. Habitat classified maps showing Scenario 1 for: a) the Causeway area & |
| Fenham Flats, b) a zoomed area within the Causeway area; c) Budle Bay, and d) a |
| zoomed area within Budle Bay65 |
| Figure 4.7. Habitat classified maps showing Scenario 2 for: a) the Causeway area & |
| Fenham Flats, b) a zoomed area within the Causeway area; (c) Budle Bay, and (d) a |
| zoomed area within Budle Bay66 |

| Figure 4.8. Habitat classified maps showing Scenario 1 for: a) the Causeway area & |
|---|
| Fenham Flats, b) a zoomed area within the Causeway area; c) Budle Bay, and (d) a |
| zoomed area within Budle Bay67 |
| Figure 4.9. Bar plots showing percent (%) cover found for each benthic class within |
| each Scenario habitat map across the Lindisfarne National Nature Reserve (LNNR). |
| (b) Stacked bar of percent cover of vegetation for each investigated area including |
| Causeway, Fenham Flats and Budle Bay for Scenario 2 |
| Figure 4.10. Classified map showing the potential movement of macroalgae along |
| the Pilgrimage track (top map) across the Causeway area (bottom map)74 |
| Figure 5.1. a) Random 3m pixel quadrat samples used to create b) UAV derived |
| training data82 |
| Figure 5.2. PlanetScope's SuperDove imagery scenes utilised for seasonal time |
| series analysis in 2021, including the months April, May, August, and October. |
| Imageries are presented using RGB bands 85 |
| Figure 5.3. PlanetScope's SuperDove imagery scenes utilised for annual time series |
| analyses. Imagery dates for the years including 2020, 2021, 2022 and 2023 were |
| chosen based on availability as close as possible to ground truth surveys and |
| seagrass peak biomass in August. Imageries are presented using RGB bands 86 |
| Figure 5.4. Spectral reflectance curves of benthic class training data. The shaded |
| area represents ± standard deviation |
| Figure 5.5. Areas chosen to assess the consistency in spectral reflectance across |
| time series imagery. a) a white roof top; b) main road; c) sandy beach area; and d) |
| vegetation area |
| Figure 5.6. Confusion matrix output of the Random Forest (RF) classification |
| method showing the correctly classified pixels (green diagonal values) and |
| misclassification between true labels and predicted labels. Values represent the |
| percent (%) numbers of pixels91 |
| Figure 5.7. Seasonal time-series classified habitat maps for the intertidal area |
| Lindisfarne National Nature Reserve (LNNR), using Random Forest classification |
| method93 |
| Figure 5.8. Classified maps showing seasonal cover for vegetation classes |
| separately, including seagrass (sparse SG and mod-dense SG), macroalgae and |
| SG/MA mixed distributions in the intertidal LNNR area94 |

| Figure 5.9. Interannual time-series classified habitat maps of the intertidal area |
|--|
| Lindisfarne National Nature Reserve (LNNR), using Random Forest classification |
| method96 |
| Figure 5.10. Classified maps showing interannual cover for vegetation classes |
| separately in seagrass (sparse SG and mod-dense SG), macroalgae and SG/MA |
| mixed distributions in the intertidal LNNR area |
| Figure 5.11. Seasonal and interannual percent change in habitat class cover for |
| LNNR, as well as for the different investigated areas (Causeway, Fenham Flats, and |
| Budle Bay, respectively) separately |
| Figure 5.12. Time series of average UK daily maximum temperatures for spring |
| 2021. (Source: Met Office, 2021: Contains public sector information licensed under |
| the Open Government Licence v3.0.) |
| |

List of Tables

| Table 2.1. Overview of classifiers used for image classification in remote sensing |
|---|
| including description of each method, strengths, weaknesses, and fitness for |
| purpose for mapping complex seagrass environments20 |
| Table 2.2. A summary of available studies that have used optical remote sensing |
| applications in temperate seagrass habitats. S=Subtidal, I=Intertidal26 |
| Table 3.1. Results of Jeffries – Matusita index, indicating spectral pair separability of |
| benthic classes for: Zostera noltii transect, Zostera marina transect, and Macroalgae |
| transect. Where a class was not present in a transect to conduct pair separability, |
| these were marked with NA = not available |
| Table 3.2. Post-classification analysis showing the accuracy assessment outputs of |
| the Maximum-likelihood classification map for a) the multispectral image and b) the |
| RGB image41 |
| Table 4.1. Reduced number of spectral bands, using the closest bands from the |
| CASI hyperspectral bands aligned to the PlanetScope SuperDove and multispectral |
| UAV band centre wavelength ± FWHM (Full Width at Half Maximum). HS = |
| Hyperspectral, MS = Multispectral57 |
| Table 4.2. Results of Jeffries-Matusita (J-M) index, indicating spectral pair |
| separability of benthic classes for the: 7-class-, 6-class- and 5-class habitat maps. 59 |
| Table 4.3. Summary table of optimal tuned parameters reached for the optimal |
| Random Forest model to create a classification habitat map for each investigated |
| Scenario61 |
| Table 4.4. Accuracy results of the Random Forest classification maps for each |
| investigated Scenario62 |
| Table 5.1. Number of training pixels for created habitat classes 82 |
| Table 5.2. Available PlanetScope satellite imagery data and the respective spectral |
| resolution for each sensor83 |
| Table 5.3. Information acquisition of imagery used in this study including tidal stage |
| and the approximate hours before or after low tide |
| Table 5.4. Results of Jeffries – Matusita (J-M) index, indicating spectral pair |
| separability of benthic habitat classes88 |
| Table 5.5. Accuracy results of the Random Forest classification for the train imagery |
| 14th August 2021 91 |

| Table 5.6. Seasonal and interannual total habitat class cover (km²) change for the | Э |
|--|------|
| investigated LNNR and different areas separately including Causeway, Fenham | |
| Flats and Budle Bay. | . 99 |
| Table 6.1: Summary of specifications of different platforms and sensors for | |
| monitoring an intertidal seagrass environment | 111 |

Chapter 1: Introduction

1.1. Importance, threats and decline of seagrass

Seagrass habitats are some of the most productive ecosystems on earth (Duarte & Chiscano, 1999). They are highly valuable, providing a wide range of ecosystem goods and services to coastal regions, including: (1) coastal protection, through their root system and above ground biomass, as they stabilise sediment by serving as natural buffer against wave actions and the protection from coastal erosion (Costanza et al., 1997); (2) improvement of water quality, through trapping pollutant run offs from land (Moore, 2004); (3) nursery grounds for commercial fish species as food source, shelter and refuge from predatory species (Beaumont et al., 2008; Bertelli & Unsworth, 2014); (4) fisheries support, as many commercial fish species rely on seagrass habitats for food and breeding (Unsworth et al., 2019); (5) and finally, their high efficiency in carbon sequestration and mitigating climate change (Röhr et al., 2018; Zou et al., 202; Gao et al., 2022). An area of seagrass may be thirty-five times more efficient at storing CO₂ than the same area of rainforest (McLeod et al., 2011), due to rapid conversion of CO2 into organic carbon and its storage in plant tissues and extensive shoot systems expanding into and stabilising the sediment (Duarte et al., 1998; Fourgurean et al., 2012).

Despite this, seagrass ecosystems are threatened, facing ongoing decline and loss due to natural and anthropogenic impacts (Orth et al., 2006; Grech et al., 2012), such as: (1) pollution from agricultural run-off and industrial waste that can cause proliferation in algal blooms and consequently limiting sunlight and thus suppressing seagrass growth (Han & Liu, 2014; Kim et al., 2015; Breininger et al., 2017); (2) coastal development that can lead to the loss or degradation of seagrass habitats due to modifications of coastal areas and sedimentation (Holon et al., 2015); (3) physical damage through boat anchoring and propeller damage (Collins et al., 2010); (4) destructive fishing practices though damaging fishing gears (Orth et al., 2002); (5) diseases that can lead to decimation in seagrass population (e.g., wasting disease) (Bull et al., 2012); (6) climate change causing rising sea water levels and increasing water temperature, which can lead to stress in seagrass and impact their growth (Tang & Hadibarata, 2022). A combination of these threats has led to an overall global

decline of seagrass habitat by 30% since the late nineteenth century (UNEP-WCMC, 2020).

Around the British Isles, seagrass meadows have not been exempt from these pressures, and have experienced widespread declines in the past decades. Many seagrass habitats are in poor condition (Jones & Unsworth, 2016). Green et al. (2021) highlighted a catastrophic loss and decline of seagrasses around the UK with an estimated loss of at least 44% since 1936, of which 39% has disappeared since the 1980s. In the early 1930s, a major decimation of *Zostera marina* (eelgrass) population was caused by an epidemic, known as the 'wasting disease' (*Labyrinthula zosterae*), which spread across the North-Atlantic Coasts of Europe and North America and impacted significantly on seagrass populations in the UK (Butcher, 1933; Den Hartog, 1989; Bull et al., 2012). As in many other parts of the world, seagrass habitats in the UK then continued to decline due to a variety of anthropogenic threats. One of the major threats in the UK is related to excessive coastal nutrient input leading to poor water quality and resultant eutrophication, for example due to agricultural activities (e.g., fertilisers), sewage and industrial activities (Jones et al., 2018).

Eutrophication has a number of potential impacts. Eutrophication can lead to light limitation, subsequently suppressing seagrass growth through increased algal blooms and overshading. Sedimentation, which is often accompanied by nutrient enrichment, can lead to both turbid waters and smothering of seagrass (den Hartog, 1994; Burkholder et al., 2007; Han & Liu, 2014). These threats are amplified by climate change in the UK, posing significant challenges to the survival of seagrass. For example, elevated sea temperatures can result in more frequent algal blooms (Short & Neckles, 1999). Additionally, increasingly changing, heavier and more dynamic precipitation patterns may lead to increased nutrient and sediment runoff from the land, resulting in higher nutrient concentrations and the subsequent rapid proliferation of algae (Gilbert et al., 2008; O'Gorman, 2015). To counteract and prevent further threats, effective seagrass and algal distribution is invaluable to track changes and implement strategies, for example, to monitor and control algal overgrowth, and mitigate seagrass decline. These tools are urgently required (Jones & Unsworth, 2016; Strachan et al., 2022).

1.2. Seagrass biology and distribution

Seagrasses are marine flowering plants (Angiosperms) (Phillips & Menez, 1988). This group consists of 73 species, which are estimated to cover an area of over 300,000 km² of the world's seabed (UNEP-WCMC, 2020). Their distribution extends across six global bioregions, and they are known to occur in 191 countries across tropical and temperate coastal zones (Short et al., 2007; McKenzie et al., 2020; UNEP-WCMC & Short, 2021). Due to their photosynthetic characteristics, occurrence in the ocean is limited to shallow coastal areas where they rely on sunlight availability for growth and survival (Zimmerman, 2006). While seagrass species are often confused with seaweeds or algae, as both are aquatic vegetation, they are different types of organisms belonging to separate taxonomic groups with distinct characteristics. Seagrasses have a more complex structure consisting of a true roots system that enables their anchoring and stabilisation in the sediment (below ground biomass) and ribbon-like leaves that grow above the sediment (above ground biomass) (Hemminga & Duarte, 2000). Algae are less structurally complex and lacking a true root system, are often only attached to substrates (Pereira, 2021) (Figure 1.1).

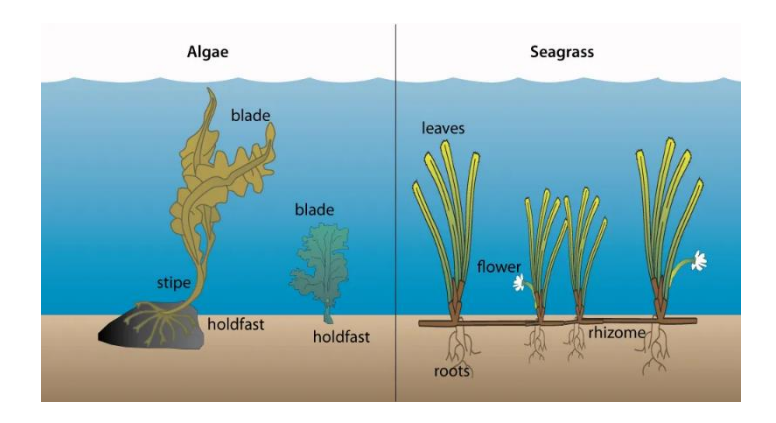


Figure 1.1. Diagram showing morphological differences between algae (left) and seagrass (right). (Source: https://ocean.si.edu/holding-tank/images-hide/algae-vs-seagrass).

Seagrasses have two main reproductive strategies that are essential to their growth and propagation. They can reproduce sexually via seed production and vegetatively through the growth of their vertical shoots, and the production of rhizomes (Figure 1.1). This enables their expansion into seagrass meadows, which can vary in density, depending on the seagrass species, stage of proliferation and environmental

conditions that they are exposed to (Akerman, 2006). They can occur both in shallow subtidal areas covered by water and intertidal areas, exposed at low tide (Short et al., 2007) (Figure 1.2). While both seagrass and macroalgae are important components of coastal ecosystems, they are in competition for space, light and nutrients to grow and expand, which can have detrimental ecological implications for seagrass habitats (McGlathery, 2001; Han & Liu, 2014; Han et al., 2016). Opportunistic growing macroalgae respond rapidly to increased nutrients, smothering seagrass and potentially outcompeting slower growing seagrass (den Hartog, 1994).

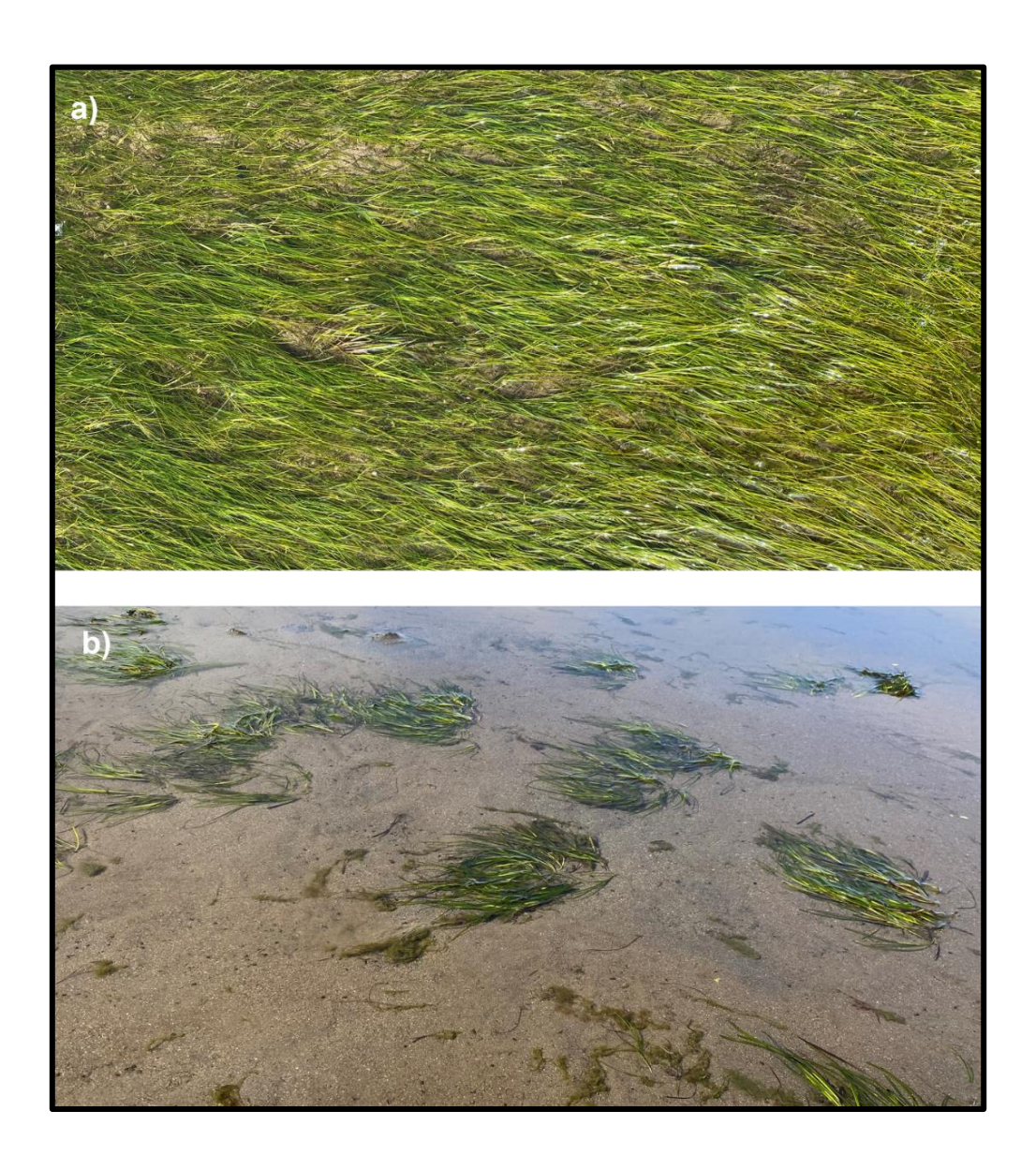


Figure 1.2. Variations in density of seagrass habitats at low tide: a) dense *Zostera noltii* patch; b) sparse *Zostera marina* patch.

1.2.1. Temperate seagrass species

In the UK temperate zone, the commonly distributed species are the intertidal seagrass species *Zostera noltii* (dwarf eelgrass) and subtidal species *Zostera marina* (eelgrass) (Short et al., 2007), note that *Z. marina* can grow intertidally. These two species differ particularly in the morphology of their leaf structure. *Z. marina* has longer ribbon-like leaf blades, whereas *Z. noltii* consists of shorter, thinner, and flat leaf blades, which are generally darker green in comparison to *Z. marina* (Figure 1.3).

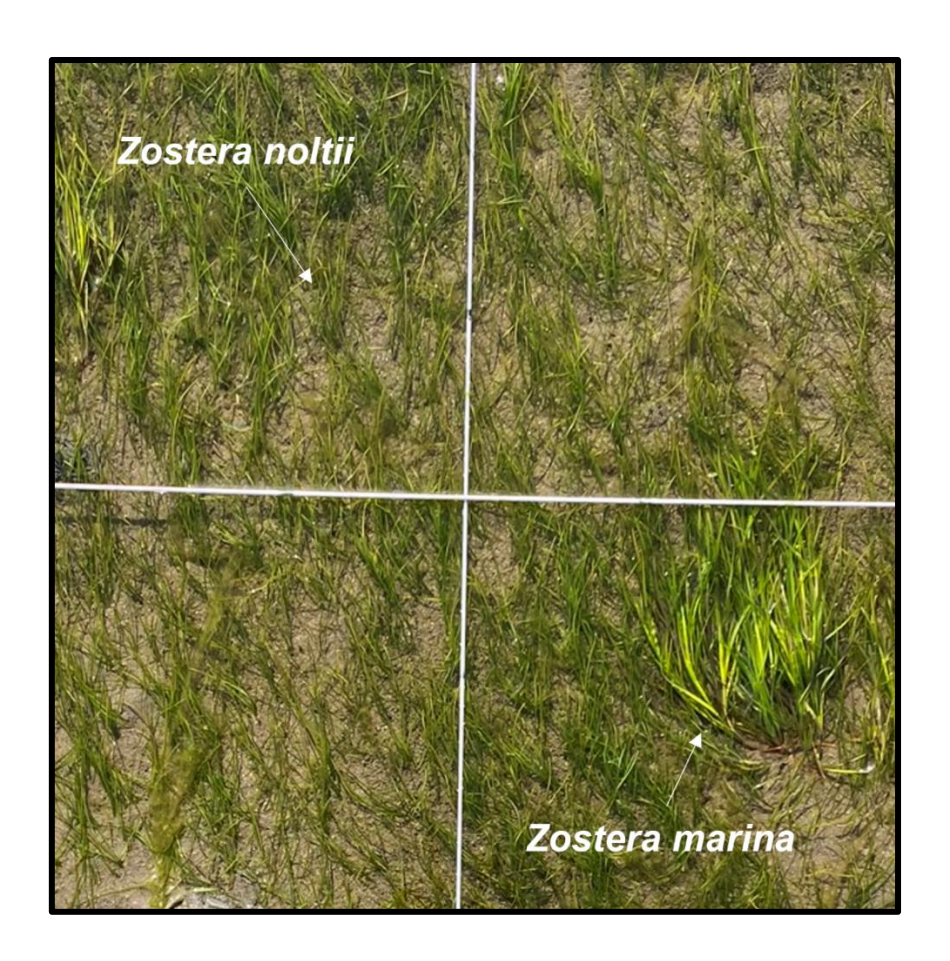


Figure 1.3. Images of the two common temperate intertidal seagrass species: *Zostera noltii* and *Zostera marina*.

1.3. Need for effective management and conservation methods

Regular monitoring and protocols enable coastal managers to assess the overall health status (condition) of seagrass habitats, which can provide information on the dynamics of species and populations, and whether these are stable or declining over time (e.g., Borum et al., 2004; Short et al., 2006). Such information allows coastal

managers to identify and quantify potential threats and stressors (e.g., pollution, algal blooms, diseases), to track long-term trends and changes in habitats, to allow for timely preventive measures and intervention to reduce potential threats.

Traditional seagrass monitoring methods involve field-based surveys through in situ collection of data. Different methods are applied to acquire direct observations and measurements of seagrass, abundance, biomass, diversity, and their distribution to evaluate the condition and health of seagrass habitats (Borum et al., 2004). Such methods include, for example, transect surveys, where seagrass data is recorded along the transect or quadrat sampling by placing a rectangular frame of known area on the seafloor to record detailed information on seagrass information (e.g., shoot density, diversity, seagrass cover) (Bunker & Green, 2019; Doggett & Northen, 2023). In the UK, such methods are well established within organisations and governmental bodies that monitor seagrass. The largest national seagrass monitoring programme is maintained by the Environment Agency (2024) which uses different ground survey methods, including quadrat sampling to acquire information on seagrass species and seagrass cover for specific locations where seagrass is present. While other governmental bodies and organisations are also known to perform seagrass surveys and monitoring, these are either limited to one or two locations, are short-term or have only recently been established. Natural England for instance, has monitored seagrass, using quadrat sampling to record seagrass cover, canopy height, shoot density and macroalgae cover in some locations in some years (Bunker & Green, 2019; Doggett & Northen, 2023). The UK-based non-profit organisation, Project Seagrass (projectseagrass.org/), surveys and monitors seagrass in Porthdinllaen, Wales as part of their established platform called Seagrass-Watch, Global Seagrass Observing Network. Finally, short-term projects (e.g., up to 5 years), smaller scale in the effort to establish seagrass monitoring programmes are in place and are currently being developed. However, they are limited to specific regions in the UK and only cover small areas (e.g., EU LIFE Wader, 2024; Stronger Shores, 2024).

In situ methods have been used for decades and continue to be valuable for seagrass habitat monitoring and management since they can provide detailed information of seagrass habitats for specific locations (Short et al., 2014), but they are often expensive, time consuming, pose safety concerns (e.g., being trapped in sediment) and lack accurate spatiotemporal information for seagrass habitat inventory and

monitoring (Mumby et al., 1999). Spatially, seagrass ecosystems can be patchy over large areas (which are difficult to monitor using *in situ* methods), and may consist of irregular seagrass meadows, species distributions and the presence of macroalgae (e.g., Leblanc et al., 2021; Ivajnšic et al., 2022). Temporally, seagrass ecosystems can be highly dynamic both annually and seasonally depending, for example, on the degree of intensity of threats, such as nutrient input and the proliferation of algae (Carr et al., 2012; Han & Liu, 2014). If only annual monitoring is carried out, spatiotemporal dynamics will not be adequately captured. Short-term fluctuations arising from events such as heatwaves, which can happen abruptly, may be overlooked, with rapid unexpected, severe consequences on seagrass populations and entire ecosystems (Thomson et al., 2015). Such fluctuations and dynamics can also occur at different spatial scales. Seagrass habitats can be spatially heterogeneous over both small and large scales. Sampling a limited number of quadrats may not adequately capture this variability crucial to understand seagrass and macroalgae dynamics (Lønborg et al., 2021).

The lack of accurate spatiotemporal information can make it challenging for managers to detect early signs of threats and decline of seagrass, potentially leading to delayed and timely management strategy responses. To address this gap of monitoring in dynamic seagrass-macroalgae environments, more frequent sampling (e.g., quarterly, or monthly) and larger coverage through increased sample size would be required. However, increasing the frequency and numbers of sampling consequently involves higher costs related to fieldwork. The trade-off between higher costs and more frequent sampling may be challenging for organisations and projects due to budget constraints, limiting their ability to increase sampling frequency and coverage. To overcome the challenge in costs associated with sampling, and to optimize the trade-offs between costs and the acquisition of accurate spatiotemporal data, technological advances such as remote sensing may provide an alternative methodology to monitor seagrass (Hossain et al., 2015; Veettil et al., 2022).

1.3.1. Habitat maps

Remote sensing techniques have revolutionised the toolbox available to coastal managers as they permit mapping and monitoring of seagrass habitats cost-

effectively, over large areas, repeatedly, and they allow acquisition of data in inaccessible areas (UNESCO, 2005; Hossain & Hashim, 2019). With increasing advancement in technology and accessibility to cost-effective high resolution imagery data such as UAVs and satellites (e.g., Sentinel-2 (10m), PlanetScope (3m)), the operationalisation of remote sensing for coastal marine monitoring programmes has gained increased attention (Ventura et al., 2022; Vitousek et al., 2023).

While remote sensing techniques are also increasingly being considered in seagrass monitoring programmes in the UK, they are often only presented in form of broadscale maps that solely provide the extent and occurrence of seagrass habitats, such as the national Seagrass layer provided by Natural England and Environment Agency (Natural England, 2024) (Figure 1.4). Such maps lack, for example, co-occurring threats to seagrass habitats such as opportunistic macroalgae, and disregard the patchiness of seagrass habitats, which is critical to accurately capture seagrass cover. In addition, these maps often represent seagrass distribution at one point in time and lack the temporal component, critical to detect seagrass habitat changes. Local scale maps that show distributional patterns of seagrass species, their densities and macroalgae cover at higher spatiotemporal resolution, may enable managers to more accurately capture seagrass-macroalgae dynamics, thus assess seagrass habitat health (condition), their decline and potential and ongoing threats and pressures. Accurate spatiotemporal habitat maps that show detailed seagrass and algae cover that can be rapidly produced are needed to aid effective informed decision-making to mitigate and prevent seagrass decline across the UK (e.g., Vahtmäe et al., 2021; Haro et al., 2022; Carlson et al., 2023).



Figure 1.4. National Seagrass Layers of current spatial extent of *Zostera* spp. (dark blue polygon area) in Lindisfarne and Plymouth Tamar that provide presence/absence data (Source: Natural England, 2024: Contains public sector information licensed under the Open Government Licence v3.0.)

1.4. Study site

The research presented here focussed on Lindisfarne National Nature Reserve (LNNR) in the northeast of England, United Kingdom. The LNNR consists of a variety of habitats including sand dunes, saltmarsh, intertidal-subtidal reefs, and intertidal mudflats. Multi-designated, the site is underpinned by a Site of Special Scientific Interest (SSSI), is also an SPA (Special Area of Protection) and sits within the Berwickshire and North Northumberland Coast Special Area of Conservation (SAC). Established as a national nature reserve, the LNNR protects important geology, habitats and species. The LNNR, for example, is ecologically important for internationally protected birds such as Light-Bellied Brent Geese (*Branta bernicla*) (regularly over 2,000 birds) and wigeon (*Mareca penelope*) (up to 40,000), that utilise the tidal mudflats as maintenance areas and foraging grounds by particularly feeding on seagrass, prevalent across the intertidal mudflat areas during late summer, autumn and into winter months (SSSI citation, 1989). National Nature Reserves also provide 'outdoor laboratories' for research.

The intertidal mudflat area in LNNR is large, covering approx. 2,300 ha, which includes three main areas of seagrass habitat, namely the Causeway area (Holy Island Sands), Fenham Flats and Budle Bay (Figure 1.5). Different vegetation types can be found across the LNNR mudflats and area of interest, including the dominating intertidal seagrass species Zostera noltii, the subtidal species Zostera marina and a mix of opportunistic green macroalgae such as Enteromorpha (Ulva intestinalis). (Figure 1.5). Distribution and density of seagrass and opportunistic macroalgae (macroalgae, hereafter) varies across the different mudflat areas, primarily attributed to increased nutrients arising from terrestrial and offshore inputs. Of particular concern is the macroalgae growth in the Causeway and Budle Bay areas, where seagrass can be often found mixed with macroalgae in the spring to summer months. The field site is managed by Natural England, a non-departmental public body (NDPB) in the United Kingdom, responsible for overseeing the management and protection of seagrass in Lindisfarne. The field site is currently monitored by the Environment Agency as part of their annual seagrass monitoring programme using quadrat sampling and hovercraft, but accurate spatiotemporal mapping for monitoring would improve monitoring and allow better understanding of trends.

The growing recognition of the ecosystem services provided by seagrass meadows, especially, as 'blue carbon ecosystems', that play a crucial role in mitigating climate change (UNEP-WCMC, 2020; do Amaral Camara Lima et al., 2023), have gained increased attention and high priority in national seagrass protection and restoration efforts. As opposed to homogeneous seagrass habitats, the complexity of the LNNR field site provides a unique opportunity to evaluate remote sensing applications and to better understand intertidal seagrass and macroalgae habitat dynamics at large-scale in the UK.

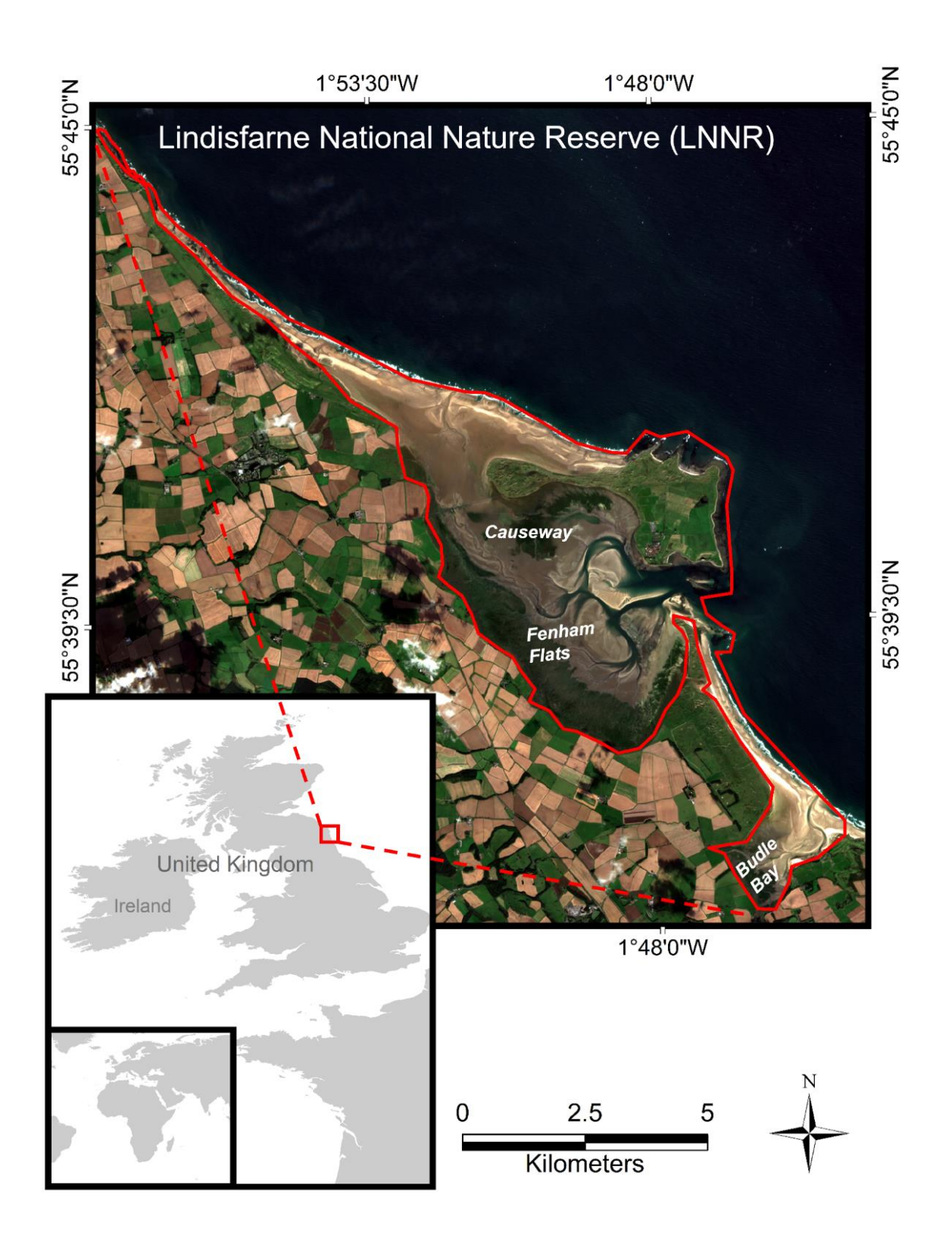


Figure 1.5. Map showing field site located in the North East of the UK (bottom left). Extent of Lindisfarne National Nature Reserve (red boundary) and different regions of studied field sites, including Causeway area, Fenham Flats and Budle Bay.

1.5. Thesis aim and structure

The overall aim of this thesis is to develop an effective remote sensing strategy for temperate intertidal seagrass monitoring for management and conservation purposes. Optical remote sensing imagery are utilised, and methods are developed to evaluate varied optical remote sensing platforms and their applications for mapping and monitoring a complex intertidal seagrass-macroalgae environment. To address knowledge gaps described in Chapter 1 and Chapter 2, the thesis is structured to reflect the multiscale approach taken by utilising imagery data from different platforms with varying spatial, spectral and temporal resolution. This permits the assessment of information that can be acquired from each different platform and sensor. The thesis is structured as follows:

Chapter 1 discusses the importance, threats and decline of seagrass habitat, their need for effective management and conservation.

Chapter 2 gives an overview on optical remote sensing technologies and classification methods and presents a literature review that identifies the knowledge gap of the application of optical remote sensing in temperate seagrass environments.

Chapter 3 evaluates the utility of an off-the shelf multispectral Unmanned Aerial Vehicle (UAV) to map an intertidal multi-species seagrass environment. This chapter investigates the level of accuracy that can be achieved, particularly focussing on additional bands at the red edge and in the near infrared in comparison to an RGB camera. This study maps seagrass at species level (*Zostera noltii* and *Zostera marina*, respectively) and aims to discriminate between seagrass species and macroalgae. Additionally, both the benefits and challenges of using UAV technology to map intertidal seagrass environments are discussed and recommendations developed to support operational and management practices.

Chapter 4 examines the utilisation of airborne hyperspectral imagery (Compact Airborne Spectrographic Imager -CASI), that has a lower spatial resolution (1m) but higher spectral resolution (23 bands) imagery data, for larger scale mapping of an intertidal seagrass environment. This chapter investigates the capability of an airborne hyperspectral imagery to accurately mapping seagrass densities and macroalgae cover, to identify where hyperspectral imagery data may augment UAV capabilities.

Additionally, benefits and challenges of airborne for large-scale seagrass intertidal mapping and monitoring for management practices are discussed.

Chapter 5 evaluates satellite multispectral imagery (PlanetScope), that has a lower spatial resolution (3m) and a lower spectral resolution (8 bands), for large scale mapping of a seagrass-macroalgae environment. Additionally, this chapter investigates the potential of satellite imagery to monitor temporal (seasonal and interannual) change in seagrass and macroalgae cover for effective management practises.

Chapter 6 discusses how these methods may combine to deliver a multiscale level mapping approach for monitoring and effective management practises and provides a synthesis of key findings, limitations, and future research of study to make recommendations to Natural England.

Chapter 2: Remote Sensing Review

2.1. Optical remote sensing

Remote sensing refers to the "process of detecting and monitoring the physical characteristics of an area by measuring its reflected and emitted radiation at a distance" (USGS, 2023). Information can be acquired via different platforms (e.g., satellite, plane, and Unoccupied Aerial Vehicle (UAV)), that have specific sensors attached, through which, detection or the measurement of electromagnetic radiation (light) reflected, emitted, or scattered by the targeted object of interest is captured (Richards, 1986). The acquisition of information through the visible to near infrared portion of the electromagnetic spectrum is referred to as optical remote sensing (remote sensing, hereafter) (Richards, 1986).

Remote sensing platforms with mounted sensors are most commonly UAV, which are operated from the ground, space -borne satellites or occupied aeroplanes (Airborne) (Figure 2.1). The amount of information and imagery data that can be acquired, depends on: temporal resolution, the revisit time between consecutive image acquisitions; spatial resolution, the level of detail represented in the image, which is determined by sensor characteristics and flight height; radiometric resolution, which represents the ability of a sensor to discriminate small changes in detected energy, thus between different levels of brightness or intensity in the electromagnetic spectrum, usually defined by whether it is 8-bit, 12-bit or 16-bit; and spectral resolution, which refers to the widths and number of spectral bands, which determines the level of detail in spectral information (Richards, 2013). Combinations of and compromises between these four sensor specifications ultimately determines the level of information attained and trade-offs are typically required. For example, an airborne hyperspectral sensor may capture data in hundreds of narrow spectral bands, which may enable detailed discrimination between vegetation types (e.g., algae and seagrass) (Garono et al., 2004; Vahtmäe et al., 2021), whereas a multispectral sensor, which consist of a few spectral bands may offer broader spectral bands with less detailed information but in turn greater spatial coverage area (Figure 2.1). Sensor and platform selection can have different implications for ecosystem habitat mapping and monitoring. These can include but are not limited to: 1) mapping of ecosystems and

habitats at spatially large scale and in inaccessible areas; 2) acquisition of ecosystem features and complexities through for example higher spatial and spectral resolution sensors, enabling the characterisation of habitats; and 3) assessment of habitat dynamics through mapping and monitoring from detailed to broad-scale level mapping (e.g., Dekker et al., 2006; Hobley et al., 2021; Zoffoli et al., 2021).

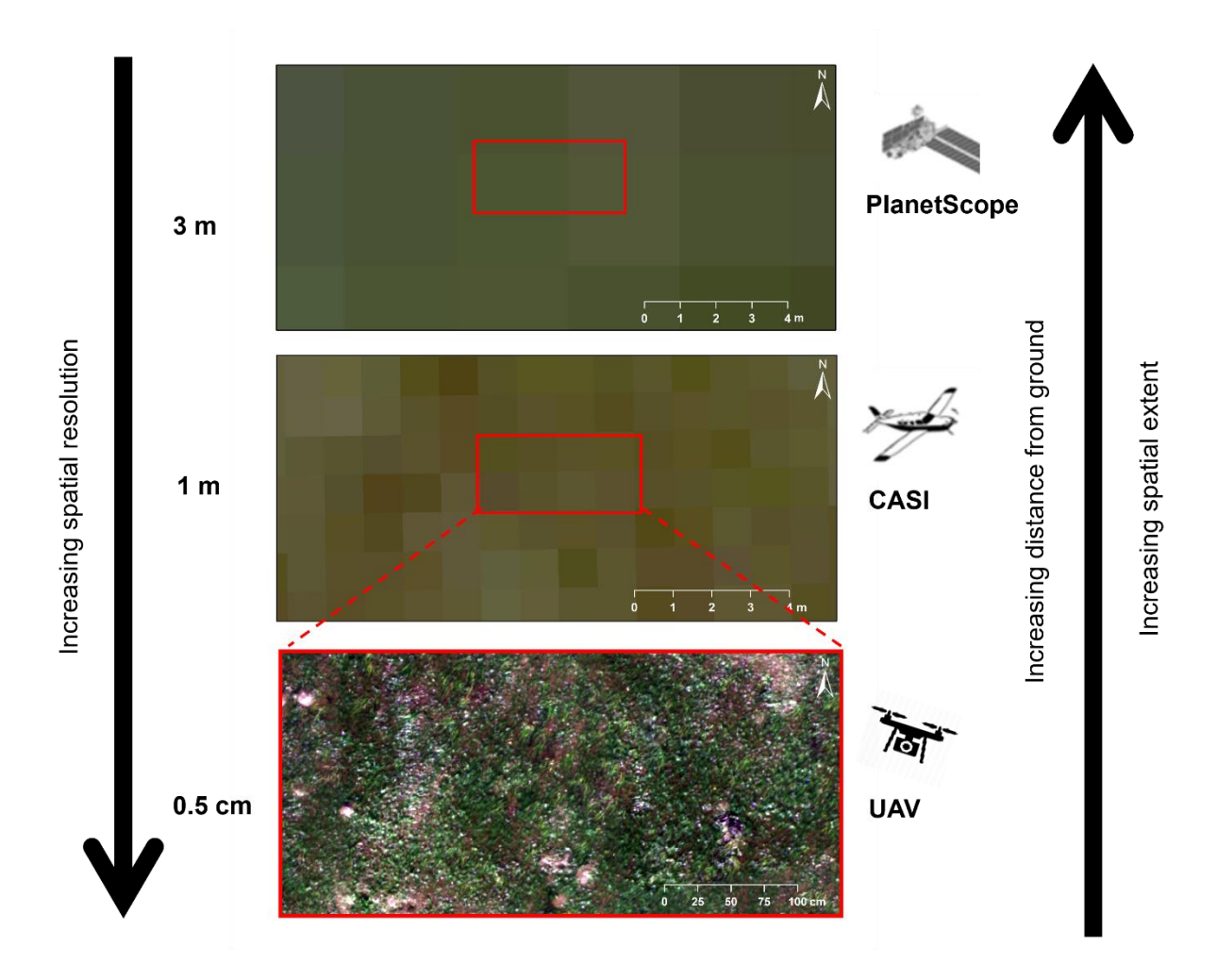


Figure 2.1. Varying spatial resolution (from high to low) of an intertidal seagrass environment taken with different platforms and sensors including an Unoccupied Aerial Vehicle (UAV), airborne and satellite imagery.

Ecosystem's constituent habitats can be complex and dynamic in their composition. These complexities and dynamics can occur from small-scale habitat patches to large-scale habitats to entire ecosystems (Phinn et al., 2018a). Often, with traditional methods, such dynamics and detailed information, critical to ecosystem management,

can be difficult to capture. By utilising appropriate platforms and sensors with optimal spatial, spectral, and temporal resolution, remote sensing derived habitat maps can provide valuable information to better understand habitat spatial complexities and dynamics (Hossain et al., 2015).

Once imagery has been collected, distinguishing characteristics in remote sensing derived data sets, classification or categorization of different features is required. Distinct classes or categories must be assigned to habitat features (e.g., vegetation, non-vegetation, water etc.). This process is performed during the analysis stage by utilising appropriate classification methods, an analytical approach where spectral data are classified, or grouped, according to similar characteristics that lead to the production of maps which represent habitats. The accuracy of classified habitat maps and their representation of the habitats and their attributes being investigated (e.g., complexity, patchiness) depends primarily on the spatial and spectral resolution of imagery data and the classification method applied to delineate the required information (Richards, 2022). For example, in complex habitats, where ecologically different features occur, i.e., seagrass and macroalgae, higher spatial resolution imagery may permit class identification to species level (Reshitnyk et al., 2014). Such detailed information can get lost in lower spatial resolution imagery, as increasing pixel size can lead to mixed pixels that contain multiple classes (Richards, 2013). However, with less habitat complexity, such as homogeneous seagrass areas, high spatial resolution imagery may not be required as relevant, unless other habitat factors such as seagrass patchiness and configuration are important.

2.1.1. Classification methods

Over the years, changes in remote sensing and sensor technologies have led to the development of new methodologies for generating classified habitat maps, improving the information on features that can be derived from remotely sensed imagery. During the early years of image analysis and classification, when spatial resolution of remotely sensed imagery was low (e.g., Landsat in the 1970s, 30m pixels), hard classification techniques, where pixels are categorised into distinct, well-defined classes based on their spectral characteristics, was the prime methodology (e.g., Weismiller et al., 1977; Ward et al., 1997). The utilisation of such hard classifiers may be effective where

seagrass mapping includes well-defined and distinct classes (Richards, 2022). For example, they may suffice for mapping homogeneous seagrass environments, where pixels contain distinct features (O'Neil & Costa, 2013). Although hard classifiers have been maintained as a traditional approach and are still needed, single pixels that contain multiple feature classes are harder to analyse, e.g., signals from seagrass, algae, shells cannot be disaggregated, making it challenging to acquire accurate information about the presence of the actual features within the pixel. To deal with such mixed pixels, fuzzy techniques, such as sub-pixel classification methods (e.g., Linear Spectral Unmixing (LSU)), which utilises the spectral information to estimate the proportion of each class within the pixel, can be applied (Keshava & Mustard, 2002; Quintano et al., 2012) (Figure 2.2).

Image classification methods and their effectiveness are especially influenced by spatial resolution. Pixel-based classification, whereby individual pixels are labelled into a specific class based on their spectral characteristics (e.g., Maximum Likelihood classifier), are often sensitive to spatial resolution (Richards, 1986; Foody et al., 1992). For example, higher spatial resolution imagery enables more detailed spectral information. Pixel-based classifiers were among the early approaches in remote sensing classification (e.g., Macleod & Congalton, 1998). With increasing higher spatial resolution imagery available through the 2000s, the concept of image segmentation and Object-Based Image Analysis (OBIA), whereby geographical objects are analysed instead of individual pixels, was introduced. For instance, Object-based image analysis groups pixels into objects or segments by considering their spectral, spatial, and contextual properties (Blaschke, 2010; Lyons et al., 2012; Roelfsema, et al., 2013) (Figure 2.2).

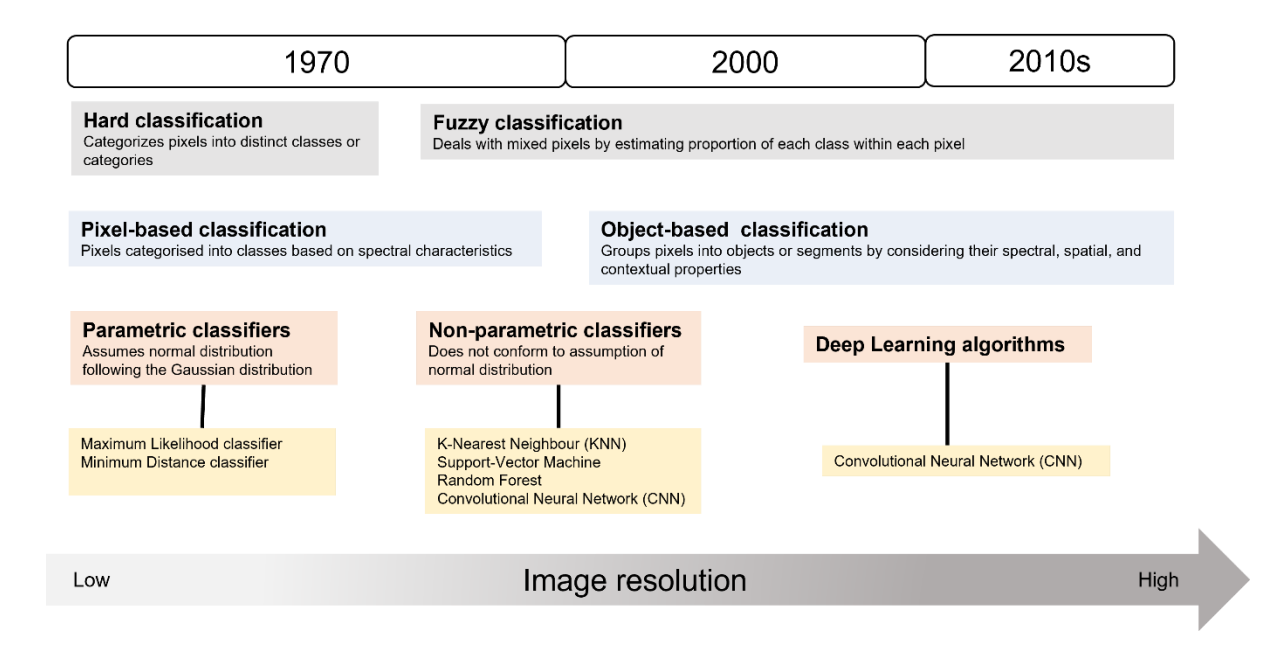


Figure 2.2. Schematic illustration of the evolution of classification methods used for remote sensing image classification.

Two main computational approaches are used for mapping. Supervised classification is a machine learning approach whereby a model is trained on labelled data, e.g., habitat classes are assigned to pixels, and unsupervised classification, where a model investigates patterns and creates categories or classes without predefined labels. Unsupervised classification can be very useful for a quick and less sophisticated, initial exploration of unknown habitat areas (Richards, 2013, 2022). For example, to investigate seagrass presence/absence and patches within an unknown area. However, in habitats with spectral distinct complex vegetation types, such as the intertidal seagrass-macroalgae environment investigated in this study, this approach may be challenging. A supervised classification method is more appropriate to account for varying vegetation features and to distinguish between these, thus enabling more accurate habitat mapping (Hossain et al., 2015).

Two main types of classifiers that differ in their underlying assumptions in statistical distribution are commonly used for image analysis. Parametric classifiers, such as Maximum Likelihood (ML) and Minimum Distance (MD) classifiers, assume a normal (Gaussian) distribution with no outliers or skewed data, and are also among the first classifiers applied in the early days of remote sensing analysis (Wacker & Landgrebe, 1972; Richards, 1986). Although parametric classifiers continue to be used and have

especially gained popularity for pixel-based image analysis, their limitations in handling data that do not conform to the assumptions of normal distribution, led to the development of non-parametric classifiers, non-parametric classifiers can handle nonnormal or complex distributions (Richards, 2022). For example, in the intertidal environment in this study the wetness of habitat classes e.g., dry seagrass/ wet seagrass, could result in bimodal distribution patterns within one ecologically coherent class. With advancing technology, computing techniques, and increasing availability of higher spatial and spectral resolution imagery data, non-parametric classifiers based on machine learning algorithms such as Support Vector Machine (SVM) were developed (Cortes & Vapnik, 1995; Sheykhmousa et al., 2020). SVM gained increased prominence due to its effectiveness in handling non-linear data and its application for pixel-based and object-based classification tasks (Pal, 2005; Mountrakis et al., 2011). The application of non-parametric methods for remote sensing classification continued to evolve, with machine learning ensemble methods, such as Random Forest (Breiman, 2001), gaining popularity due to its versatile applications in handling complex and high dimensional imagery data (e.g., hyperspectral data) (Pal, 2005; Belgiu & Drăgu, 2016). În parallel, a significant advancement în image classification analysis was made through the development of Deep Learning techniques (e.g., Convolutional Neural Networks; CNNs), which has improved the potential and capability of automated image classifications in remote sensing (Maggiori et al., 2017; Hobley et al., 2021; Kattenborn et al., 2021).

While many techniques are available for remote sensing image classification, today, choosing the appropriate method requires consideration of many factors, including the: (1) objectives of project, applications and utilisation of end product; (2) required level of accuracy and spatial extent; (3) platform, sensors and data characteristics (i.e., spectral/spatial/temporal resolution; data dimensionality i.e., multispectral/hyperspectral); (4) availability of training data; (5) complexity of habitat homogeneous/heterogeneous; (6) distribution assumptions (parametric/nonparametric); (7) computational resources i.e., processing time; hardware and software limitations; (8) Budget and resources. As such, different methods have their strengths and weaknesses depending on the purpose and the application of interest (Table 2.1).

Table 2.1. Overview of classifiers used for image classification in remote sensing including description of each method, strengths, weaknesses, and fitness for purpose for mapping complex seagrass environments.

| Classifier | Description | Strength | Weakness | Fit for purpose |
|-----------------------------|--|--|---|--|
| Unsupervised | | | | |
| K-means clustering | Pixels are grouped into a class, based on their spectral values, whereby the dataset is partitioned into specified number of clusters by assigning each data point to the nearest mean (centroid); is considered as non-parametric, as it, instead, uses an interactive algorithm /approach to group data points based on similar spectral features (Hartigan & Wong, 1979). | Simplicity and speed to explore and identify initial spatial patterns; computationally efficient; no ground data required. | Due to lack of training data may lead to inaccurate results; does not provide class labels, thus may lead to misinterpretation of identified patterns if areas and potential classes of imagery are not known. | Initial exploration of seagrass habitats; user friendly and low computational demands, which makes it accessible to managers for rapid habitat mapping. |
| Supervised | | | | |
| Maximum-Likelihood (ML) | Parametric classifier that assumes that the distribution of class is normally distributed (Gaussian) and calculates the probability that a pixel belongs to a given class based on their spectral variance and covariance (Foody et al., 1992; Richards, 1986). | Performs very well when assumptions of normal distribution are met; suitable for multispectral imagery data; simple implementation; no extensive and complex parameter tuning required; well established for the application in remote sensing classification. | Sensitive to outliers and non-normal distributed data; sensitive to small training sample size; depends on high quality and accurate training data that represents the class categories well; does not handle mixed pixels well and performs best with pure pixels. | Beneficial in homogeneous non- complex seagrass habitats when using low spatial resolution imagery data; Can be useful in complex and heterogeneous seagrass habitats with very high spatial resolution imagery data; user friendly and low computational demands, which makes it accessible to managers for rapid habitat mapping. |
| Spectral Unmixing (SU) | A method used to extract information of the composition of mixed spectral signatures pixels, by estimating the fraction of the abundance of each endmember (cover material) within a pixel (Keshava & Mustard, 2002; Quintano et al., 2012). | Can aid in identifying various materials/cover in each pixel thus enabling the handling of mixed pixels; can be used in combination with other remote sensing methods as a complementary methodology. | Imagery with high variability in complex mixtures may lead to challenging identification of materials within each pixel; some spectral unmixing algorithms may be computationally extensive and expensive. | Beneficial in low spatial resolution imagery data where mixed pixels contain seagrass and macroalgae to get accurate quantification of each class. |
| Spectral Angle Mapper (SAM) | SAM algorithm classifies pixels based on their spectral signatures. It identifies spectral similarity of pixels by calculating the angle | Highly effective for hyperspectral data; no assumption of class distribution required, non-parametric approach. | Sensitive to unbalanced and low training sample size; sensitive to spectral variation due to noise leading to inaccurate classification results; sensitive to mixed pixels and works best on pure | Beneficial where spatial resolution of imagery data allows distinct seagrass and macroalgae pixels with well-defined spectral characteristics. |

between a reference spectrum (end member) and the spectra of the pixel in an image (Richards, 1986; Rossiter et al., 2020).

pixels that represent distinct spectral signature; depending on the size of scene and spatial resolution it may be computationally extensive when working on large datasets; sensitive to changes in lightning conditions and variation in illumination leading to misclassification thus lower accuracy; not suitable for temporal change detection.

Support Vector Machine

A binary classifier that identifies a hyperplane divides the data into two classes, whereby only those that lie on defined margins (support vectors) are used. Its focus is on finding the optimal hyperplane while maximising the margin between classes thus minimising misclassification (Mountrakis et al., 2011; Pal, 2005).

Non-parametric; Can handle complex and high dimensional data e.g., hyperspectral imagery data; insensitive to small sampling data; robust to noise and outliers due to support vectors. SVM can be computationally intense; sensitive to highly imbalanced training samples; parameter tuning can be time extensive and might impact results if chosen inappropriately.

Beneficial for complex intertidal seagrass-macroalgae habitats, which can be complex in their spectral reflectance thus often not conform to normal distribution.

Random Forest (RF)

Ensemble learning method based on decision trees whereby decision trees are combined to make robust predictive models using label training data to create classification maps (Breiman, 2001; Pal, 2005).

Non-parametric; can handle complex and high dimensional data e.g., hyperspectral and multispectral imagery data; provides reliable and robust predictions due to ensemble methodology; insensitive to unbalanced and small sampling data; robust to noise and outliers; well -suited for change detection applications.

While less computationally intensive in comparison to SVM, depending on the data set it may still pose challenges with large memory, especially when dealing with large ensembles or deep trees; hyperparameter tuning needs to be performed carefully to achieve optimal performance and accuracy.

Beneficial for complex intertidal seagrass-macroalgae habitats, which can be complex in their spectral reflectance thus often not conform to normal distribution. Suitable for temporal seagrass mapping and monitoring.

Deep learning

Convolutional Neural Network (CNN) A deep learning method trained to automatically learn and extract spatial data within imagery for remote sensing classification (Kattenborn et al., 2021; Maggiori et al., 2017). Automatic approach thus reduced manual handling; can handle complex and high dimensional data e.g., hyperspectral, and multispectral imagery data.

Requires a large amount of labelled data for effect training; training CNNs can be highly computationally extensive and time consuming and requires access to powerful hardware which may be expensive; does not perform well on small data sets.

If well trained and reliable, automated systems can be highly useful, practical, and cost-effective for intertidal seagrass monitoring.

2.2. Applications of optical remote sensing in seagrass habitats

Use of optical remote sensing for seagrass mapping can be traced back to the late 1970s and early 1980s (Ackleson & Klemas, 1987), and has increased gradually with the advances in remote sensing technology and accessibility, especially in the past decade (Hossain et al., 2015; Veettil et al., 2020; Rowan & Kalacska, 2021). Remote sensing has been applied to better understand seagrass ecology at spatial and temporal scales. Studies have successfully created remote sensing derived seagrass maps to assess distribution and extent in both species diverse (Kovacs et al., 2018; Traganos & Reinartz, 2018) and homogeneous seagrass meadows (Topouzelis et al., 2018). They have measured seagrass densities (Lyons et al., 2011) assess seagrass health by identifying and assessing disease outbreaks and their distributions (Yang et al., 2023); measure seagrass biomass and make productivity assessments (Phinn et al., 2008); describe seagrass growth patterns both seasonally and interannually (Lyons et al., 2013); evaluate the success of various restoration and rehabilitation methods via the creation of pre- and post-habitat maps (Ventura et al., 2022); and finally to assess temporal change of seagrass to evaluate habitat declines or increases (e.g., Traganos et al., 2018; Zoffoli et al., 2021).

Multiple optical remote sensing technologies and methods for seagrass habitat mapping have been applied successfully, but these studies have mostly focused on tropical regions, due to their clear, calm waters (Hossain et al., 2015). Fewer studies are available that have investigated the application of optical remote sensing methods in temperate seagrass habitats. This is mainly due to factors challenging to optical methods, such as water turbidity and cloud cover, which limits the detection of seagrass habitats (Barillé et al., 2010; Armitage et al., 2013; Dierssen et al., 2019). Nevertheless, studies have demonstrated the application of optical remote sensing to assess spatial distribution and spatiotemporal changes in temperate seagrass habitats (Ward et al., 1997; O'Neill & Costa, 2013; Hogrefe et al., 2014; Wilson et al., 2019). These applications have particularly increased in the past decade and more so over the past few years with increasing awareness for the value of seagrass habitats and need for their protection and need for effective management approaches (Table 2.2). In parallel, new and improved platforms with higher spatial, spectral and temporal resolution imagery have been developed using satellite, airborne and UAV techniques, which offer low-cost and increasingly open access spatiotemporal data, that have led to a surge in applications to temperate seagrass mapping and monitoring. However, notably the majority of these studies have been applied to subtidal seagrass environments, with lower numbers of studies in intertidal seagrass. There is a significant lack of studies available for the UK (Table 2.2).

2.3. Application of optical remote sensing in temperate seagrass habitats

Investigation of the potential of remote sensing technologies for temperate seagrass habitat mapping and monitoring began with the utilisation of Landsat imagery in the 1980's when Ackelson and Klemas (1987) showed that two different Landsat sensors (Multispectral Sensor (MSS) and Thematic Mapper (TM) where similarly effective in detecting submerged seagrass habitat in the USA, and some other studies demonstrated the potential of Landsat (TM) for monitoring and change detection (Macleod & Congalton, 1998; Lundén & Gullström, 2003). The utilisation of Landsat satellite imagery has been used especially for baseline and broad scale mapping and long-term series analysis (Hogrefe et al., 2014; Leblanc et al., 2021; Zoffoli et al., 2021), mainly due to its low spatial resolution for accurate mapping but its highly relevant historic data archive since 1972 for long-term change detection. For instance, Leblanc et al. (2021), used Landsat time-series data to evaluate the distribution and abundance of subtidal Zostera marina from 1984 to 1917 elucidating the dynamics in Z. marina habitats in north-eastern New Brunswick, Canada. The benefit of Landsat data lies in its accessibility at no cost which has the potential for cost-effective seagrass mapping and monitoring.

The launch of Sentinel-2 in 2015, provided easy access to satellite imagery with higher spatial resolution (10-20m) and increased revisit time (≤ 5 days) became available at no cost for download and increased the potential for more accurate seagrass habitat mapping and monitoring (Kovacs et al., 2018; Wicaksono et al., 2021). The higher temporal resolution may have advantages for intertidal seagrass, due to the increased probability of capturing seagrass environments at low tide when exposed. This is evident in the surge in applications of Sentinel-2 data to intertidal seagrass mapping (Zoffoli et al., 2021; Haro et al., 2022; Benmokhtar et al., 2023). Other cost-effective satellite imagery that provides higher spatial resolution includes, for example, PlanetScope (3m) with a daily revisit time. To date, this has only been applied in

tropical and Mediterranean seagrass habitats (e.g., Traganos & Reinartz, 2018; Astuty & Wicaksono, 2019; Lee et al., 2023), not in temperate seagrass environments (Table 2.2.). For instance, Wicaksono and Lizuardo (2018) mapped five seagrass species classes with a 74% overall map accuracy, revealing the potential of PlanetScope for a multispecies seagrass environment in the tropics. In temperate environments, such accurate habitat mapping using multispectral satellite imagery, where, seagrass could be segregated from algae, has mainly applied using commercially available imagery to date that consist of higher spatial resolution (e.g., WorldView2; 1.8m spatial resolution) (Wilson et al., 2019).

Although, the ability to discriminate between different vegetative taxa (e.g., *Zostera* spp. and macroalgae) has been proven using higher spectral resolution imagery, studies that have used hyperspectral imagery (satellite and airborne) to map multispecies environments are limited for temperate seagrass (Levings et al., 1999; O'Neill et al., 2011), with only one study available that has used hyperspectral imagery for intertidal seagrass mapping (Garono et al., 2004).

While spectral resolution can help to successfully discriminate between different vegetation types, ultra-high spatial resolution (sub-cm level) imagery can also prove beneficial for accurate and detailed mapping and enable the discrimination at taxonomic levels. Advances in technology and accessibility of Unoccupied Aerial Vehicles (UAVs), which provide very high spatial resolutions, for example, have led to a surge in the use of remote sensing for mapping intertidal seagrass habitats (Table 2.2). UAVs have great potential for intertidal seagrass mapping due to their flexibility in acquiring imagery data in ideal conditions such as at low tide and under cloud cover. One of the earliest studies was conducted by Duffy et al. (2018), that evaluated the application of light weight consumer-grade UAV to map the distribution for a Zostera noltii environment. While this study and following studies by Nahirnick et al. (2019a, b) also highlighted limitations of using UAV in temperate seagrass (e.g., limited in large scale mapping, logistical matters), its applications for mapping and monitoring for intertidal and subtidal temperate seagrass mapping continued to develop. However, applications of UAVs for temperate seagrass began with mainly RGB-cameras to map homogeneous seagrass habitats but transitioned into utilising multispectral camera UAVs in more complex and heterogeneous seagrass habitats, which started to emerge only recently in the early 2020s (Table 2.2.).

Overall, the literature indicates a lack of studies of temperate seagrass habitats across all platforms and sensors. This gap is particularly noted for multispectral satellite and hyperspectral satellite/airborne remote sensing (Table 2.2). Large-scale habitat mapping and monitoring studies are scarce and close to non-existent for intertidal seagrass environments across temperate regions. Moreover, the majority of studies have been conducted in subtidal seagrass in the USA and in Canada (Table 2.2). Some studies have also utilised remote sensing including, Satellite, airborne and UAV imagery in intertidal seagrass environment in southern Europe (e.g., France, Spain, Portugal) (Sousa et al., 2019; James et al., 2020; Haro et al., 2022) and New Zealand (Martin et al., 2020; Chand & Bollard, 2021), but only two studies were found for seagrass habitat around the UK, of which both have used UAV technology (Duffy et al., 2018; Hobley et al., 2021), with no studies available that have used satellite and airborne multispectral and hyperspectral technology for large-scale habitat mapping in UK's coastal waters. Investigating and understanding the potential and limitations of remote sensing applications in UK's intertidal coastal areas is critical, as methods from other temperate regions may not be suitable and comparable. Mainly, due to differences in biological, environmental, and physical properties such as, benthic substrate and species composition, e.g., different vegetation taxa have different reflectance spectra. Additionally, weather patterns may be different in coastal regions in the UK, which are commonly prone to high cloud cover and frequent precipitation throughout the year (Bergsma & Almar, 2020), in comparison to, for example southern Europe and New Zealand. Although there is a growing recognition in the application of remote sensing for seagrass management and conservation in the UK (Duffy et al., 2018; Hobley et al., 2021; Unsworth et al., 2022), robust and effective monitoring programmes that utilise remote sensing are still lacking significantly, both at local and national levels (Table 2.2). Efforts to address the potential, challenges, and improvements of remote sensing application in UKs seagrass habitats may support and initiate effective management practices and programmes.

Table 2.2. A summary of available studies that have used optical remote sensing applications in temperate seagrass habitats. S=Subtidal, I=Intertidal.

| | Year | Location | Platform and Sensor | Application | Species | Methods | Reference |
|-----------------|------|------------------|--|--|--|---|------------------------------|
| | 1987 | USA | Landsat MSS and TM | Detection of submerged aquatic vegetation (SAV) | Z. marina (S) | Unsupervised clustering algorithm: CLUSTER (within ERDAS) | (Ackleson & Klemas, 1987) |
| | 1998 | USA | Landsat TM | Temporal mapping | Z. marina (S) | ISODAT & Maximum Likelihood | (Macleod & Congalton, 1998) |
| | 2003 | Sweden | Landsat TM | Temporal mapping | Z. marina (S) | Discussed in (Baden et al., 2003) | (Lundén & Gullström, 2003) |
| | 2003 | Sweden | Polygon boundaries | Temporal mapping | Z. marina (S) | Polygon boundaries using GPS | (Baden et al., 2003) |
| - Multispectral | 2014 | Canada | WorldView2 | Mapping the distribution of SAV | Z. marina; green algae (Ulva spp.); brown algae (Fucus spp.) (S) | Maximum Likelihood | (Reshitnyk et al., 2014) |
| ltispe | 2014 | USA | Landsat TM & ETM+ | Spatial extent and distribution mapping; baseline mapping | Z. marina (S) | Maximum Likelihood | (Hogrefe et al., 2014) |
| | 2015 | Korea | Landsat TM and ETM; Aster; Spot 4; Kompsat-2 | Temporal mapping | Z. marina (S) | Mahalanobis Distance | (K. Kim et al., 2015) |
| Satellite | 2019 | Canada | SPOT 6/7 | Spatial extent and distribution mapping | Z. marina (S); seaweed (S, I) | ISOCLUST; Maximum Likelihood | (K. L. Wilson et al., 2019) |
| Sat | 2020 | Canada | WorldView2 | Spatial extent mapping; presence/absence | Z. marina (S) | Maximum Likelihood; Random Forest | (Forsey et al., 2020) |
| | 2020 | Germany | Aerial Photography; Sentinel-2; Landsat OLI | Spatial density mapping; temporal mapping | Z.noltei (I) | Decision trees | (Kohlus et al., 2020) |
| | 2020 | France &Spain | Sentinel-2 | Percent cover and biomass mapping; temporal mapping (seasonal) | Z. noltei (I) | - | (Zoffoli et al., 2020) |
| | 2021 | Estonia | CASI and Sentinel-2 | Percent cover and biomass mapping | Z. marina; green algae; brown algae (S) | Spectral Angle Mapper | (Vahtmäe et al., 2021) |

| | 2021 | France | Landsat TM & TM+; SPOT1-5; Sentinel-2 | Temporal mapping | Z. noltii (I) | NA? | (Zoffoli et al., 2021) |
|--------------------------|------|------------|---|--|--|---|-----------------------------|
| | 2021 | Canada | Landsat TM & ETM+; 8-OLI | Temporal mapping | Z. marina (S) | Automatic Adaptive Signature Generalization | (Leblanc et al., 2021) |
| | 2022 | Spain | Sentinel-2 | Temporal biomass mapping; | Zostera sp.; Caulerpa sp.; green algae (I) | Random Forest | (Haro et al., 2022) |
| | 2023 | Morocco | Sentinel-2; Orthophotography mosaics | Temporal mapping | Z. noltei; algae (I) | OBIA; Random Forest | (Benmokhtar et al., 2023) |
| | 2023 | Greenland | Sentinel-2 | Spatial extent and distribution mapping | Z. marina; algae (Ascophyllum nodosum, and Fucus spp); Kelp (Saccharina latissima and Agarum clathratum) (S) | NDVI | (Carlson et al., 2023) |
| ਰ | 1999 | Canada | CASI | Spatial extent and distribution mapping | Z. marina; algae (S) | Polygon boundaries | (Levings et al., 1999) |
| pectr | 2004 | USA | CASI | Spatial extent and distribution mapping | Z. marina; green algae; brown algae (I) | ISODTA; Maximum Likelihood | (Garono et al., 2004) |
| Airborne - Hyperspectral | 2011 | Canada | AISA | In situ hyperspectral measurement of spectral characteristics; Spatial extent and distribution mapping | Z. marina; green algae (Ulva fenestra and Enteromorpha spp.) (S) | Maximum Likelihood | (O'Neill et al., 2011) |
| ne - I | 2013 | Canada | AISA; IKONOS | Spatial extent and distribution mapping | Z. marina (S) | Maximum Likelihood | (O'Neill & Costa, 2013) |
| Airbor | 2021 | Finland | CASI; Sentinel-2 | Spatial extent and distribution mapping | Z. marina; brown algae; green algae (S) | Minimum Distance; Spectral Angle Mapper | (Vahtmäe et al., 2021) |
| | 2006 | USA | Aerial Digital Camera: RGB- NIR | Spatial extent and distribution mapping | Z. marina, Ruppia marítima; algae (Ulva lactuca) (S) | Image segmentation/object- oriented | (Lathrop et al., 2006) |
| | 2016 | USA | Fixed-Wing: RGB | Spatial extent and distribution mapping | Z. marina, Halodule wrightii, Ruppia maritima (S) | Linear Spectral Unmixing | (Uhrin & Townsend, 2016) |
| 74 | 2018 | UK (Wales) | UAV: RGB | Spatial extent and distribution mapping | Z. noltii (I) | K-means clustering; Support Vector machine; Object-Based Image Analysis | (Duffy et al., 2018) |

| 2019 | Canada | UAV: RGB | Spatial extent and distribution mapping | Z. marina (S) | Object-Based Image Analysis | (Nahirnick et al., 2019b) |
|------|---|--|--|--|--|---------------------------|
| 2019 | Canada | UAV: RGB | Spatial extent and distribution mapping | Z. marina (S) | Object-Based Image Analysis | (Nahirnick, et al., 2019a |
| 2019 | Portugal | UAV: RGB | Spatial extent and distribution mapping; temporal mapping | Z. noltei (I) | Polygons created from mosaics and areal extend calculated in ArcGIS | (Sousa et al., 2019) |
| 2020 | New Zealand | UAV: RGB-RE- NIR | Temporal mapping (seasonal) | Z. mulleri (I) | Random Forest | (Martin et al., 2020) |
| 2020 | France | UAV: RGB; RGB- RE-NIR | Spatial extent and distribution mapping | Z. marina; algae (I) | Maximum Likelihood | (James et al., 2020) |
| 2021 | UK, Northumberl and, Lindisfarne | UAV: RGB; RGB- RE-NIR | Spatial extent and distribution mapping | Z. noltii, Z. angustifolia; algae (I) | Fully Convolution Neural Network (FCNN); Object-Based Image Analysis | (Hobley et al., 2021) |
| 2021 | Canada | UAV: RGB-RE- NIR; Sentinel-2 | Spatial extent and distribution mapping | Z. marina; algae (S) | Random Forest | (Gallant et al., 2021) |
| 2021 | New Zealand | UAV: RGB-RE- NIR | Spatial extent and distribution mapping | Z. mulleri (I) | Maximum Likelihood; Object- Based Image Analysis | (Chand & Bollard, 2021) |
| 2021 | Spain | UAV: 10 spectral bands | Spatial extent and distribution mapping | Z. noltei, Cymodocea nodosa; algae (Ulva sp.); saltmarsh (Spartina maritima) (S, I) | Maximum Likelihood; Minimum Distance; Spectral Angle Classifier | (Román et al., 2021) |
| 2021 | Japan | UAV: RGB | Spatial extent and distribution mapping; temporal mapping (seasonal) | Z. marina, Z. caulescens, and Z. japonica (S, I) | Feature Pyramid Network (FPN) | (Chen & Sasaki, 2021) |
| 2022 | Canada | UAV RGB-RE- NIR & 10 spectral bands) | Spatial extent and distribution mapping | Z. marina (S) | Random Forest | (Leblon et al., 2022) |
| 2022 | Denmark | UAV: RGB | Spatial extent and distribution mapping; temporal mapping | Z. marina; algae (F. vesculosus) (S) | Object-Based Image Analysis; Support vector Machine | (Svane et al., 2022) |
| 2023 | USA & Canada | UAV: RGB; RGB- RE-NIR | Detection and spatial distribution mapping of disease | Z. marina (S) | Object oriented image segmentation | (Yang et al., 2023) |
| 2023 | Canada | UAV: RGB | Spatial extent and distribution mapping; temporal mapping (seasonal) | Z. marina; macroalgae (S) | Random Forest | (Prystay et al., 2023) |

Chapter 3: Evaluating multispectral UAV imagery for mapping a multispecies intertidal seagrass environment

3.1. Introduction

In recent years Unoccupied Aerial Vehicles (UAV) have gained increased attention for application in seagrass habitat mapping and monitoring (e.g., Ventura et al., 2018; Yang et al., 2020; Price et al., 2022). Their utilisation has been successful in intertidal (Duffy et al., 2018; Yang et al., 2023) and subtidal (Nahirnick et al., 2019a,b; Prystay et al., 2023) seagrass environments, since they offer affordable ways of acquiring very high resolution images and fill important gaps in remote sensing capability in temporally dynamic and complex environments with a potential to revolutionise the toolbox of coastal managers (Doukari et al., 2021; Bremner et al., 2023).

Specific benefits of UAVs in comparison to other optical remote sensing technology (e.g. satellite imagery) for monitoring programmes include: (1) very high spatial resolution, which increases ability to capture detailed features in imagery permitting identification of seagrass species and other benthic organisms (Duffy et al., 2018; James et al., 2020); (2) control of temporal resolution as appropriate weather conditions for image acquisitions can be chosen; (3) coverage of areas inaccessible on the ground; (4) relatively small, portable and user-friendly; (5) customised and repeatable flight planning is possible as flight paths can be saved making data acquisition reproducible to enable repetitive inventories, relevant to monitoring programmes (Nahirnick et al., 2019a,b). To effectively map and monitor seagrass environments that contain multiple vegetation taxa with similar spectral properties (i.e., *Zostera* spp. and green macroalgae), higher spectral resolution sensors are required. Such sensors may enable discrimination and permit accurate habitat mapping (Davies et al., 2023).

The vulnerability of different seagrass species to threats, and their response to environmental changes can be different, such as varying tolerance thresholds to temperature fluctuations and nutrient levels, impacting survival to varying degrees (Massa et al., 2009; Grech et al., 2012; La Nafie et al., 2012; Kaldy, 2014). Additionally, seagrass species may differ in their provision of ecosystem services and functioning such as, for example, efficiency in carbon storage (Postlethwaite et al., 2018; Sousa et al., 2019), their suitability as a habitat for many threatened seagrass dependent

species and commercially important fish species (Hughes et al., 2009; Bertelli & Unsworth, 2014). The accurate identification of seagrass and spatial distribution at species level is imperative to coastal managers for informed decision-making in prioritising areas of protection. It will enable effective consideration of the vulnerability of seagrass species to threats and decline to achieve species-specific targeted management and conservation goals (Wilson et al., 2005).

In temperate seagrass meadows, most studies to date have used consumer grade UAVs with either limited spectral resolutions, for example, simple red-green-blue (RGB) or 5-band multispectral cameras (RGB, red edge, near infrared). These have mapped monospecific seagrass habitats, with a focus successfully presence/absence and/or density of seagrass cover (Duffy et al., 2018; Martin et al., 2020; Chand & Bollard, 2021; Svane et al., 2022), but few have disaggregated more complex vegetative habitats (for example, Hobley et al., 2021). Although some studies have also used multispectral UAV cameras to discriminate between vegetation taxa (i.e., seagrass and macroalgae) in temperate intertidal areas, these have limitations. For example, Román et al. (2021) used a MicaSense RedEdge-MX dual 10-band multispectral camera to map the only presence of Zostera noltii in the intertidal area, and the seagrass species Cymodocea nodosa and green macroalgae in the subtidal area (submerged), but not to distinguish co-occurring and mixed seagrass species. In contrast, Hobley et al. (2021), used a MicaSense RedEdge 3 multispectral camera, and successfully mapped and discriminated algal species in a multispecies intertidal seagrass environment, but no discrimination was made between seagrass species. In addition, available studies have used computationally intensive analysis (e.g., Deep Learning; Hobley et al., 2021), or required a high number of spectral bands (up to 10) to achieve accurate map outputs (Román et al., 2021). This requires cameras that need to be custom mounted on the UAV, increasing operational costs. With improving UAV technology, affordable off-the-shelf consumer grade UAVs that are equipped with multispectral cameras have recently become available, which may simplify logistics and analysis, and support management actions. However, their application and efficacy in mapping complex heterogeneous intertidal seagrass environments still require testing, to develop a foundation and guidelines for coastal managers.

This Chapter aims at using an off-the shelf consumer grade multispectral camera UAV (Phantom 4 RTK multispectral), to create habitat maps of highly mixed and complex intertidal multispecies seagrass environment exposed at low tide. Objectives were: (1)

To use Maximum Likelihood classification method and evaluate the ability of a 5-band (RGB, red edge, near infrared) multispectral UAV to discriminate between *Zostera* spp. (*Zostera noltii* and *Zostera marina*, respectively) and macroalgae on three transects with varying benthic community composition and compare to detailed field surveys; (2) To compare accuracy of classification using multispectral and RGB-only data, with a view to assessing the operational need for multispectral imagery for seagrass mapping; (3) To discuss field logistics and the operational potential of UAV utilisation for intertidal seagrass habitat monitoring, with a view to moving such methods towards operational use.

3.2. Methods and Materials

3.2.1. Study site

The study was performed in the Causeway area within the Lindisfarne National Nature Reserve (LNNR) (Figure 3.1). The field site is an intertidal mudflat and sandflat, which is exposed during low tide and consists of sparse to dense *Zostera* spp. habitats. Two seagrass species, *Zostera noltii* and *Zostera marina* were present in the field. *Z. noltii* is the dominant species and can form large dense meadows across the site. Other benthic substrates such as sand, lugwormcasts and a mixed complex of green opportunistic macroalgae (macroalgae hereafter) were also present.

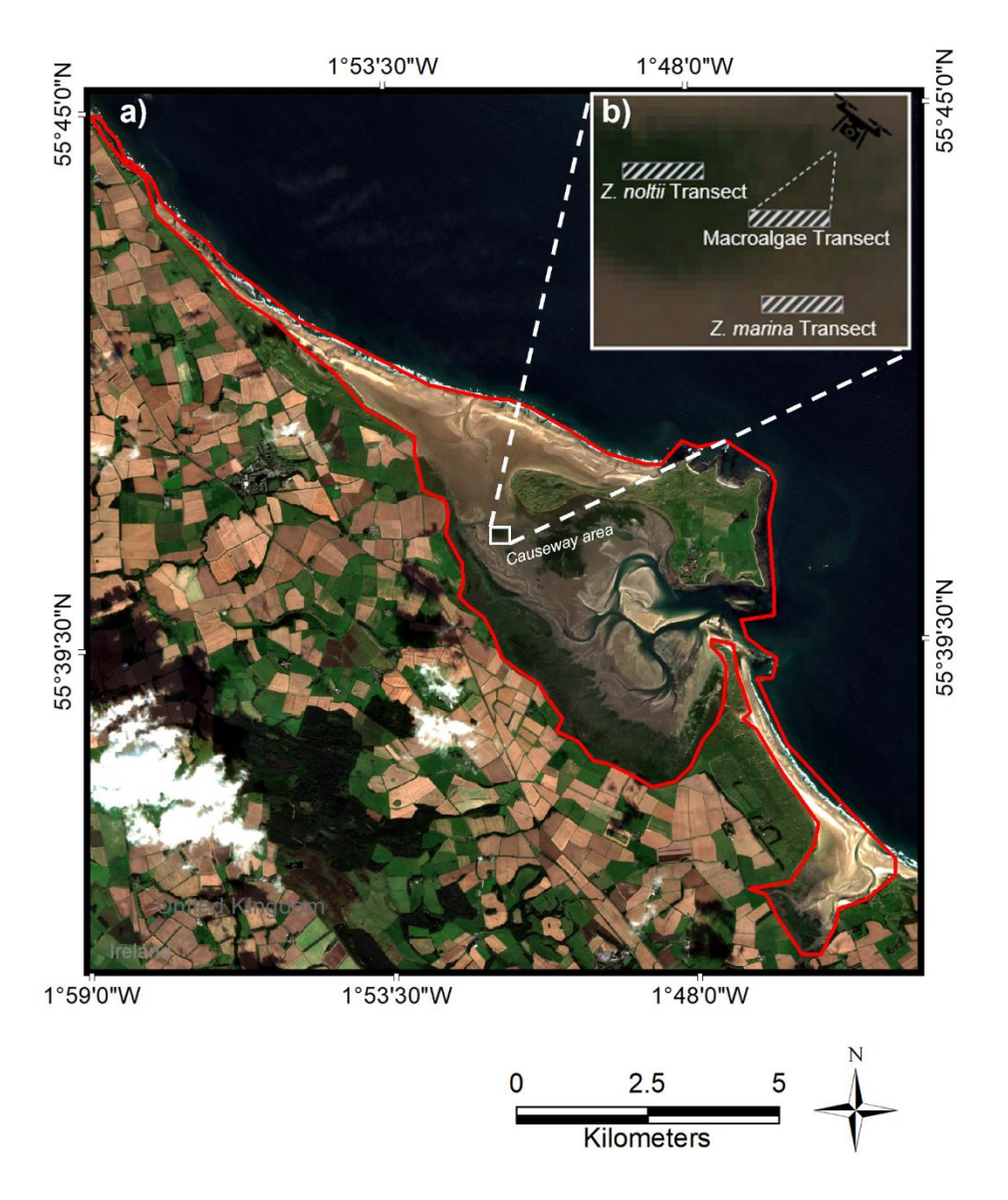


Figure 3.1. a) Map showing LNNR (red boundary outline) indicating the field survey area (white square) in the Causeway area and b) the flight transects surveyed in this study.

3.2.2. Equipment specifications

A DJI Phantom 4 Multispectral Real-Time Kinematic (RTK) UAV was used to perform flight missions. The UAV has a camera attached that consists of five in-built 1/1.29" CMOS monochrome sensors with an image size of 1600×1300 pixels (2.02 MP) including the following bands: blue (B: $450 \text{ nm} \pm 16 \text{ nm}$), green (G: $560 \text{ nm} \pm 16 \text{ nm}$), red (R: $650 \text{ nm} \pm 16 \text{ nm}$), red edge (RE: $730 \text{ nm} \pm 16 \text{ nm}$), and near infrared (NIR: $840 \text{ nm} \pm 26 \text{ nm}$). The aircraft includes a spectral sunlight sensor to detect the solar irradiance, which allows reflectance calibration of images. Flight planning was conducted using the DJI Ground Station Pro app (v. 2.0.16) that enabled prepreparation of flight settings. A Labsphere SRT-99-100 Spectralon Diffuse Reflectance

Target calibration reflectance panel was used for radiometric calibration. The panel was calibrated, and the data provided by the Natural Environment Research Council Field Spectroscopy Facility (NERC FSF). Prior to flights, images of the reflectance panel were taken with the UAV camera. These images were then used in the imagery pre-processing stage.

3.2.3. UAV and ground-truth survey

Flight missions were conducted around seagrass peak biomass on 24th August 2021, during exposed low tide, to minimise the effect of surface water. Three 100m x 20m transects (2.000 m²) were surveyed, with each survey taking approximately 19 minutes flight time. Images were captured at 10m altitude with a 5.4mm/pixel spatial resolution, using a 70% side- and fore overlap, at an equal distance interval, within the 2D mode. An off-nadir angle, with a gimbal pitch of - 80° was used. The Geographic position of the camera was established using the fitted RTK GNSS corrected against a DJI D-RTK 2 base station service. The location of each transect was selected based on species coverage and composition to capture widespread heterogeneous vegetated areas. Transects constituting the three different dominant vegetation types were then surveyed: *Zostera noltii* dominated (55°40'39"N 1°51'29"W), *Zostera marina* dominated (55°40'34"N 1°51'19"W), and macroalgae dominated (55°40'37"N 1°51'21"W) (*Zostera noltii* transect, *Zostera marina* transect and Macroalgae transect, hereafter).

To train and validate UAV images, photographs of 1m² ground quadrats were taken immediately on the ground after flight missions. In total, 20 quadrat photographs were taken at predefined regular intervals every 10 metres across two rows within the flight transect, resulting in a total number of 60 quadrats across all transects (Figure 3.2a). The Google Pro app was used to locate approximate location of the pre-defined quadrats sampling points in the field. To enable geo location of quadrats for the purpose of georeferencing in the analysis stage, GPS positions of the north and south corner of each quadrat were taken using a Trimble Catalyst receiver with the Trimble Network RTK Precision service (± 0.2 cm accuracy) (Figure 3.2b).

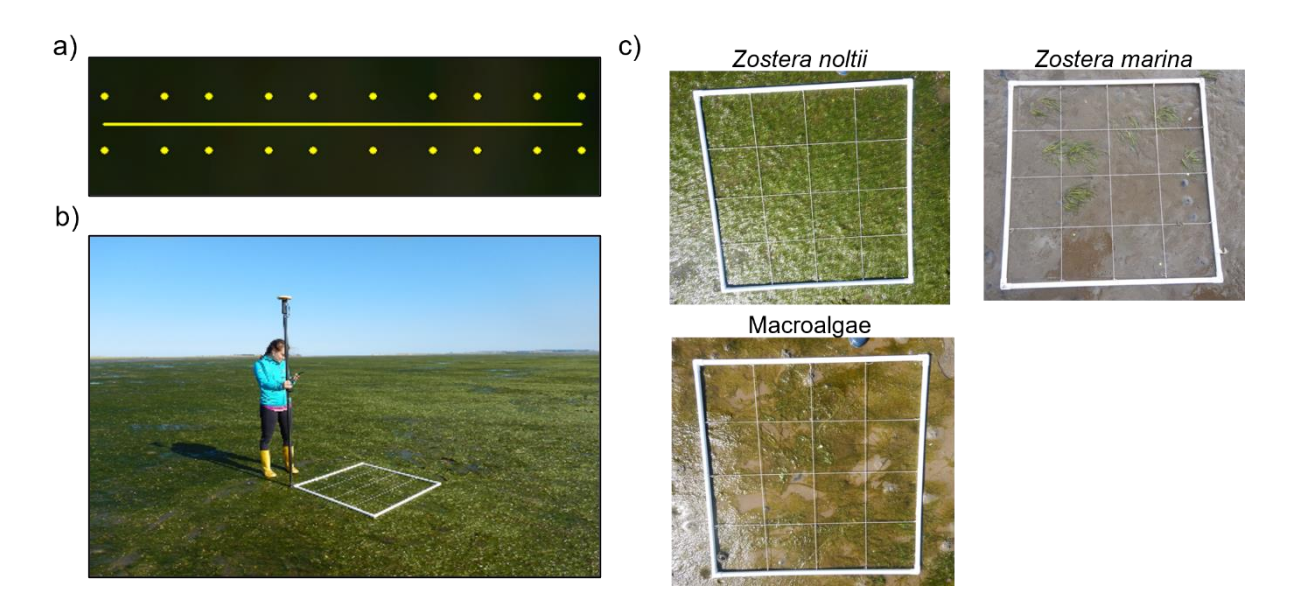


Figure 3.2. a) Flight transect showing the pre-defined regular points for photo quadrats (n=20) across a flight transect. b) Image showing the quadrat and a Trimble receiver to record the northern corner of the quadrat sample. c) Photographs of a *Zostera noltii*, *Zostera marina* and Macroalgae dominated quadrats.

3.2.4. Image pre-processing

Agisoft Metashape (v. 1.7.3) was used to create orthomosaics using TIFF files acquired by the UAV. Prior to processing, the quality of images was checked. The image quality assessment is scaled between 0-1 (unitless), whereby the quality assessment value of 1 corresponds to the highest possible image quality. Images were considered based on an image quality value of > 0.5, to facilitate the removal of blurred imagery (Agisoft, 2021; Over et al., 2021). To calibrate reflectance, panel calibration data provided by NERC Field Spectroscopy Facility (FSF) was resampled to the sensor spectral bands by assigning calibrated reflectance to the five band wavelengths of UAV images using the Calibrate Reflectance tool. Prior to conducting the reflectance calibration, calibration images were masked so that only the reflectance panel area was marked. Sun sensor data was also used within the calibration to account for the sun's position and irradiance and improve the accuracy of the reflectance calibration process. Photo alignment and sparse cloud generation were performed using, i) the highest accuracy setting, ii) a key point limit of 40.000, and iii) a zero-tie point limit. Afterwards low-quality tie points within the generated sparse cloud point were selected and removed by filtering by reconstruction uncertainty, projection uncertainty and projection error. Error was reduced by iteratively selecting and deleting points and re-optimizing the camera after each removal. This procedure was performed manually until the self-reported

standard error of unit weight (SEUW) was close to 1 (Over et al., 2021). Afterwards, a dense cloud was created, which was followed by the generation of a Digital Elevation Model (DEM). The DEM was used to create an orthomosaic consisting of reflectance values for each individual band, whereby pixel values were normalised ranging from 0-1 (Chand and Bollard, 2021).

3.2.5. Training data and image classification

Quadrat photographs were aligned with the orthomosaic, using ArcGIS (v.10.6.1) to aid in the assignment of habitat classes. Afterwards, based on visual assessment of photo quadrats, Regions of Interest (ROIs/pixels) were created randomly within each quadrat area, using ENVI (v.5.6.2). Where certain benthic classes were not found sufficiently within the quadrat sampling areas, random samples were created outside of the quadrat. Pixels were assigned to the following benthic classes: Zostera noltii, Zostera marina, macroalgae, bare ground, lugwormcasts, decomposing vegetation, anoxic sediment, shadow (i.e., from leaves or part of lugwormcasts), sunglint, and shells (Figure 3.3). The primary interest of this study was in mapping the vegetation species. Therefore, benthic substrates other than vegetation (i.e., bare ground, lugwormcasts, decomposing vegetation, anoxic sediment, shadow, sunglint, and shells) were compiled into two classes with similar spectral reflectance. Anoxic sediment, shadow, and dark areas within the decomposing vegetation substrate were compiled into the class, dark material/shadow, respectively. Sunglint, shells and white areas within the decomposing vegetation substrate were compiled into the class, sunglint/shells, respectively (Figure 3.3 e-h). This resulted in a total of six benthic classes: Zostera noltii, Zostera marina, macroalgae, bare ground, dark material/shadow, sunglint/shells. The data were then split into two sets of 50% for each: 50% for training the classification algorithm, and the remaining 50% for validation of classified map output.

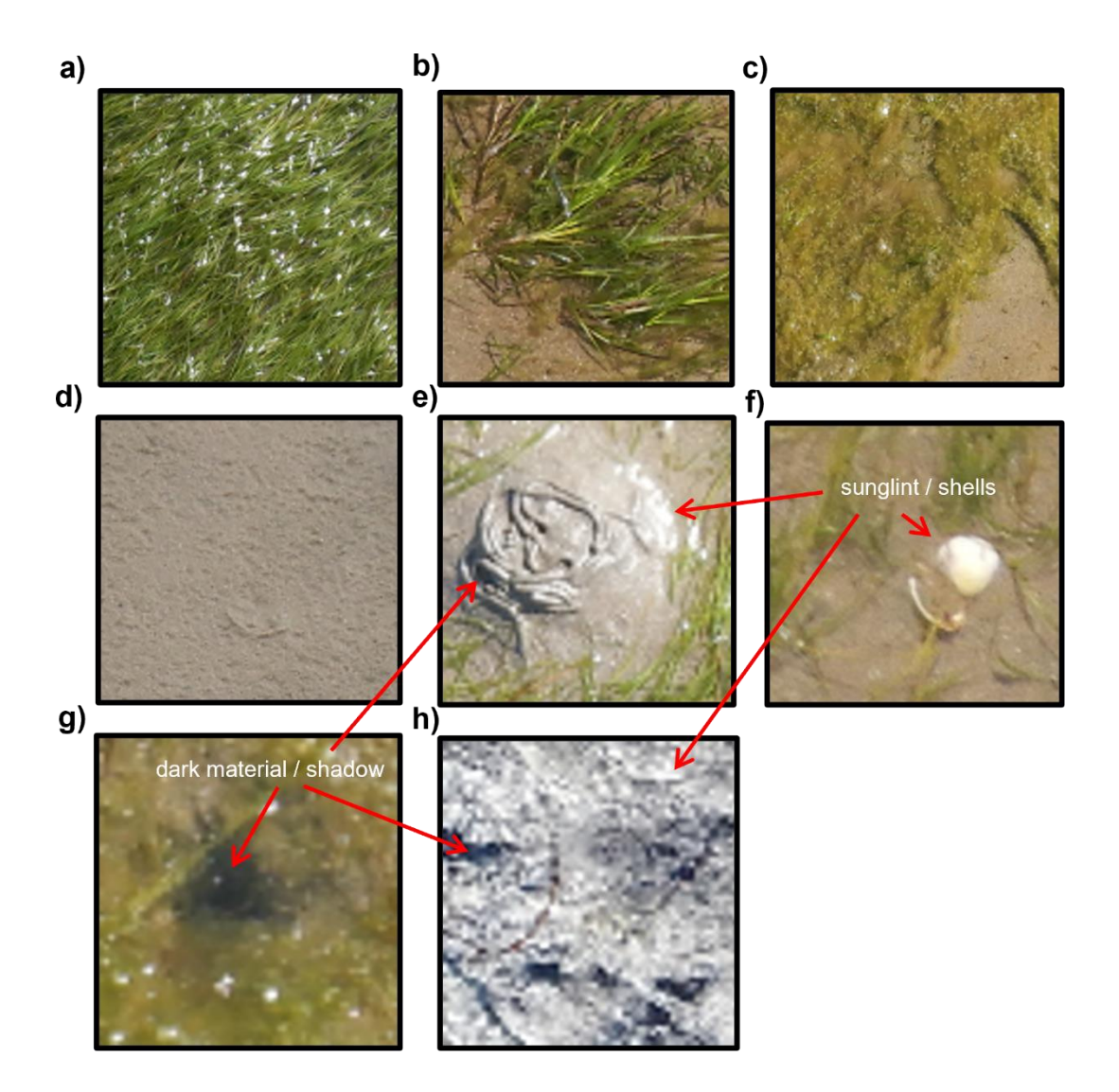


Figure 3.3. Images of benthic substrates initially identified in quadrat photographs before aggregation benthic classes in further analysis. a) *Zostera noltii*, b) *Zostera marina*, c) macroalgae, d) bare ground, e) lugwormcasts, f) shells, g) anoxic sediment h) decomposing vegetation. Arrows highlight examples of categories including dark material/shadow and sunglint/shells.

The Jeffries-Matusita (J-M) distance measure, a widely used measure for spectral discrimination of vegetation types (Schmidt & Skidmore, 2003), was applied to assess the statistical separation between created ground-truth classes (Richards, 2013). The index value ranges between 0 and 2, whereby a 0 value indicates a complete overlap of spectral signatures and a value of 2 a complete separation of spectral signatures between two classes. To evaluate the strength of separation between classes, the following values were used: poor (0.0 < x < 1.0), moderate (1.0 < x < 1.9), good separability (1.9 < x < 2.0) (ENVI, 2022).

The Maximum Likelihood Classifier (MLC), a supervised pixel-based classification method, whereby spectral information of pixels is used to assign pixels to habitat classes, was used for benthic habitat classification. The classifier is based on the assumption that each training class follows a normal distribution. It considers the mean and covariance of the training class signature when assigning pixels to each class. The selection of this classifier was based on the dataset meeting normality assumptions and its proven success and reliability of application in seagrass habitats often outperforming other classifiers (e.g., Román et al., 2021). MLC is also widely available as a classifier in multiple commercial and open source geospatial and image processing software, increasing its availability for operational applications. To evaluate the operational need for accurate multi species habitat mapping, a comparison of the accuracy classification between an RGB and multispectral imagery was made. Here, the MLCs were trained on three bands (RGB) and five bands (RGB, red edge, near infrared), for each transect separately.

3.2.6. Accuracy assessment

A confusion matrix was generated to assess the accuracy of the classified habitat maps. The Overall Accuracy (OA) gives information about the percentage of the total number of pixels contained within the ground truth area that have been correctly classified by the classification. User,s(UA) and producer's accuracy (PA) then permits the assessment of the accuracy of each individual class. The confusion matrix outputs will be used to identify the nature of misclassifications between habitat classes.

3.3. Results

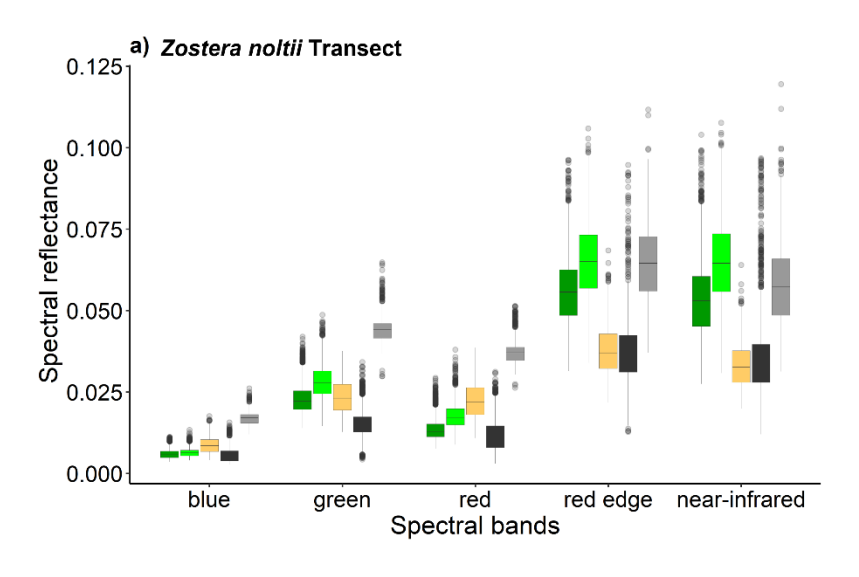
3.3.1. Training data separability

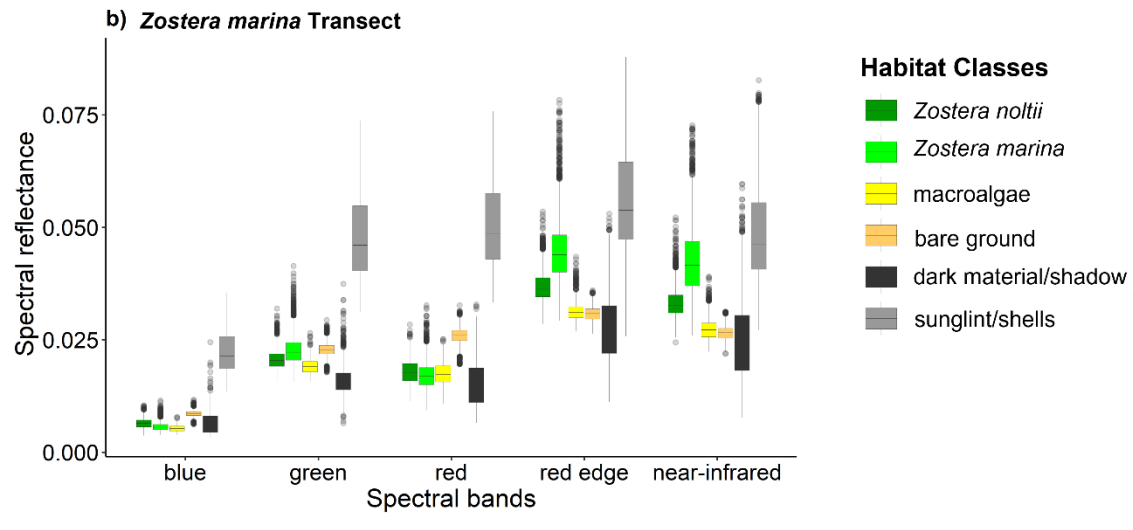
While spectral separation between all recorded benthic substrates was least within the blue band, benthic classes including bare ground, sunglint/shells, and dark matter/ shadow appeared to be separable from vegetation across nearly all bands. However, the multispectral sensor showed least separability between *Zostera noltii*, *Zostera marina* and macroalgae across the red-green-blue (RGB) bands, and a distinct separation between these vegetation types within the red edge (RE) and near infrared (NIR) bands (Figure 3.4). When considering all spectral bands to investigate spectral

separability of the training data of benthic classes, Jeffries-Matusita's separability values indicated the lowest pair separation between the two seagrass species, *Zostera noltii* and *Zostera marina*, among all vegetation species, for all three transects (Table 3.1). Respectively, the *Z. noltii* and *Z. marina* transects showed lower separability (J-M value: 0.9 and 1.0, respectively), compared to the Macroalgae transect (J-M value: 1.3). Where macroalgae was present in the image, i.e., *Z. marina* transect and Macroalgae transect, results indicated a moderate pair separation between the two seagrass species and macroalgae (J-M value: ranging between 1.4 and 1.7). All pairwise separation values between the vegetation species and the other benthic categories indicated a moderate to good separability (Table 3.1).

Table 3.1. Results of Jeffries – Matusita index, indicating spectral pair separability of benthic classes for: *Zostera noltii* transect, *Zostera marina* transect, and Macroalgae transect. Where a class was not present in a transect to conduct pair separability, these were marked with NA = not available.

| Benthic pair c | elasses | Z. noltii transect | Z. marina transect | Macroalgae transect |
|------------------------------|---|-----------------------|-----------------------|------------------------|
| Z. noltii | Z. marinamacroalgaemacroalgae | 0.9 | 1 | 1.3 |
| Z. noltii | | NA | 1.7 | 1.4 |
| Z. marina | | NA | 1.6 | 1.7 |
| Z. noltii | dark material/shadowdark material/shadow | 1.4 | 1.7 | 1.7 |
| macroalgae | | NA | 1.8 | 1.9 |
| bare ground Z. marina | dark material/shadowdark material/shadow | 1.5 1.6 | 1.9 1.9 | 2 |
| bare ground <i>Z. noltii</i> | sunglint/shellsbare ground | 1.8 1.8 | 2 2 | 2 2 |
| Z. marina | bare groundsunglint/shells | 1.9 | 2 | 2 |
| Z. marina | | 1.9 | 2 | 2 |
| sunglint/shells Z. noltii | dark material/shadowsunglint/shells | 1.9 2 | 1.9 2 | 2 2 |
| macroalgae | bare groundsunglint/shells | NA | 2 | 2 |
| macroalgae | | NA | 2 | 2 |





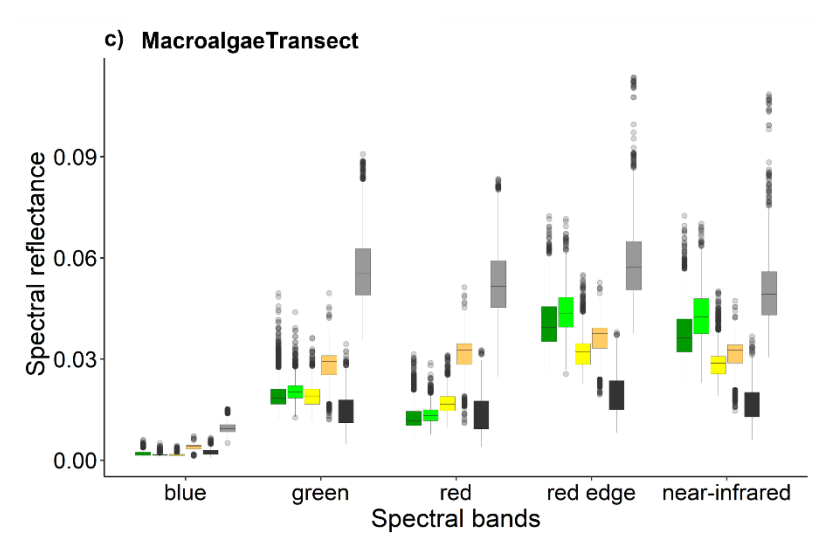


Figure 3.4. Spectral signatures of generated training data including all benthic classes across the multispectral bands for a) *Zostera noltii* transect b) *Zostera marina* transect, and c) Macroalgae transect. Boxplots show the median value (horizontal line), the interquartile range representing the dispersion of the data (size of the box), the upper and lower quartiles, and outliers.

3.3.2. Maximum-likelihood classification and accuracy assessment

Using the Maximum Likelihood Classifier, detailed benthic maps were produced with very high Overall Accuracy (OA) when considering all five spectral bands (multispectral image) in comparison to RGB only bands (Figure 3.5). The lowest accuracy was found for the *Z. noltii* transect classified map with an OA of 84% for the multispectral image, and 57% OA for the RGB image. The Z. marina transect and the Macroalgae transect maps indicated very high OA for the multispectral image (91% and 89%, respectively) and lower OA for the RGB image (63% and 72%, respectively) (Table 3.2). Considering the multispectral images only, class level accuracy for each transect map indicated a general pattern of lower Producer's Accuracy (PA) and User's Accuracy (UA) for all vegetation classes (Z. noltii, Z. marina and Macroalgae, respectively) in comparison to non-vegetation classes (bare ground, sunglint/shells, material/shadow, respectively). Vegetation classes indicated PA and UA ranging between 73% and 99%, and non-vegetation classes indicated PA and UA ranging between 79% and 100% in all transect maps (Table 3.2), except for distinctly lower UA values for the macroalgae class (UA 54%) in the Z. marina transect map, which may be due to small sample size because of its sparse representation in the studied transect area, and PA for dark material/shadows (64%) in the Z. noltii transect map, due to small validation sample size.

Similar to J-M results for training data, the post-classification accuracy assessment results indicated notably higher misclassification among vegetation classes in comparison to all other benthic classes, across all classified transect maps. The largest misclassification among habitat classes was found between *Z. noltii* and *Z. marina*. In the *Z. noltii* transect, 24.7% proportion of sampled pixels of *Z. noltii* were incorrectly classified as *Z. marina* class, and 6.7% of the class *Z. marina* were incorrectly classified as *Z. noltii*. The *Z. marina* transect indicated a lower misclassification of sampled pixels of *Z. noltii* as *Z. marina* (13% proportion of sampled pixels), and only 2% of *Z. marina* pixels were incorrectly classified as *Z. noltii* class. Finally, Macroalgae transect indicated 14.8% of sampled pixels of *Z. noltii* as *Z. marina* and similarly, 14.7% of *Z. marina* pixels were incorrectly classified as *Z. noltii*. Misclassification between macroalgae and *Zostera* spp. was notably lower in transects where macroalgae was present (*Z. marina* transect and Macroalgae transect, respectively). In both transects, between 4% to 9% of macroalgae pixels were incorrectly classified as *Z. noltii* or *Z. marina*, whereas up to 10% of *Z. noltii* pixels and 2% *Z. marina* pixels were incorrectly

classified as macroalgae. Other notable misclassification was found between *Z. noltii* and dark material/shadow with 28% of *Z. noltii* pixels incorrectly classed as dark material/shadow within the *Z. noltii* transect. All other benthic class combinations across all transect maps showed low misclassification cover ranging between 0 and 7.5%.

Table 3.2. Post-classification analysis showing the accuracy assessment outputs of the Maximum-likelihood classification map for a) the multispectral image and b) the RGB image.

| a) | Zostera noltii transect 84 % | | Zostera marina transect 91 % | | Macroalgae transect 89% | |
|---|------------------------------------|---------------------------|------------------------------------|---------------------------|-------------------------------|---------------------------|
| Overall Accuracy (OA) | | | | | | |
| Habitat classes | Producer's Accuracy (%) | User's Accuracy (%) | Producer's Accuracy (%) | User's Accuracy (%) | Producer's Accuracy (%) | User's Accuracy (%) |
| Zostera noltii | 90 | 80 | 84 | 85 | 76 | 80 |
| Zostera marina Macroalgae bare ground dark material/shadow | 73 - 90 64 | 84 - 92 79 | 82 87 100 92 | 87 54 99 99 | 80 99 100 90 | 73 91 98 96 |
| sunglint/shells | 95 | 84 | 99 | 97 | 100 | 93 |
| b) | Zostera trans | | | n marina sect | Macro- trans | |
| Overall Accuracy (OA) | 57 | % | 63 | 3% | 729 | % |
| Habitat classes | Producer's Accuracy (%) | User's Accuracy (%) | Producer's Accuracy (%) | User's Accuracy (%) | Producer's Accuracy (%) | User's Accuracy (%) |
| Zostera noltii | 61 | 68 | 56 | 61 | 40 | 56 |
| Zostera marina Macroalgae bare ground dark material/shadow | 37 - 86 33 | 54 - 55 46 | 57 37 77 68 | 68 9 72 86 | 54 59 93 81 | 65 71 70 76 |
| sunglint/shells | 67 | 39 | 69 | 87 | 94 | 85 |

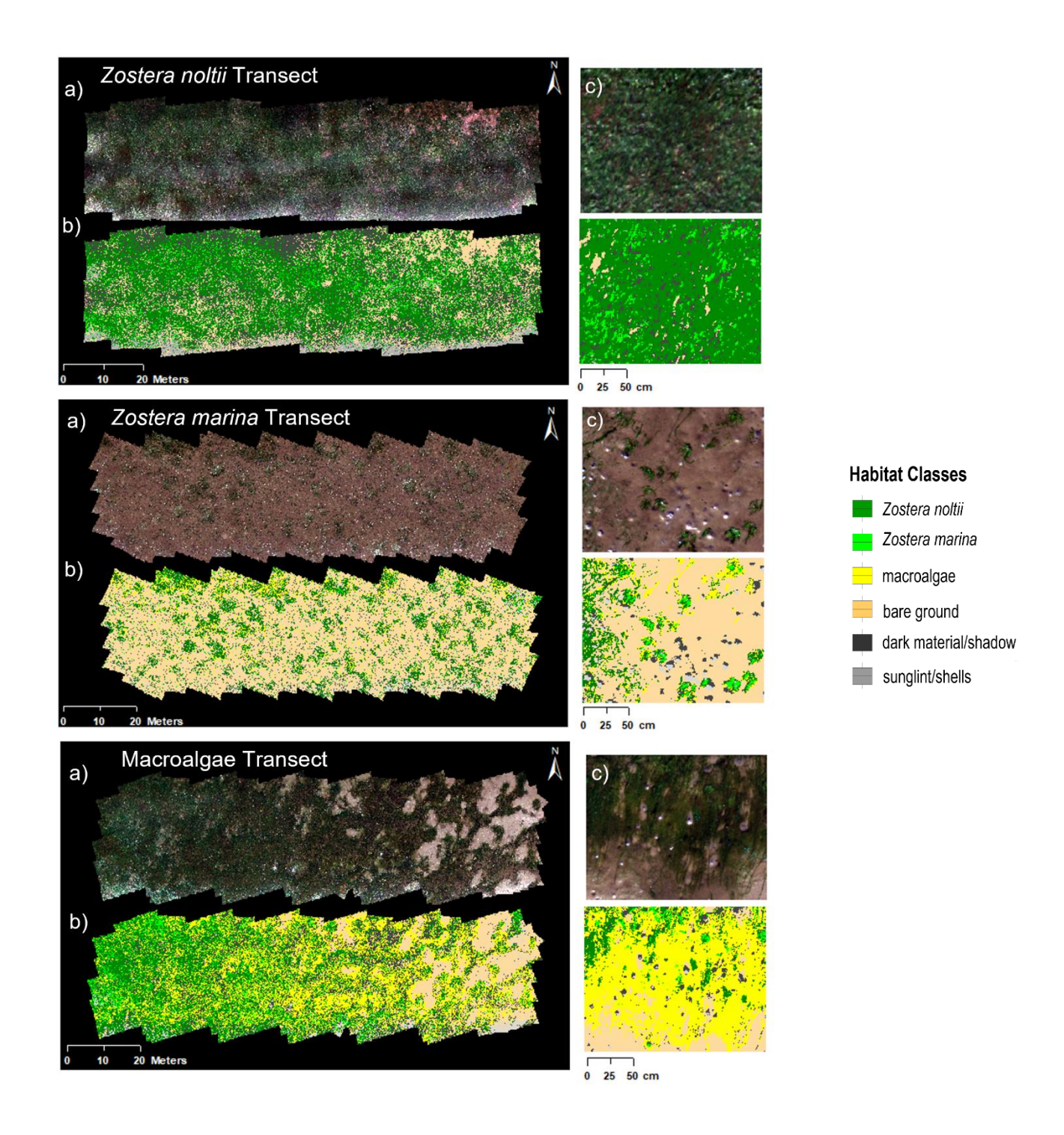


Figure 3.5. a) Raw UAV orthomosaic are displayed using the red, green, and blue colour composite, b) classified map and, c) a close-up example for each transect survey (*Zostera noltii*, *Zostera marina* and Macroalgae).

3.4. Discussion

3.4.1. Habitat classification

This chapter aimed to evaluate a consumer grade UAV multispectral camera for mapping a multispecies intertidal temperate seagrass environment. The objective was to discriminate between macroalgae and different Zostera spp., to capture accurate species-specific distribution patterns. This is essential to coastal managers to effectively address mitigating strategies for the prevention of seagrass species decline, and the growth of detrimental macroalgae growth. Findings show that despite the complex environment and similar spectral properties of Zostera spp. and green macroalgae, five-band multispectral UAV camera and the MLC method can yield maps with overall accuracies ranging between 84% and 91%. When considering only the RGB bands, the OA was reduced by up to 28% across all transects. Likewise, Producer's and User's -accuracy associated with vegetation classes declined substantially, highlighting the significant advantage that the red edge and near infrared bands can provide to effective mapping of an intertidal multispecies environment, increasing accuracy discriminating particularly between Zostera spp. and macroalgae. This provides the key to an operationally viable method for monitoring multispecies intertidal seagrass habitats. The high OA here also aligns with prior studies that used 5-10 band multispectral UAVs to map intertidal seagrass-macroalgae environments. For example, in less complex intertidal seagrass-macroalgae environments, James et al., (2020) and Román et al., (2021) demonstrated an OA of 98.6% and 90.3%, respectively, using the MLC method. Hobley et al., (2021), used more sophisticated analysis, a deep learning method (Convolutional Neural Networks; FCNNs), in a similarly complex intertidal seagrass-macroalgae environment in LNNR, and achieved an average accuracy of 88.4%, although without discriminating separate seagrass species.

The three vegetation types, *Zostera* spp. and macroalgae were spectrally distinct across all investigated transects. This distinction may be attributed to their differences in leaf pigmentation enabling the discrimination between the different vegetation types (Fyfe, 2003; Davies et al., 2023). While *Zostera noltii* and *Zostera marina* have similar leaf pigmentation, macroalgae with its brighter pigmentation in green colour indicated greater separability in comparison to that between *Z. noltii* and *Z. marina*. Notably, the

peak reflectance of all vegetation types and a maximum separation in the spectral reflectance between Zostera spp. and macroalgae occurred in the green, red edge and near infrared wavelength bands. These observations conform with generally observed spectral reflectance patterns in healthy plants that are known to absorb radiation in the blue and red wavelengths (around 450nm and 670nm, respectively), and reflect radiation in the green (around 530nm), red edge and near infrared wavelengths (around 730nm, 840nm, respectively) (Schmidt and Skidmore, 2003; Chand and Bollard, 2021; Davies et al., 2023). Although this study showed low spectral separability between Z. noltii and Z. marina, and higher misclassification between these two species, their separability could still be observed in the red edge and near infrared bands. These results also align with Fyfe (2003) who showed that seagrass species could most easily be discriminated between 700 and 900nm and Davies et al. (2023) that demonstrated a steep reflectance signature from ~680nm onwards for intertidal seagrass and algae. However, results contradict another study conducted by Román et al., (2021), who showed that the peak reflectance of *Z. noltii*, in an intertidal coastal area in Cadiz, Spain, was highest between 500 and 700nm and declined from 700nm. Such disparities between studies may be related to differences in spectral responses of seagrass due to for example, the influence of epiphytes and epibionts (Fyfe, 2003; Hwang et al., 2019), or sediment background (Bargain et al., 2012).

A further advantage in creating accurate habitat maps from UAVs may be related to the ultra-high spatial resolution that the camera offers. The high resolution minimises mixed pixels (i.e., the representation of more than one class within a pixel). This may not only have aided in discriminating between the vegetation types (beyond the addition of red edge and near infrared bands alone), but also reduced classification errors between vegetation types and non-vegetative classes. For example, when *Z. noltii* is found in sparse density, their thin leaves lie on the bare ground and could easily be misclassified with other benthic classes within the pixel when using a lower spatial resolution imagery, but this issue is avoidable, if a pixel contains *Z. noltii* features entirely. Finally, high spatial resolution imagery enables the identification of seagrass habitats to species level, critical to coastal managers for the monitoring of biodiversity and species distribution of seagrass.

Overall, results indicate significant potential for mapping an exposed multispecies intertidal seagrass environment using an off-the shelf multispectral consumer grade UAV. We show that by using a 5 band and a user-friendly and easily accessible

classifier, similar accuracy results can be achieved with a study that has for example, applied more computationally intensive methods (e.g., Hobley et al., 2021). We demonstrate the potential of a cost-effective approach in creating accurate multispecies intertidal seagrass habitat maps, which may be operationally more accessible to coastal managers. This approach may be used to develop new monitoring programmes or be integrated into existing monitoring programmes to support the effective protection and conservation of *Zostera* spp..

3.4.2. Limitations, challenges, and recommendations

Although this study indicates high potential for using multispectral UAV imagery for mapping a complex multispecies intertidal seagrass environment, some limitations and challenges need to be considered from the planning stage and prior to flight missions of data collection, during field surveys and in the interpretation phases: (1) Despite successful creation of multispecies seagrass habitat maps, results showed that some misclassification among vegetation is still likely and may impact the accuracy of species distribution maps, especially between the two Zostera spp. investigated in this study. These inaccuracies need to be considered and critically evaluated for management and conservation planning, when aiming for species-specific targeted protection and management plans. Moreover, to reduce misclassification errors, an Object-Based Image Analysis (OBIA) approach, instead of a pixel-based approach, could improve classification accuracies when using ultra-high imagery data (Blaschke, 2010; Hobley et al., 2021). (2) Unfavourable environmental conditions can pose numerous challenges during field surveys and hamper logistics: In cases where the field site of interest cannot be surveyed outside the mudflat areas, such as in this study, similar to traditional field surveys, UAV surveys can remain challenging in terms of accessing areas with soft sediments on foot, with potential hazards of getting stuck in soft bottom areas; (3) Protected site specific restrictions e.g., prohibition of surveys during the period of nesting and breeding birds, and foraging seasons, need to be considered to minimise impact on protected features, to minimise and avoid the potential of collision of UAV with birds; (4) Given the restricted and limited periods of time during low tide available to conduct the surveys, and that all the necessary conditions (e.g., wind speed, weather) to fly a UAV must be met within a particular time slot, a well-planned manageable operation is recommended for maximum efficiency and safety; (5) It is important to consider that large-scale mapping can be restricted

due to short battery autonomy and Visual Line Of Sight (VLOS) restrictions, on flight altitude and distance (Nahirnick et al., 2019a; Walker et al., 2023). In the UK, for example, the current flight limit is typically restricted to 120 m altitude and within VLOS, with further qualifications required when flying a UAV beyond these limits. To overcome this challenge, it is recommended to either have additional batteries on field site or increase battery capacity by increasing flight altitude at the cost of lower spatial resolution; and (6) Other technological issues that may be encountered in the field can be related to GNSS accuracy, which can fail depending on satellite configuration and result in inaccurate positioning of ground-truth surveys or the UAV, thus may impact the post-processing and map results and should be considered.

3.4.3. Benefits for management

The proposed methodology could support effective management by overcoming expensive, time consuming and exhaustive quadrat sampling in challenging mud flat environments, by simply using a number of UAV-derived classified transects as samples to assess the condition of seagrass habitats (Figure 3.5). The UAV derived maps could be utilised as ground-truth for large-scale habitat mapping, using freely available satellite imagery to create broad scale habitat maps for presence/absence and density maps (Carpenter et al., 2022). Moreover, multispectral UAV derived habitat maps could be developed as an integral part for multi-temporal seagrass habitat monitoring, allowing for greater reproducibility and repeatability of habitat mapping (Prystay et al., 2023; Ventura et al., 2022). Finally, UAV-derived habitat maps may provide a foundation to develop effective communication tools used for decision-and policy.

3.4.4. Conclusion

This Chapter demonstrates the viability of using an off-the shelf multispectral UAV to accurately map a complex intertidal seagrass environment. The ultra-high image resolution and additional red edge and near infrared bands enabled discrimination between vegetation classes at species level and ultimately the creation of fine-scale habitat maps. The study may provide a foundation to aid coastal managers to develop effective monitoring programmes by integrating multispectral UAV derived habitat maps in monitoring programmes. The methodology of this study can be utilised to

implement targeted management practices to identify areas of concern and potential threats to effectively manage *Zostera* spp. decline, and detrimental macroalgae growth.

Chapter 4: Mapping intertidal seagrass and macroalgae using Hyperspectral CASI imagery

4.1. Introduction

While UAV Imagery can be useful for prioritising detailed information on small seagrass areas, as discussed in previous chapter, a major limitation is its suitability for largescale habitat mapping, due to limited flight time and line of sight restrictions as discussed in Chapter 3 (Carpenter et al., 2022). Accurate large-scale habitat maps are required to fully investigate seagrass habitat extent, distribution, and spatial patterns (Hossain et al., 2015; Veettil et al., 2020). Capturing seagrass environments at a habitat and/or ecosystem scale, is important to coastal managers to gain insights and overview of seagrass - macroalgae ecology and dynamics relevant for effective holistic management plans. While satellite derived imagery data (e.g., Sentinel 2, Landsat) can provide cost-effective and rapid seagrass habitat mapping over large areas and may benefit regular and long-term monitoring, sensors typically lack high spatial resolution (e.g., Dekker et al., 2005; Knudby et al., 2010; Kovacs et al., 2018; Zoffoli et al., 2020; Benmokhtar et al., 2023). This can limit their ability to map small or fragmented seagrass patches accurately. Although they typically have spectral bands similar to for example, the multispectral UAV used in Chapter 3, (e.g., Sentinel has 4-12 bands), this varies by platform, and the wavelengths available may not permit discrimination between different vegetation types with similar spectral signatures due to their low spatial resolution. These limitations are reflected in literature, where low spatial/spectral resolution satellite data have typically been used to map either relatively homogeneous seagrass habitats, or to derive coarse seagrass habitat extents (e.g., Wabnitz et al., 2008; Topouzelis et al., 2018).

Other factors that may prove challenging in temperate seagrass regions, are associated with clouds covering imagery data, and turbidity. Both cloud and turbidity can physically obscure the habitat features of interest, making it impossible for most satellite sensors to detect submerged vegetation in temperate regions (Dierssen et al., 2019; Kuhwald et al., 2022). For example, Armitage et al. (2013) showed that the Moderate Resolution Imaging Spectroradiometer (MODIS) exhibited an average yearly probability of cloud-free images of 21.3% for the UK and between 13% and 25% in the North East of England. To overcome sensor specific spatial and spectral limitations and platform related environmental challenges, airborne hyperspectral imagery may

prove beneficial for intertidal temperate seagrass mapping, as the accurate mapping of different vegetation classes at large-scales may be possible (Dierssen et al., 2019). Flexibility in data acquisition is possible, as platforms can be flown at different altitudes, below cloud cover, and at low tide when seagrass is exposed, to avoid potential turbidity in the water column, consequently enhancing data quality. The inherent flexibility of airborne remote sensing technology can enable users to develop flight plans and attach hyperspectral sensors tailored to specific interests, offering considerable potential for detailed vegetation mapping (Jia et al., 2020).

While studies have used airborne hyperspectral imagery to map seagrass habitats, the majority of these have been conducted in shallow clear tropical waters. Airborne hyperspectral sensors have successfully mapped tropical seagrass distribution, biomass, species composition and extent (e.g., Phinn et al., 2008; Clarke et al., 2021). Although scarce, as outlined in Chapter 2 (Table 2.2), the few studies available, that have utilised airborne hyperspectral imagery in temperate seagrass environment, have demonstrated its potential for mapping seagrass- macroalgae environments. Among these few studies, most were conducted in submerged seagrass and macroalgae environments. For example, a study conducted in Finland by Vahtmäe et al. (2021), demonstrated that a temperate benthic habitat of submerged aquatic vegetation (SAV) which included green macroalgae and seagrass (Zostera marina), could be mapped with higher accuracy using hyperspectral Compact Airborne Spectrographic Imager (CASI) sensor (Overall Accuracy 78%), in comparison to Sentinel-2 imagery (Overall Accuracy 69%). Moreover, O'Neill & Costa (2013) mapped a subtidal Zostera marina and macroalgae habitat in Canada, comparing high spatial resolution satellite imagery (IKONOS; 4m) and two-metre airborne hyperspectral imagery (Airborne Imaging Spectrometer for Applications - AISA). This study showed successful discrimination between seagrass and green macroalgae with hyperspectral imagery outperforming the satellite imagery. However, the mapped habitats in these studies entailed segregated seagrass and macroalgae areas with less habitat complexity, as can be found, for example, in the intertidal areas of LNNR. Here, exposed intertidal seagrassmacroalgae habitats, can be different in their ecological complexity due to intermingled macroalgae and seagrass and the presence of mudflat which can often blend in together, consequently increasing the optical complexity, thus spectral signatures of different components. For example, assessing the habitat maps created in Chapter 3, benthic classes including seagrass, macroalgae and bare ground can be found at subcm spatial resolution adjacent to each other, requiring both higher spatial and spectral resolution.

Studies that have investigated the application of airborne hyperspectral imagery in complex intertidal seagrass environments are scarce or close to non-existent (Chapter 2, Table 2.2). The only study found, Garono et al., 2004, used CASI airborne hyperspectral imagery to discriminate between intertidal and subtidal eelgrass (*Zostera marina*) and green macroalgae cover in the US. While this study also mapped seagrass and macroalgae densities, denoting some habitat complexity using a spatial resolution of 1.5m, hyperspectral imagery with higher spatial resolution may be required for more accurate mapping in LNNR to capture the complexity in more detail.

Despite the potential benefits of using hyperspectral imagery to distinguish between seagrasses and macroalgae (Garono et al., 2004; O'Neill & Costa, 2013), multispectral satellite imagery remains the predominant technology for mapping seagrass habitats (Hossain et al., 2015; Veettil et al., 2020). This is mainly due to high costs of operation and expensive equipment often associated with the acquisition of airborne hyperspectral imagery data. However, the regular (annual) acquisition of hyperspectral CASI imagery in coastal areas including the LNNR by the Environment Agency (EA) in the UK, which is accessible to managers, provides great potential for coastal monitoring programmes. Although UK's coastal areas consist of many intertidal seagrass areas (Natural England, 2024), no studies were found that have utilised airborne hyperspectral imagery to map a complex seagrass -macroalgae environment in the UK. To advance the knowledge and better understand the feasibility of airborne hyperspectral imagery for an intertidal seagrass-macroalgae environment, and its potential for monitoring and management to effectively conserve seagrass habitats, reliable and validated studies are urgently required.

This Chapter investigates the potential of CASI airborne hyperspectral imagery for the mapping of intertidal seagrass-macroalgae environments in the UK at a large-scale. Objectives were: (1) To use Random Forest classification method to identify the optimal benthic class level (7 - class map; 6 - class map and 5 - class map, respectively) for accurate seagrass-macroalgae habitat mapping; (2) To establish the extent to which the hyperspectral nature of the imagery contributes to mapping complex intertidal seagrass-macroalgae environments by reducing the number of spectral bands to 5-8 bands similar to the multispectral UAV (Chapter 3) and satellite PlanetScope (Chapter 5) for comparison, and assess impacts on classification

accuracy; (3) To discuss seagrass-macroalgae distribution patterns in the context of management and conservation implications.

4.2. Materials and Methods

4.2.1. Ground truth sampling

To validate the hyperspectral image classification, in situ ground surveys were carried out in August 2021 in the Causeway area due its safer environment and accessibility in comparison to Fenham Flats and Budle Bay, which are known to consist of softer sediment thus increasing the likelihood of being trapped (Chapter 1, Figure 1.5). To achieve large-scale area sampling and ensure even sampling of benthic categories including seagrass, macroalgae, seagrass and macroalgae mixed and bare ground, the positions of 31 suitable transects of 100m x 20m were identified in a GIS, based on apparent seagrass and macroalgae cover. The same method of quadrat sampling and geo location of quadrats as described in Chapter 3, Section 3.2.3., were undertaken to obtain detailed information on the benthic cover across the Causeway Area (Figure 4.1). Same as in Chapter 3, photographs of quadrats and GPS positions of the north and south corner of each quadrat were taken using a Trimble Catalyst receiver with the Trimble Network RTK Precision service (± 0.2 cm accuracy). In total, 630 quadrat photographs were taken. To account for bright surface covers encountered across the field site identified in the UAV imagery, 26 additional quadrat samples were targeted on known large cockle shell beds.



Figure 4.1. Map showing the ground-truth sampling points where quadrat photographs were taken in the Causeway area (red boundary).

4.2.2. Benthic Classes

Percent cover of each benthic class within quadrat photographs were visually estimated. Classes included, seagrass, macroalgae, seagrass/macroalgae mixed, bareground (including shells). To capture density of cover, the seagrass class was further divided into sparse, moderate- and dense- seagrass, according to the following percent cover ranges similar to Zoffoli et al. (2020): sparse (5-40%); moderate (41-70%) and dense (71%-100%) (Figure 4.2a). Within the mixed seagrass/macroalgae quadrats, macroalgae was often found on top of seagrass or intertwined in seagrass patches. In some cases, only a string of macroalgae was found in the quadrat that was dominated by seagrass and vice versa. To reduce spectral misclassification between pure seagrass and pure macroalgae classes, quadrats that indicated less than 15% difference in percent cover between seagrass and macroalgae were assigned the seagrass/macroalgae mixed class. This low threshold was set to maintain higher dominance of either seagrass or macroalgae in order to reduce potential misclassification between these two classes. Otherwise, the dominating habitat class (seagrass or macroalgae, respectively) was assigned. Although not observed in the quadrats, an additional class "water" was produced to account for channels of water occurring in the imagery (Figure 4.2a). In total, seven benthic classes were identified: sparse seagrass (sparse SG, hereafter), moderate seagrass (moderate SG), dense seagrass (dense SG), macroalgae, seagrass and macroalgae mixed (SG/MA mixed), bare ground, and water (Figure 4.2a). To investigate how much detailed information can be acquired accurately from the hyperspectral imagery, using 3 scenarios of benthic class combinations were investigated, producing 7- class, 6- class and a 5class benthic habitat maps. Here, the 7-class Scenario entailed all possible seagrass densities, including sparse SG, moderate SG and dense SG. For the 6-class Scenario, the moderate and dense SG class were grouped into the class moderate/dense SG (mod-dense SG). And finally for the Scenario 3, all three seagrass classes were grouped into one seagrass class. All Scenarios included the benthic classes, macroalgae, SG/MA mixed, bare ground and water (Figure 4.2b). Notably, the number of training samples was unbalanced and varied across classes (Figure 4.2b). Training data were created using a pixel-based approach, where each identified class of quadrat was assigned to a pixel relative to the location of the quadrat.

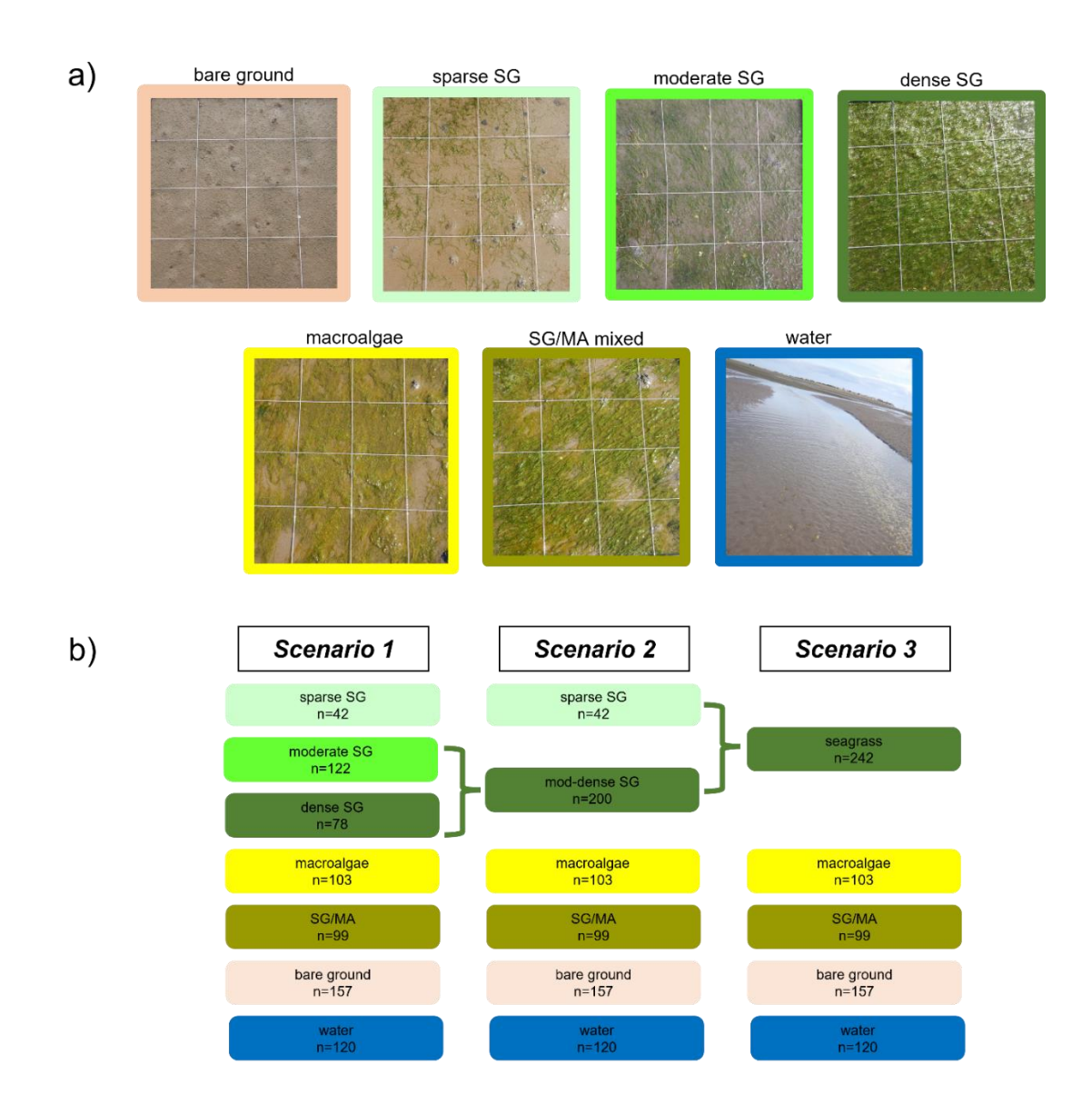


Figure 4.2. a) Quadrat photographs of identified benthic classes. b) Diagram of the three different investigated Scenarios with differing numbers of benthic classes including the number of training sample data for each benthic class. Sparse SG = sparse seagrass, moderate SG = moderate seagrass, dense SG = dense seagrass, SG/MA mixed = seagrass/macroalgae mixed, bare ground = bare ground, water = water.

4.2.3. CASI information and Image acquisition

Airborne imagery was collected on the 20^{th} September 2021 using the mounted Compact Airborne Spectrographic Imager (CASI). The CASI sensor is a push-broom sensor that captures narrow spectral bands in the visible and near infrared (VNIR) region of the electromagnetic spectrum covering wavelengths between 400-1000nm. While the sensor offers up 288 bands, the number of spectral bands can be adjusted according to user interest. The spatial resolution depends on the flight height and ranges between 0.3-1.5m. The imagery used in this study was acquired by the

Environment Agency as part of their monitoring programme and was flown during spring low tide across the Lindisfarne National Nature Reserve (LNNR) (Figure 4.3). The spatial resolution of the data was 1m including a spectral resolution of 33 spectral bands (Appendix A).

Atmospheric absorption bands are specific wavelength regions, commonly observed in the VNIR, where a significant amount of incoming radiation is absorbed by the Earth's atmosphere, caused by the occurrence of atmospheric constituents (e.g., water vapour (H₂O) and carbon dioxide (CO₂)). To avoid a steep slope in spectral reflectance curves, atmospheric absorption features, which were observed around 750nm and 790nm (band 20-29, respectively) were removed. This resulted in a total of 23 spectral bands for further analysis.

4.2.4. Pre-processing of imagery

CASI data were acquired from the Defra Survey Data Portal (Geomatics Hub, 2024), and downloaded in GeoTiff formats within compressed .zip files. It had undergone the following pre-processing stages: (1) Calibration; (2) Radiometric correction, which performs radiometric and spectral corrections to the image; (3) Dark correction and; (4) geometric correction for the production of accurate geo-referenced images. In addition to the pre-processing stages applied by the Environment Agency, this study performed a Quick Atmospheric Correction (QAC), which is a rapid method to correct data from atmospheric effects. In comparison to many other atmospheric correction algorithms such as the FLAASH, the QAC algorithm uses an empirical approach where no ancillary data other than band wavelengths are required. It can be applied on multispectral and hyperspectral imagery data spanning across the spectral range of the visible- near infrared-short wave infrared range (~ 400-2500 nm) (Bernstein et al., 2012). The final step before analysis and the creation of habitat maps, included the stitching of tiles into a mosaic to have a seamless single image, prior analysis (Figure 4.3).

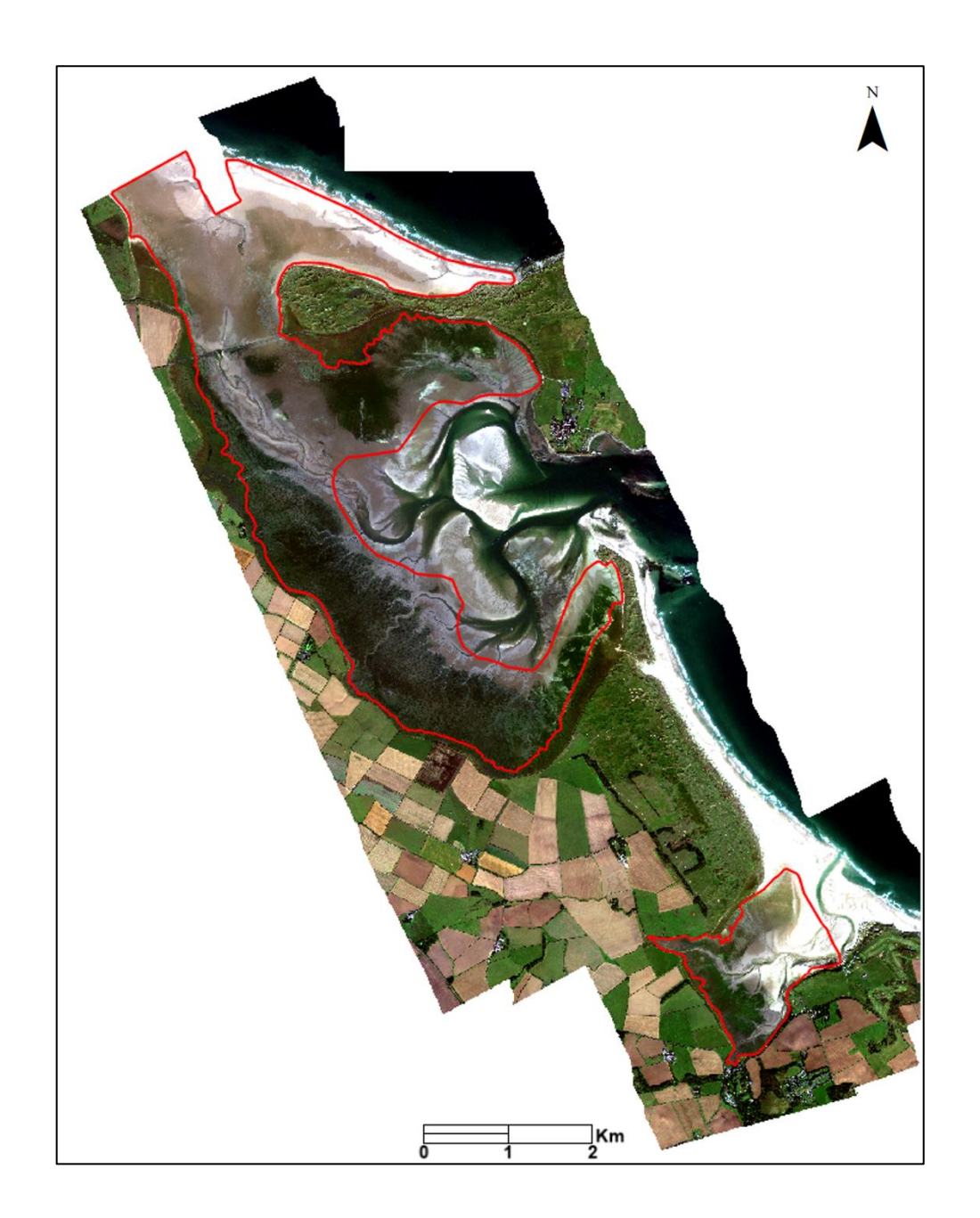


Figure 4.3. The Mosaic of the hyperspectral imagery scene and the investigated intertidal area in Lindisfarne National Nature Reserve (LNNR) (red boundary) (Source: Geomatics, 2024: Contains public sector information licensed under the Open Government Licence v3.0.)

4.2.5. Classification method and accuracy assessment

Due to the high dimensionality of spectral data across a wide range of wavelengths, creating habitat maps of hyperspectral imagery can be challenging. For example, the high dimensionality of data can result in variability within classes, often requiring a large amount of training data to capture the high variation present (Ghamisi et al., 2017). Different classifiers such as the Spectral Angle Mapper (SAM) and Maximum Likelihood Classifier (MLC) have previously been used for hyperspectral imagery and

habitat mapping of vegetation (Chan & Paelinckx, 2008; Vahtmäe et al., 2012), the machine learning (ML) classifier, Random Forest (RF), has gained in popularity due to its versatility in handling high dimensional data, it's robustness to noise and reliability in higher accuracy performance (Breiman 1996, 2001; Dietterich 1999).

Random forest is a supervised non-parametric classifier which uses ensemble learning method by using decision trees to make predictions through a bootstrapping method called bagging (Breiman, 1996, 2001). These features help the classifier handle low and unbalanced training samples, with no separate validation data set required (Pal, 2005; Sheykhmousa et al., 2020). The RF classifier has also been successfully applied in seagrass habitat mapping and shown to outperform other classifiers such as the Maximum Likelihood and Support Vector Machine (SVM) classifier (Ha et al., 2021). To overcome the existence of unbalanced and low training samples in this study, the RF classifier was used to produce the classified habitat maps. A separate training data set is not required for cross-validation, making it useful for the low training data samples in this study. The RF classifier can use an Out-of Bag (OOB) prediction error method, through a bootstrap sampling approach that provides an estimate of models' performance. This procedure is applied during the training process and simultaneous creation of the habitat classification map. The OOB- score provides an internal error estimation of unseen data. During the creation of bootstrap samples and the building of each tree in the Random Forest, a random subset of the original dataset is selected with some samples included multiple times in the training set, but others excluded entirely (unseen data) (Belgiu & Drăgu, 2016).

The model prediction performance can be tuned/improved through adjustment of three parameters: (1) number of classification trees (*ntree*; (2) the depth of each tree (max_depth), and (3) the number of feature classes to be considered at each node (*mtry*) (Scornet, 2017). To avoid excessive computation time, the model was performed systematically by increasing the parameter *ntree* and adjustment of the parameters including max_depth and *mtry* until a stable OOB- error rate was reached. The model's performance being validated by observing the OOB-score (Benmokhtar et al., 2021),

To get more insight into the performance of the classifier, additional metrics including *precision*, *recall* and *F1-score*, were examined. *Precision* (*User's Accuracy*) measures the accuracy of positive predictions made by the model i.e., how many of the positive predictions made are correct; *Recall* (*Producer's Accuracy*), measures the rate of true

positive predictions i.e., to correctly predict identified by the model to evaluate the model's ability to avoid false negatives; *F1-score* is a weighted average of precision and recall. Furthermore, an *Accuracy score* (*Overall Accuracy*), which describes the number of correct predictions over all predictions and a confusion matrix that enables to assess misclassifications between true labels and predicted labels for each class, are also produced.

To investigate whether increasing the number of spectral bands achieves better map accuracy results, hyperspectral imagery (23bands) was compared with a reduced number of spectral bands. The number of spectral bands were reduced (from *Scenario* 2) to match the PlanetScope satellite used in Chapter 5 and DJI UAV multispectral sensors used in Chapter 3. The 8-spectral bands closest to the PlanetScope SuperDove sensor were extracted, as were the 5 spectral bands closest to the DJI multispectral UAV sensor wavelengths utilised in Chapter 3 (*Scenario 2 PS* and *Scenario 2 UAV*, hereafter) (Table 4.1).

Table 4.1. Reduced number of spectral bands, using the closest bands from the CASI hyperspectral bands aligned to the PlanetScope SuperDove and multispectral UAV band centre wavelength ± FWHM (Full Width at Half Maximum). HS = Hyperspectral, MS = Multispectral.

| Airborne: CASI-HS | Satellite: PlanetScope SuperDove-MS | Airborne: CASI-HS | UAV: DJI-MS |
|-----------------------|---|----------------------|--------------|
| 442.246nm ± 14.195 nm | 442nm ± 10nm | 442.246nm ± 14.195nm | 450nm ± 16nm |
| 487.186nm ± 14.188 nm | 490nm ± 25nm | 554.561nm ± 15.362nm | 560nm ± 16m |
| 513.195nm ± 11.821 nm | 526.5nm ± 13.5nm | 643.166nm ± 5.905nm | 650nm ± 16nm |
| 554.561nm ± 15.362 nm | 565nm ± 18nm | 727.018nm ± 5.90nm | 730nm ± 16nm |
| 611.273nm ± 5.907 nm | 610nm ± 10nm | 852.204nm ± 12.993nm | 840nm ± 26nm |
| 663.244nm ± 5.905 nm | 665nm ± 15nm | | |
| 712.846nm ± 5.905 nm | 705nm ± 8nm | | |
| 879.372nm ± 11.813 nm | 865nm ± 20nm | | |

4.3. Results

4.3.1. Spectral signatures

The spectral signature of training data assessed using Jeffries-Matusita (J-M) distance measure, from each benthic class varied distinctly between the non- vegetation classes (i.e., bare ground and water) and the vegetation classes (i.e., seagrass, macroalgae and SG/MA mixed) (Table 4.2). Spectral separability varied among investigated vegetation classes both within Scenario 1 and Scenario 2, the benthic class sparse SG was distinctively separable (1.7 – 1.9 J-M value) from all other benthic vegetation classes (dense SG, moderate SG, macroalgae and, SG/MA mixed, respectively). The least spectral separation within Scenario 1 and Scenario 2 was found between the classes including: moderate SG, SG/MA mixed and macroalgae, mod-dense SG (1.4 – 1.6 J-M value). Similarly, the Scenario 3 image indicated the least spectral separation (1.4 – 1.6 J-M value) among all vegetation classes (seagrass, macroalgae and SG/MA mixed classes, respectively) (Table 4.2). However, when assessing the spectral curves of individual vegetation classes, the observed separability between vegetation classes differed across the spectrum (Figure 4.4). Within Scenario 1 and Scenario 2, the benthic class sparse SG appeared distinctly separable across all wavelengths compared to all vegetation classes, except its separation with macroalgae from around 700nm onwards. In contrast, all other seagrass classes (mod SG, dense SG, mod-dense SG, SG/MA mixed, respectively) did not show major separability across the entire wavelength spectrum from each other. However, the class macroalgae showed a distinct separation from all seagrass classes, except sparse SG, from 700nm onwards. All vegetation classes indicated peak reflectance between 550nm and 610nm (green wavelength) with a slight decline until 680nm (red wavelengths) and sharp increase to a peak reflectance at around 720nm (Red Edge wavelengths). From here the peak reflectance plateaued and followed a typical vegetation spectral response with a slight increase to the highest reflectance at around 880nm (NIR) (Figure 4.4).

Table 4.2. Results of Jeffries-Matusita (J-M) index, indicating spectral pair separability of benthic classes for the: 7-class-, 6-class- and 5-class habitat maps.

| | | 1 | |
|--|---|---|---|
| Benthic pair separation | J-M | Benthic pair separation | J-M |
| 7-class Habitat | | 6-class Habitat | |
| moderate SG - SG/MA mixed SG/MA mixed - macroalgae moderate SG - macroalgae dense SG - Moderate SG dense SG - SG/MA mixed moderate SG - Sparse SG dense SG - macroalgae sparse SG - macroalgae sparse SG - macroalgae sparse SG - bare ground moderate SG - bare ground SG/MA mixed - bare ground bare ground - macroalgae dense SG - Sparse SG water - bare ground sparse SG - water sense SG - water sense SG - water water - macroalgae SG/MA mixed - water dense SG -water | 1.4 1.4 1.5 1.7 1.8 1.8 1.9 1.9 2.0 2.0 2.0 2.0 2.0 2.0 2.0 2.0 2.0 2.0 | SG/MA mixed - macroalgae SG/MA mixed - mod-dense SG macroalgae - mod-dense SG sparse SG - mod-dense SG sparse SG - SG/MA mixed sparse SG - macroalgae sparse SG - bare ground SG/MA mixed - bare ground bare ground - macroalgae bare ground - mod-dense SG water - bare ground sparse SG - water water - mod-dense SG water - macroalgae SG/MA mixed - water | 1.5 1.6 1.9 1.9 1.9 2.0 2.0 2.0 2.0 2.0 2.0 2.0 |
| 5-class Habitat | J-M value | | |
| SG/MA mixed - macroalgae SG/MA mixed - seagrass macroalgae - seagrass bare ground - seagrass SG/MA mixed - bare ground bare ground - macroalgae water - bare ground water - seagrass water - macroalgae SG/MA mixed - water | 1.4 1.5 1.6 1.9 2.0 2.0 2.0 2.0 2.0 2.0 | | |

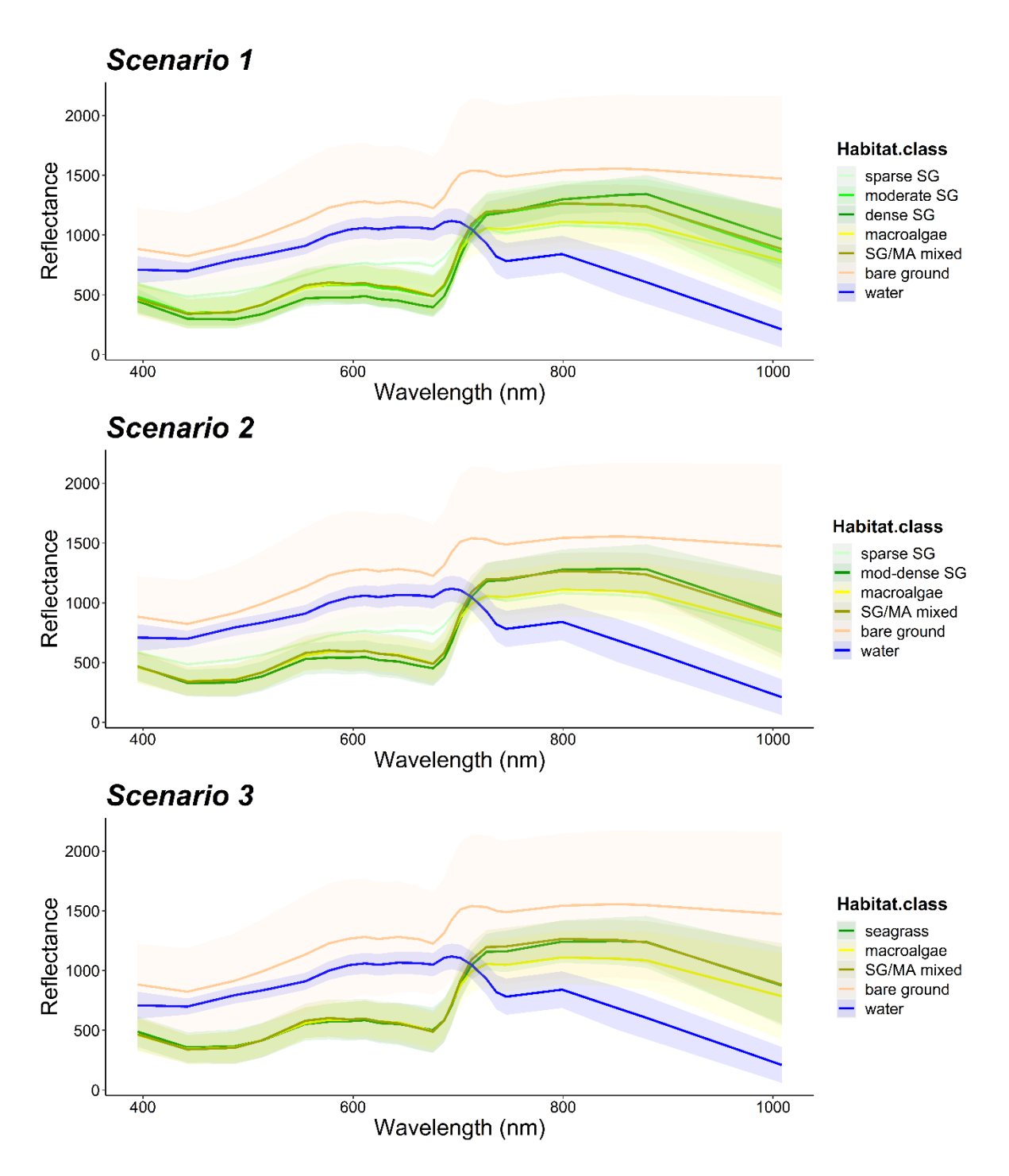


Figure 4.4. Spectral reflectance curves of benthic class training data across all hyperspectral bands for *Scenario 1*, *Scenario 2*, and *Scenario 3*. The shaded area represents ± standard deviation.

4.3.2. Accuracy assessment

The model's performance reached the best OOB- score, which ranged between 0.66 and 0.75, at parameters of *ntree*:150-200; *max-depth*:5-9; *mtyr*: 4-6, across all investigated Image Scenarios (Table 4.3).

Table 4.3. Summary table of optimal tuned parameters reached for the optimal Random Forest model to create a classification habitat map for each investigated Scenario.

| | ntree | max_depth | mtry | OOB-score |
|---|-------|-----------|------|-----------|
| Scenario 1 (7 benthic classes) | 200 | 5 | 4 | 0.66 |
| Scenario 2 (6 benthic classes) | 150 | 8 | 5 | 0.73 |
| Scenario 2 PS 6 benthic classes) | 150 | 8 | 5 | 0.75 |
| Scenario 2 UAV (6 benthic classes) | 200 | 8 | 5 | 0.73 |
| Scenario 3 (5 benthic classes) | 200 | 9 | 5 | 0.73 |

The Random Forest yielded the lowest Overall Accuracy (OA) of 76% for the 7-class habitat map (*Scenario 1*) (Table 4.4; Figure 4.6), followed by the 6-class habitat maps (*Scenario 2*) 93% OA (Table 4.4; Figure 4.7). The highest OA was found for the 5-class habitat map (*Scenario 3*) with an OA of 97% (Table 4.4; Figure 4.8). When investigating *Scenario 2* with a reduced number of spectral bands, both the *Scenario 2-PS* imagery and the *Scenario 2-UAV* revealed similar OA in comparison to the *Scenario 2* imagery (93% and 92%, respectively) (Table 4.4).

Habitat class accuracies varied between image Scenarios (Figure 4.5; Table 4.4). The highest class accuracy was achieved for the habitat classes bare ground and water across all images (Precision: 87%-100%; Recall; 93%-97%), whereas the highest misclassification for these classes was found within image $Scenario\ 1$, whereby 6% of the sampled pixels of bare ground was incorrectly misclassified as sparse SG. While vegetation classes indicated lower class level accuracies, there was large variation found between Scenarios. Notably, the lowest vegetation class accuracies were found for $Scenario\ 1$ (Precision: 56%-81%; Recall: 45%-76%) and the highest class accuracies were found for Scenario 3 (5-class map) (Precision: \ge 94%; Recall: \ge 93%). The Scenarios that entailed seagrass density classes (Scenario 1 and $Scenario\ 2$, respectively) showed very high-class accuracy for the class sparse SG ($Scenario\ 1$: Precision: 81.25%; Recall: 62%; all $Scenario\ 2$: Precision: \ge 95%; Recall: \ge 86%) (Figure 4.5; Table 4.4).

Table 4.4. Accuracy results of the Random Forest classification maps for each investigated Scenario.

| | Precision | Recall | F1-score | Overall Accuracy |
|----------------|-----------|--------|----------|------------------|
| Scenario 1 | | | | 0.76 |
| sparse SG | 0.81 | 0.62 | 0.70 | |
| moderate SG | 0.56 | 0.70 | 0.62 | |
| dense SG | 0.66 | 0.76 | 0.71 | |
| macroalgae | 0.82 | 0.64 | 0.72 | |
| SG/MA mixed | 0.61 | 0.45 | 0.52 | |
| bare ground | 0.87 | 0.97 | 0.92 | |
| water | 1.0 | 1.0 | 1.0 | |
| Scenario 2 | | | | 0.93 |
| SG sparse | 0.97 | 0.86 | 0.91 | |
| SG mod-dense | 0.85 | 0.96 | 0.91 | |
| macroalgae | 0.97 | 0.84 | 0.90 | |
| SG/MA mixed | 0.91 | 0.81 | 0.85 | |
| bare ground | 0.98 | 1.0 | 0.99 | |
| water | 1.0 | 1.0 | 1.0 | |
| Scenario 2-UAV | | | | 0.92 |
| SG sparse | 0.95 | 0.86 | 0.90 | |
| SG mod-dense | 0.84 | 0.95 | 0.89 | |
| macroalgae | 0.95 | 0.80 | 0.87 | |
| SG/MA mixed | 0.82 | 0.76 | 0.79 | |
| bare ground | 0.98 | 1.0 | 0.99 | |
| water | 1.0 | 1.0 | 1.0 | |
| Scenario 2-PS | | | | 0.93 |
| SG sparse | 0.97 | 0.88 | 0.93 | |
| SG mod-dense | 0.85 | 0.96 | 0.90 | |
| macroalgae | 0.93 | 0.85 | 0.89 | |
| SG/MA mixed | 0.91 | 0.76 | 0.83 | |
| bare ground | 0.99 | 1.0 | 1.0 | |
| water | 1.0 | 1.0 | 1.0 | |
| Scenario 3 | | | | 0.97 |
| SG | 0.95 | 0.98 | 0.97 | |
| macroalgae | 0.98 | 0.89 | 0.93 | |
| SG/MA | 0.94 | 0.93 | 0.93 | |
| bare ground | 0.99 | 1.0 | 1.0 | |
| water | 1.0 | 1.0 | 1.0 | |

Within Scenario 1, moderate SG class indicated the lowest class accuracy (Precision: 56.29%; Recall: 70%) (Table 4.4), which was 44.9% incorrectly classified as the other vegetation classes (sparse SG (12.5%), dense SG (12.4%), macroalgae (7.5 %) and SG/MA mixed (12.5%), respectively) (Figure 4.5). However, the habitat class, dense SG, indicated a slightly higher accuracy (Precision: 66.29%; Recall: 76%), but showed a misclassification of 9.93% with the moderate SG class, and 4.17% with SG/MA mixed class, but substantially lower misclassification with the macroalgae class (1.25%) (Table 4.4; Figure 4.5). When grouping mod SG and dense SG into one class in Scenario 2, class accuracies improved overall across all vegetation classes. The moddense SG habitat class indicated a high accuracy (Precision: 84%-85%; Recall:95%-96%) across all investigated Scenario 2 (Table 4.4). However, some misclassification with the other vegetation classes (SG/MA mixed, macroalgae, and sparse SG, respectively) where still observed, whereby mod-dense SG was incorrectly classified between 1.16% and 6.67% with these vegetation classes. Here, the Scenario 2-UAV indicated the lowest misclassification with macroalgae (1.16%) and the highest misclassification with SG/MA mixed class (6.67%) (Figure 4.5).

The habitat class macroalgae indicated high Precision accuracy ranging between 82.5% and 98.95% but lower Recall accuracies ranging between 64% and 89% across all Scenarios, with the lowest class accuracies observed for Scenario 1 and highest accuracy for Scenario 3, respectively (Table 4.4). Here, within all Scenarios, the largest misclassification was found between macroalgae and SG/MA mixed class. Scenario 1 and Scenario 2-UAV showed the largest amount that was incorrectly classified as SG/MA mixed (18.06% and 11.1%, respectively) (Figure 4.5). All other Scenarios showed less misclassification (≤ 5.7%). The habitat class SG/MA mixed indicated the lowest class accuracy (Precision: 61.11%; Recall: 45%) within Scenario 1 in comparison to all other Scenarios (Precision: ≥ 82%; Recall: 76%) and was mostly incorrectly classified as moderate SG (21.85%), followed by dense SG (10.11%) and macroalgae (7.5%). Within all Scenario 2 maps, SG/MA mixed class was mostly incorrectly classified as mod-dense SG (8%-9%) (Table 4.4; Figure 4.5). Scenario 3, in which seagrass density classes were compiled into one seagrass class, indicated high vegetation class accuracies (Precision: ≥ 94%; Recall: ≥ 89%) (Table 4.4). Here the only notable misclassification, however very low, within Scenario 3 was found between the classes macroalgae and SG/MA mixed (3.13%) and the classes

macroalgae and seagrass (2.4 %). Unclassified pixels were also present in classified maps, however consisted of only a very low number of pixels (< 0.07%) (Figure 4.5).

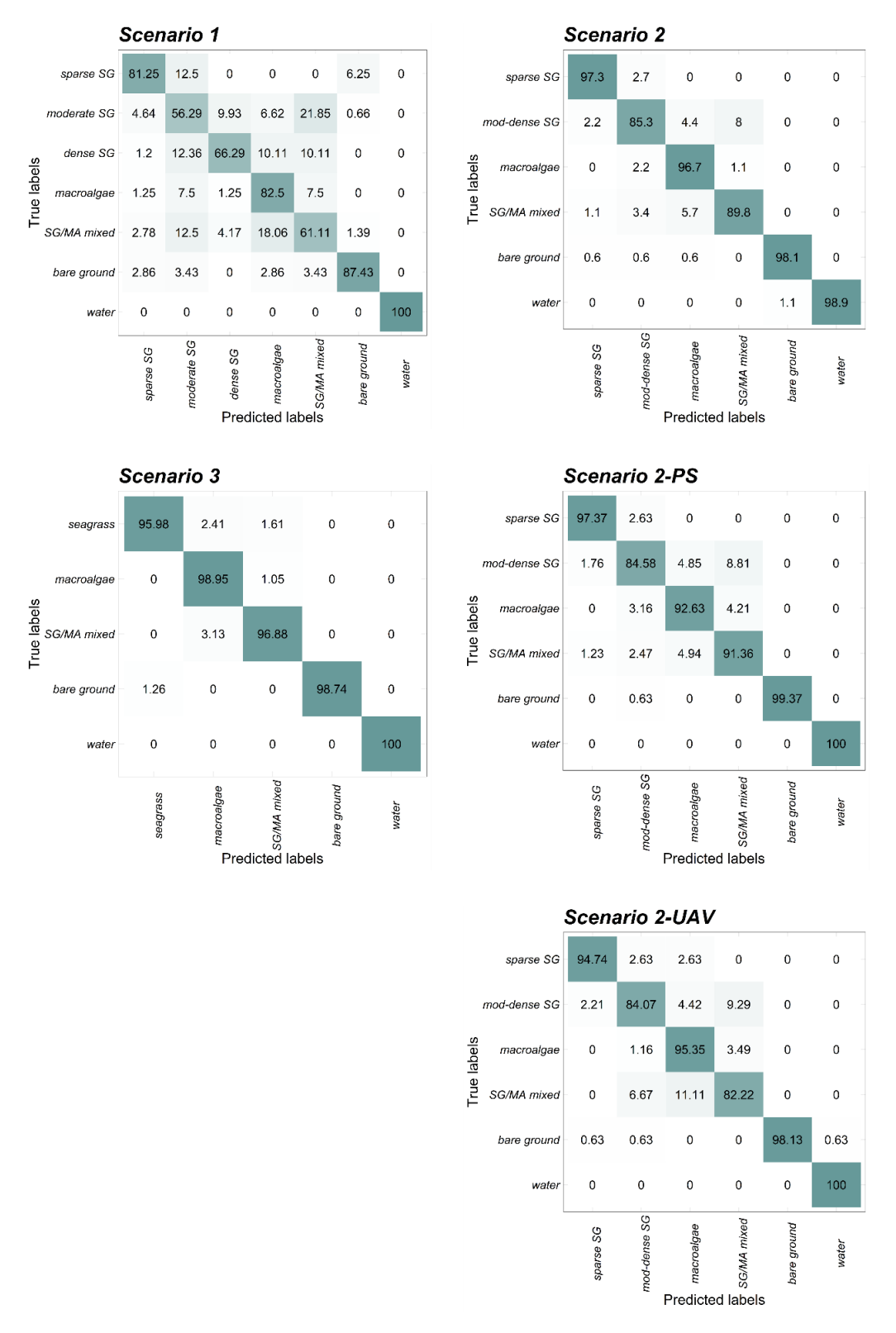


Figure 4.5. Confusion matrix outputs of the Random Forest classification method showing misclassification between true labels and predicted labels. Values represent the percent (%) numbers of misclassified pixels.

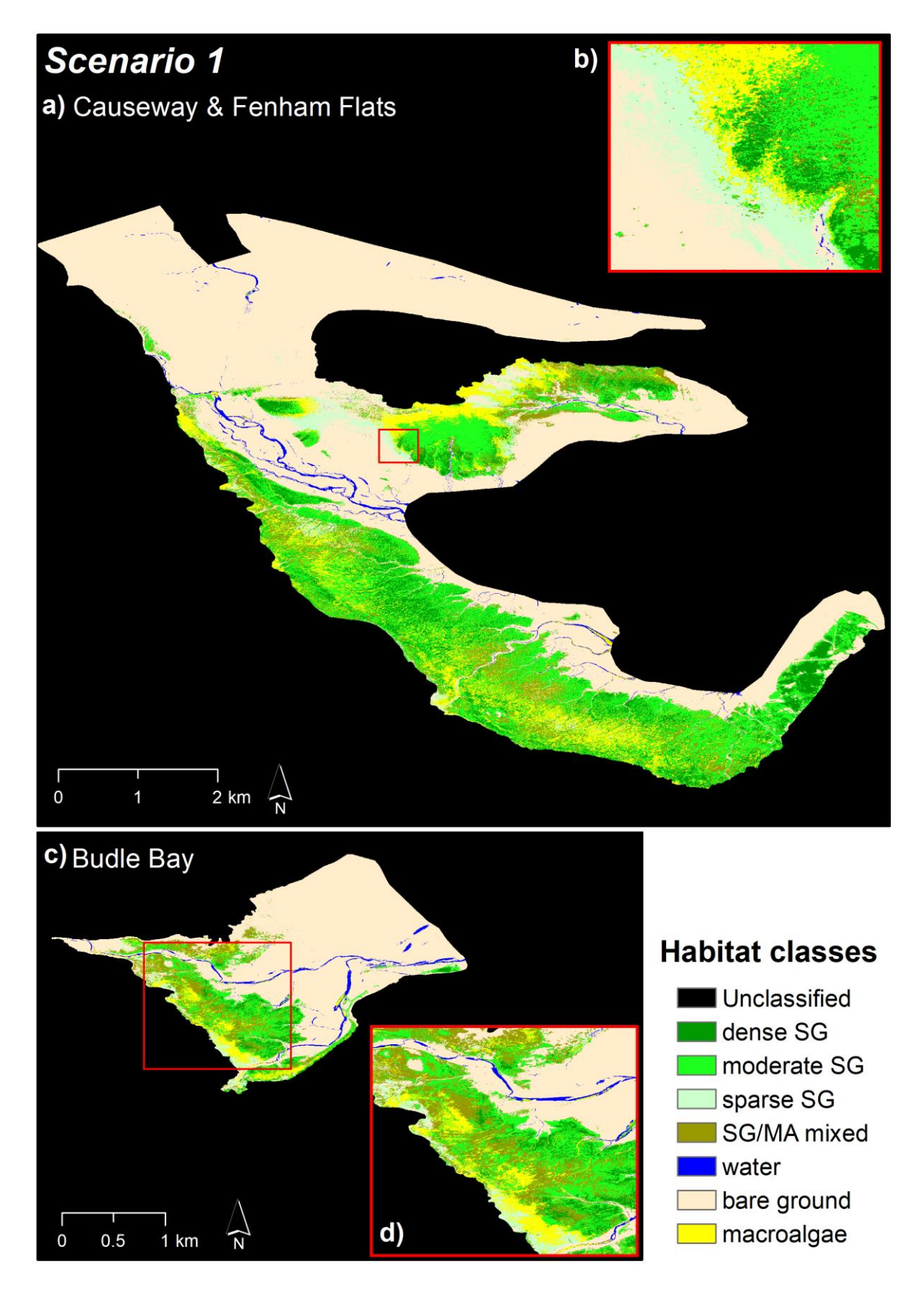


Figure 4.6. Habitat classified maps showing *Scenario 1* for: a) the Causeway area & Fenham Flats, b) a zoomed area within the Causeway area; c) Budle Bay, and d) a zoomed area within Budle Bay.

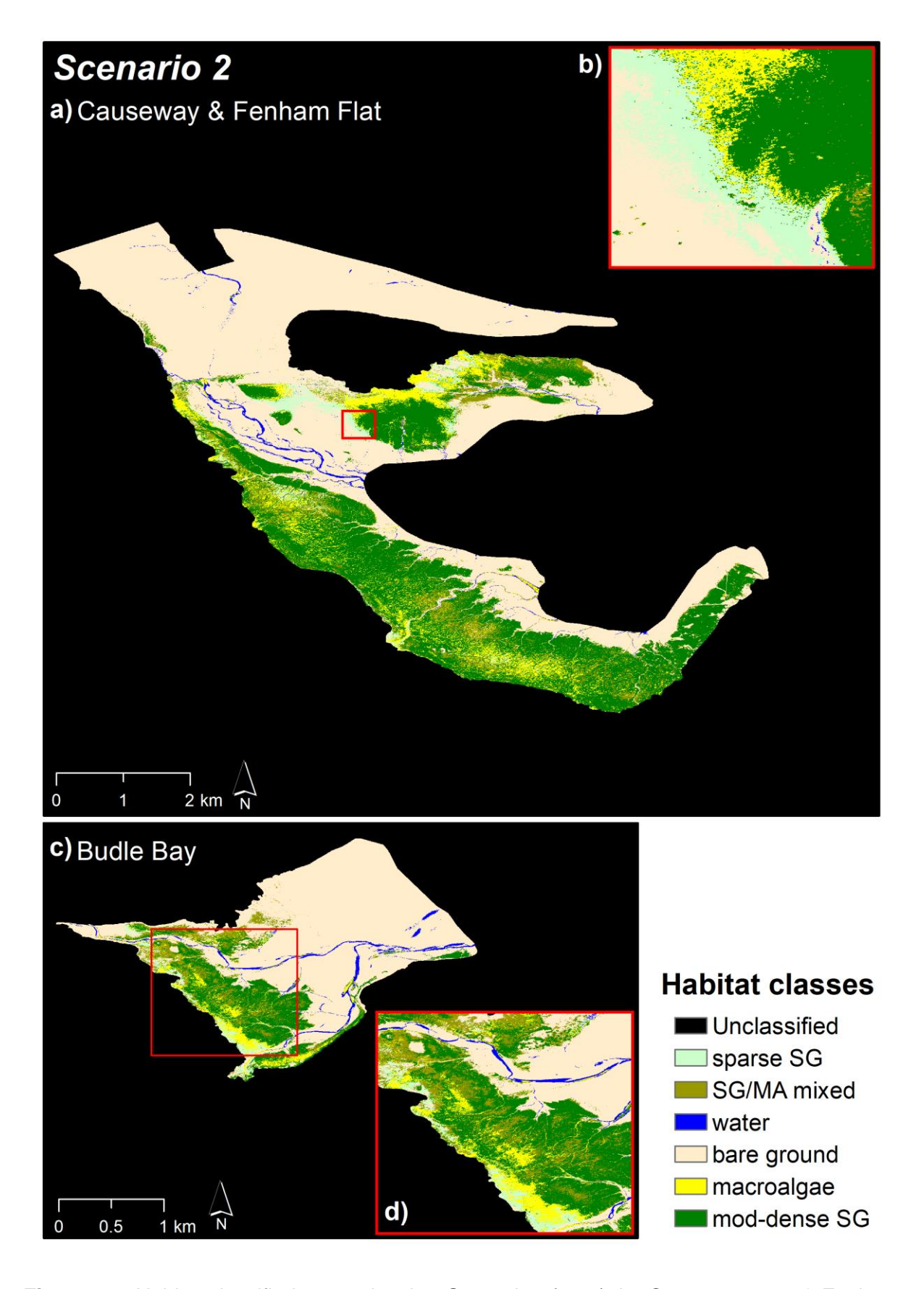


Figure 4.7. Habitat classified maps showing *Scenario 2* for: a) the Causeway area & Fenham Flats, b) a zoomed area within the Causeway area; (c) Budle Bay, and (d) a zoomed area within Budle Bay.

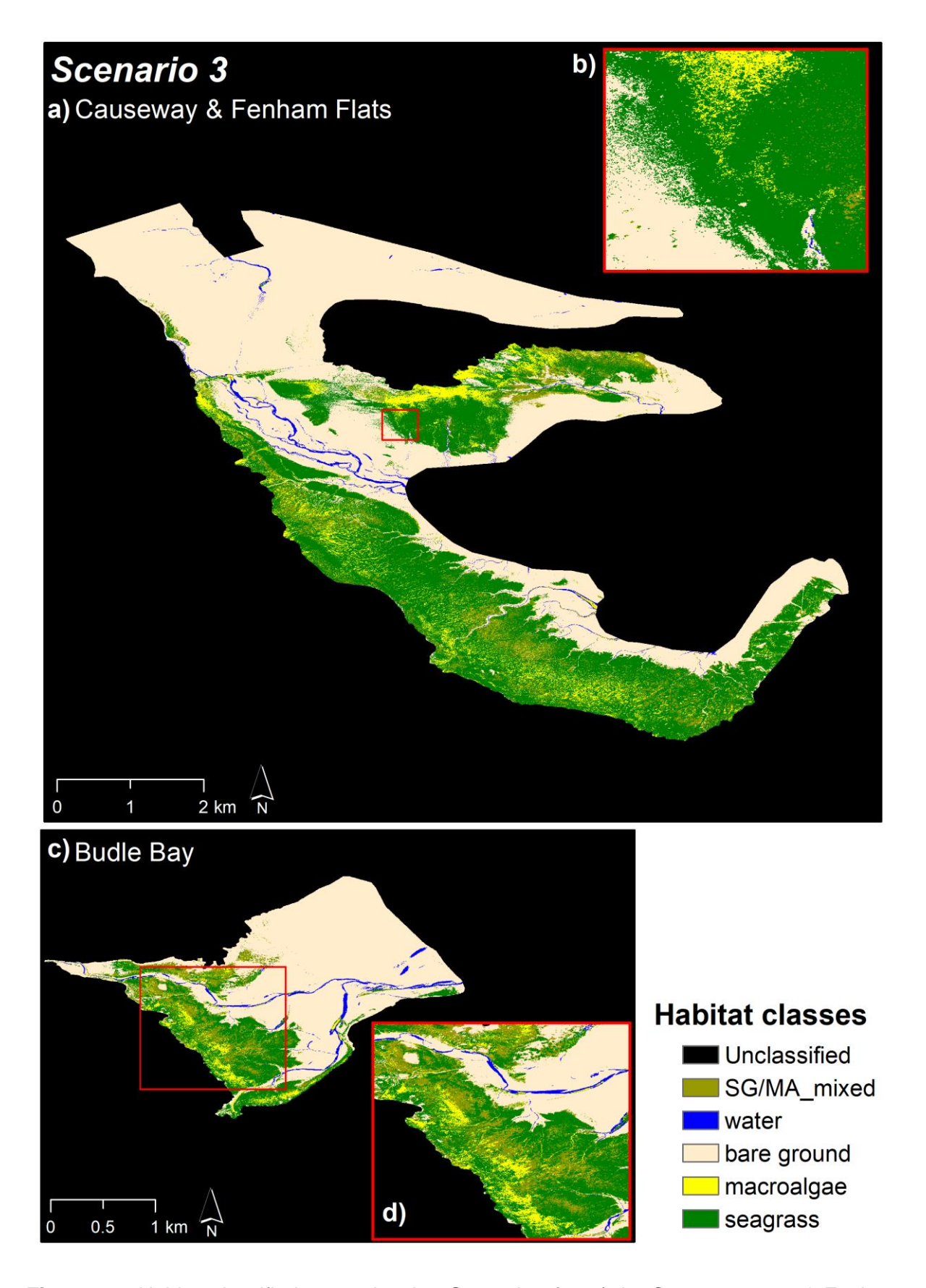


Figure 4.8. Habitat classified maps showing *Scenario 1* for: a) the Causeway area & Fenham Flats, b) a zoomed area within the Causeway area; c) Budle Bay, and (d) a zoomed area within Budle Bay.

The classified habitat maps showed a large variation in the cover of benthic classes across the investigated LNNR intertidal area (Figure 4.6 - 4.8; Figure 4.9a). Within all classified habitat maps, the benthic class water represented the lowest cover (1%) followed by macroalgae cover (~6%) and SG/MA mixed cover (6-7%). The largest benthic cover was found for bare ground (~57%), whereas seagrass cover ranged between 26% and 30% in habitat cover (Scenario 1 = 26%; Scenario 2 = 28%; Scenario 3 = 30%). However, where benthic classes of seagrass density were considered (Scenario 1 and 2, respectively), sparse SG showed the lowest cover (2%) in both the Scenario 1 and Scenario 2 maps. The Scenario 1 map indicated a moderate seagrass (mod SG) cover of 17% and a dense seagrass (dense SG) cover of 6%, which combined in Scenario 2 map indicated a similar cover of 25% (Figure 4.9a). When considering Scenario 2 only to assess and compare the vegetation classes, the largest mod-dense SG cover was found for the Fenham Flats area (67% cover) whereas Causeway area and Budle Bay showed similar coverage (48%). The largest cover in macroalgae was found in the Causeway area (22%), whereas Budle Bay indicated nearly double cover of SG/MA mixed (28%) in comparison to Fenham Flats and Causeway area in which both had similar cover (14.3% and 15.9%, respectively) (Figure 4.9b).

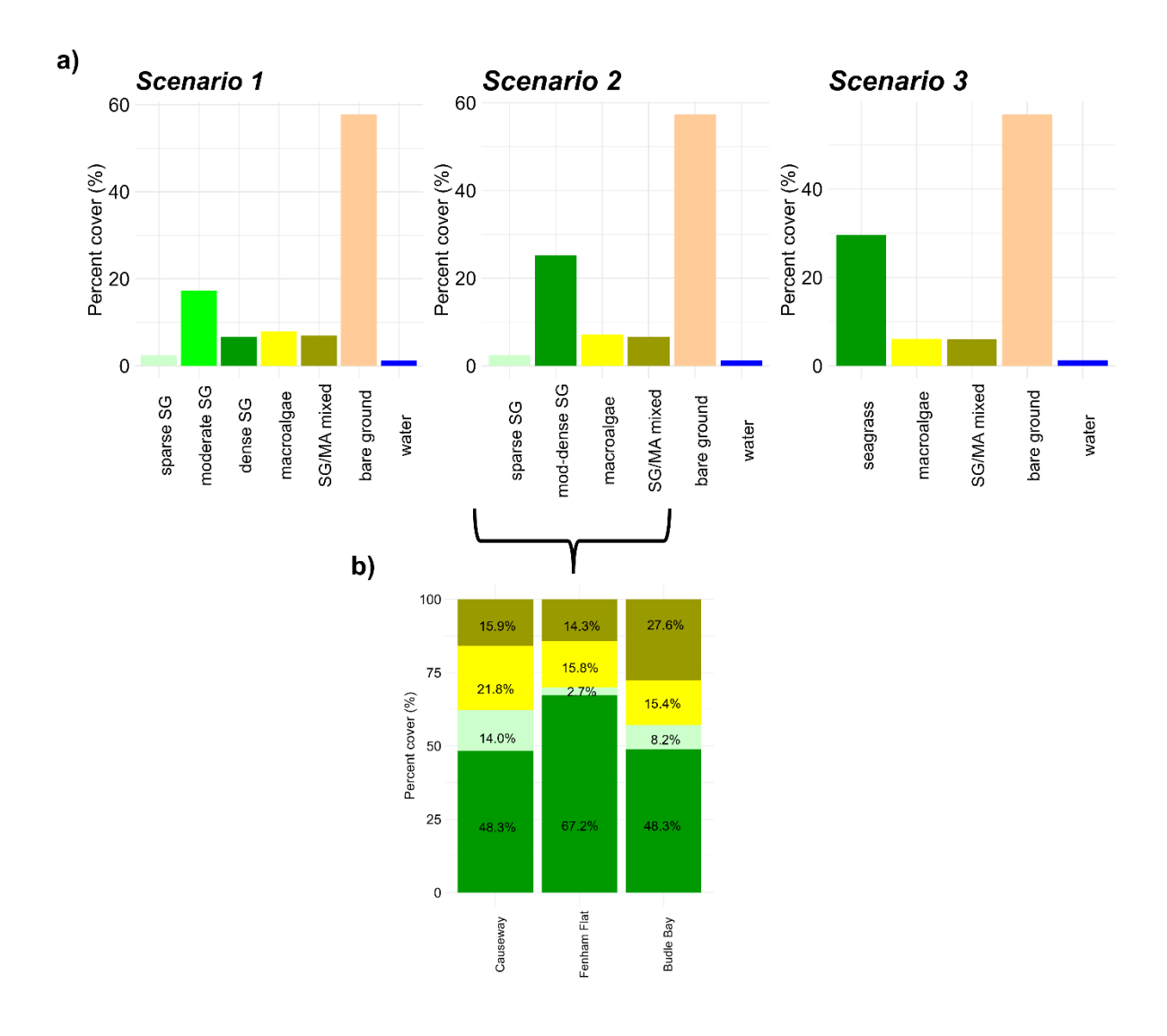


Figure 4.9. Bar plots showing percent (%) cover found for each benthic class within each Scenario habitat map across the Lindisfarne National Nature Reserve (LNNR). (b) Stacked bar of percent cover of vegetation for each investigated area including Causeway, Fenham Flats and Budle Bay for *Scenario 2*.

4.4. Discussion

In situ quadrat sampling and small area UAV derived habitat maps can only provide limited information on seagrass and macroalgae distribution patterns and their dynamic interaction. Large-scale maps that present the full extent of seagrass and macroalgae distributions, are needed for management practitioners to better understand distribution patterns and dynamics for effective management and conservation decision making (Lengyel et al., 2008; Neckles et al., 2012). Using an airborne CASI hyperspectral imagery, this Chapter demonstrated the successful accurate mapping of a complex seagrass-macroalgae environment at large scale. The Random Forest classification indicated an Overall Accuracy (OA) ranging between 76% and 97%

across all investigated Scenarios. While maps could be successfully generated, to demonstrate distributions and discriminate between seagrass and macroalgae at 1m resolution, accurate finer class level habitat maps were less consistently generated. Higher map accuracies were achieved with lower habitat class levels, (i.e., 5-class map with an OA of 97%), while the finer 7-class map showed substantially lower map accuracy with misclassification mainly observed among vegetation classes. Furthermore, this study showed that a 6-class habitat map (*Scenario 2*) using fewer spectral bands (5 and 8 bands) may be sufficient to achieve similar OA in comparison to a 23-band imagery. Similar to Chapter 3, the red edge and near infrared bands appeared to be most effective in terms of spectral separability between vegetation classes, implying that lower cost solutions may be as effective, as long as these bands are present. The ability to capture relevant information including the discrimination between seagrass and macroalgae classes at lower spectral resolution, may provide insights for more cost-effective solutions for management purposes, such as the requirement of less expensive sensors.

4.4.1. Habitat classification

Variation found in OA across map Scenarios can be primarily explained by the number of benthic habitat classes. Regardless of the habitat complexity, higher number of habitat classes commonly result in lower map accuracies (Pu et al., 2012). In this study, the complexity and similar spectral signatures across vegetation classes, especially within the 7-class habitat map (*Scenario 1*) can be explained by the observed higher misclassification found among vegetation classes including, moderate SG, dense SG, macroalgae, and SG/MA mixed, due to similar spectral reflectance (O'Neill & Costa, 2013). However, the lower misclassification found between sparse SG and the other vegetation classes, but higher misclassification found with bare ground, may be due to its inherent high percentage cover of bare ground (up to 60%) in the sparse SG benthic classes, consequently leading to spectral signature favourable for bare ground (Bargain et al., 2012).

The high OA achieved for *Scenario 2* and *Scenario 3* (OA > 90%) do not conform to other studies where hyperspectral airborne imagery has been used to map co-occurring seagrass and macroalgae environments. For example, O'Neil et al. (2011, 2013), utilised AISA airborne hyperspatial imagery (2m spatial resolution) and reduced

the spectral resolution from >200-band to 4 key bands (between 530nm and 602nm) to map eelgrass and green algae habitats along a water depth gradient and achieved an OA of 83%. Vahtmäe et al (2021) used a CASI hyperspectral imagery (1m resolution) to map higher plants (including *Zostera marina*) and green macroalgae yielding an OA of 78%. However, it is important to note that these studies were conducted on submerged vegetation and the lack of scientific references and studies for intertidal segrass-macroalgae environment when exposed do not conform the exact comparison of results. The higher map accuracies achieved in this study may be due to the lack of water column, the higher spatial resolution of 1m (Haro et al., 2022; Leblanc et al., 2021), and the additional red edge and near infrared spectral wavelengths, known to benefit spectral signature of vegetation (Schmidt & Skidmore, 2003; Zeng et al., 2021) and as demonstrated in Chapter 3.

Generally, discriminating seagrass mixed with green macroalgae can be challenging when using remote sensing, often due to required higher spatial and/or spectral resolution imagery (Phinn et al., 2018b; Veettil et al., 2020) (Chapter 3). However, the observed spectral separability between macroalgae and seagrass as found across all Scenarios, is probably related to their distinct hues of green (Figure 4.2a), that enables the separation in spectral signature between macroalgae and seagrass pixels thus the effective discrimination by the hyperspectral sensor. The distinct spectral signature between green macroalgae and seagrass have also been shown through the creation of spectral libraries using in field spectrometers and multi-and hyperspectral imagery (Davies et al., 2023), which are also comparable with spectral curves observed in this study.

While several studies have mapped algae and seagrass as separate classes (Garono et al., 2004; Hobley et al., 2021), those investigating mixed seagrass and macroalgae pixels are scarce (Benmokhtar et al., 2023). However, the utilisation of hard classifiers can lead to classification errors, particularly when near class boundaries across a continuum are used, whereby for example, seagrass densities as used in this study, are put into classes with subtle distinction between the classes. This may also explain the high misclassification between moderate SG and dense SG habitat classes (up to 12.4% of total pixels) observed in *Scenario 1*. While this issue could have been mitigated by using a fuzzy classification method as explained in Chapter 2, misclassifications were reduced by up to 14% when aggregating these two classes in

Scenario 2, which substantially improved the OA accuracy of classified habitat map (6-class habitat map).

As demonstrated in Chapter 3, and in alignment with other studies, red edge and near infrared bands can be beneficial in discriminating between vegetation types (Casal et al., 2013; Fyfe, 2003). Such patterns were also observed in this Chapter, where seagrass and macroalgae indicate large separation between spectral curves along this spectrum of wavelengths. However, the consistent reflectance in the red edge and near infrared wavelengths region, may indicate that numerous spectral bands are not needed in this region. This may be strengthened by the similar OA achieved between *Scenario 2* (23 bands) and *Scenario 2-PS* (8 bands) and *Scenario 2-UAV* (5 bands), which may suggest that potentially no benefit is acquired from a higher spectral resolution imagery beyond an 5-8 band multispectral imagery, as long as red edge and near infrared bands are included. These results may provide insights to consider more cost-effective remote sensing applications, where expensive hyperspectral sensors may not be required.

4.4.2. Ecology and implications for management

Interactions between seagrass and macroalgae in coastal ecosystems are dynamic and can be influenced by several factors. Major factors that may influence distribution and growth are related to competition for space, light and nutrients (Davis & Fourqurean, 2001). These abiotic factors may consequently determine the spatial patterns of seagrass and macroalgae proliferation and their cover (Han et al., 2016; Han & Liu, 2014; Hauxwell et al., 2001). For example, it is well known that Lindisfarne has reached a high level of pollution (Maier et al., 2009). Excessive nutrient run-off from agricultural activities surrounding the intertidal mudflats may stimulate algal growth (Howarth, 2008; Jones et al., 2018). When considering the entire intertidal area, the classified *Scenario 2* habitat map indicated the highest cover in seagrass (moddense SG and sparse SG), and lower cover in macroalgae and SG/MA mixed. However, at large spatial scales, nutrient levels may vary across the site and could explain the high variation in macroalgae and SG/MA mixed cover in the different areas. Findings here would suggest that Budle Bay may be exposed to higher nutrient levels, due to the observed high cover in SG/MA mixed.

When further assessing the Scenario 2 habitat map, macroalgae cover was mostly present around the edges of large seagrass beds, whereas the SG/MA mixed habitat class cover was mostly found within seagrass beds (Figure 4.7). The competition between macroalgae and seagrass in coastal areas is well documented (e.g., Stafford & Bell, 2006; Young et al., 2018). While the presence of macroalgae around the edges may occupy potential space, hampering seagrass proliferation, macroalgae may also be distributed across seagrass beds, covering seagrass, indicated by observed SG/MA mixed class within beds. Such dynamic proliferation of macroalgae from their source towards seagrass habitats, could be caused through for example, tidal and wave driven currents by facilitating the transportation of loose macroalgae strings/patches and their spores to settle towards seagrass habitats (Bell and Hall 1997; Holmquist 1997; Pihl et al. 1999). Other macroalgae proliferation mechanisms may be caused through physical disturbance by humans as vectors of spread (Firth et al., 2023). For example, specific to this field site, the LNNR offers a walk ("pilgrimage walk"), across the Causeway area to tourists as part of their recreational management plan. These walks may promote the transportation of macroalgae and their spores through the attachment to footwear and clothing, consequently dislodging macroalgae from its source to new locations. Such a potential distributional pattern was also observed within the Scenario 2 classified habitat map, where the walking area indicated a cover of SG/MA mixed habitat class along this path (Figure 4.10). However, it is important to consider that these patterns may also be a result of misclassification errors, whereby either seagrass or macroalgae may have been misclassified as SG/MA mixed.

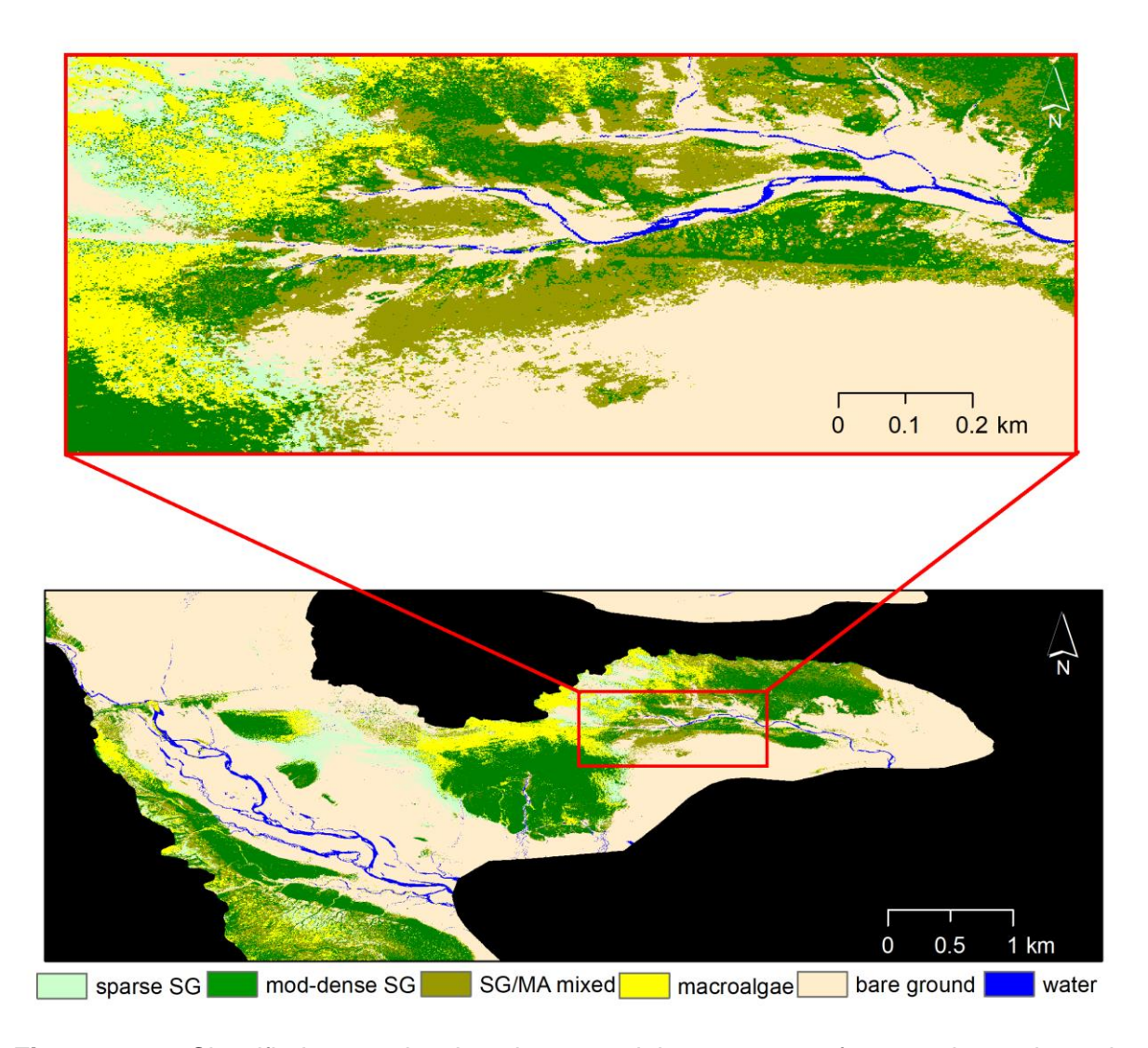


Figure 4.10. Classified map showing the potential movement of macroalgae along the Pilgrimage track (top map) across the Causeway area (bottom map).

Although, in comparison to Chapter 3, habitat mapping was not possible at very fine scales, the hyperspectral imagery provides the advantage of mapping at larger scale, enabling assessment of seagrass and macroalgae distribution patterns across the LNNR. The 1m spatial resolution may be sufficient to identify small seagrass and macroalgae patches and to assess the heterogeneity of these classes across the field site. Such information may support the assessment of seagrass and macroalgae patterns at large-scale to identify threats, and thus may provide a foundation to identify seagrass-macroalgae distributional patterns and dynamics for management practices to effectively reduce macroalgae proliferation (Ivajnšic et al., 2022). This method could enable resource managers to prioritise target areas for monitoring and management of threatened sites by utilising the produced maps as a communication tool (Nagendra et al., 2013). For example: 1) areas that indicate high cover in macroalgae e.g., Budle

Bay, could be controlled for nutrient levels by investigating the sources of nutrients in specific area; 2) in order to reduce the spread of macroalgae, tourism could be managed by reducing numbers allowed to walk across the field site; 3) maps could help to find and target macroalgae areas to be removed.

Although the produced maps can provide a useful tool to identify spatial patterns of seagrass and macroalgae cover, understanding the drivers of macroalgae cover is essential to effectively managing algal growth. Here, ancillary data including, for instance, nutrient levels (e.g., phosphorus, nitrogen) and water quality, could be combined and correlated with the generated maps to identify the root causes of algal growth. This approach could enable locally targeted management strategies for effective seagrass habitat protection.

4.4.3. Limitations, challenges, and recommendations

While this study has shown the potential of airborne hyperspectral imagery to accurately map a complex intertidal seagrass-macroalgae environment has various advantages for monitoring programmes, it comes with several limitations and challenges (Myers & Miller, 2005; Nagendra et al., 2013): (1) The limitation of classification exists within this study. To reduce classification error, a fuzzy classification such as spectral unmixing where the % cover of seagrass in pixels are taken into account rather than density classes, may reduce classification errors and improve accuracy; (2) While the collection of airborne hyperspectral imagery has been established for Lindisfarne National Nature Reserve (LNNR) monitoring, imagery acquisition and operation can be cost intensive, which often limits use for seagrass monitoring, especially for organisations with limited budget; (3) While seagrass at its peak biomass (August-September), may show less variability in cover, macroalgae may be more variable due to their fast growth rate and loose attachment to sediment. Given these dynamic interactions between seagrass and macroalgae cover, a single point survey during peak seagrass biomass may not be sufficient and representative to capture the extent of true seagrass cover. Therefore, it is recommended to acquire multiple images each year to monitor macroalgae cover to be able to capture an imagery that shows the lowest macroalgae cover, so that the full seagrass cover can be assessed. However, this in turn, would increase costs; (4) Airborne Hyperspectral images are suitable for limited coverage at local scale but may not be appropriate for

regional assessment. Although it would be suitable for monitoring known seagrass habitat locations and is currently gathered in specific locations across the UK, unknown seagrass habitats or newly established habitat may be neglected; (5) Increasing spectral resolution often comes at the expense of spatial resolution, inherently due to the high data volume and data acquisition time when using airborne hyperspectral imagery. This trade-off may limit the ability to acquire fine spatial details such as being able to achieve more accurate cover between seagrass and macroalgae. Without compromising the number of spectral bands, a higher spatial resolution imagery could be achieved by flying at lower altitude, but often this comes with other trade-offs: Flying at lower altitudes would for example, reduce the flight swath requiring more flight lines and passes and extended data acquisition time consequently associated with increasing operational costs. Given that this study showed that a 5-8 band multispectral sensor would achieve similar map accuracy results, an alternative recommendation would be to increase the spatial resolution at the expense of spectral resolution, which may provide a more cost-effective option; (6) Hyperspectral sensors require frequent calibration to ensure consistency to maintain spectral integrity and reliability. Changes in performance of the sensor may have an impact in comparing multitemporal imageries, hence making data comparison unreliable for monitoring purposes.

Despite these challenges, airborne hyperspectral imagery can be an increasingly valuable tool for conservation and management efforts for mapping and monitoring to better understand seagrass-macroalgae dynamics. Furthermore, assessing and evaluating the reliability and possibilities of using hyperspectral imagery in complex intertidal seagrass environments may become more relevant for future applications as the advancement and launch of more satellite based hyperspectral remote sensing may enable increasing accessibility and affordability in the future, such as the German Spaceborne Imaging Spectrometer Mission EnMAP (Environmental Mapping and Analysis Program) (EnMAP, 2023; Minghelli et al., 2021; Pandey et al., 2020).

4.4.4. Conclusion

This chapter demonstrated the potential of using airborne hyperspectral imagery to successfully map a large-scale complex intertidal seagrass-macroalgae environment. Results showed that using Random Forest classifier, a very high accuracy 6-class map

could be produced with the ability to discriminate between different seagrass densities and macroalgae vegetation classes using 23-spectral bands. When down sampling these spectral bands to 5-8 bands, results indicated similar outputs making these findings highly valuable information for the potential of more cost-effective and operationally viable seagrass mapping and monitoring approaches when using large-scale remote sensing applications. While major limitations using airborne imagery include limited area coverage and associated high costs, the produced maps can be used to better understand seagrass-macroalgae distributions and dynamics and may aid coastal practitioners in management decision making to promote effective protection and conservation of seagrass habitats. Finally, the procedure and methods applied in this study may provide a foundation for future work using hyperspectral imagery in intertidal seagrass habitats to improve its operational use for management practitioners.

Chapter 5: Using PlanetScope imagery to map and assess spatiotemporal intertidal seagrass-macroalgae dynamics

5.1. Introduction

Managing seagrass habitats requires accurate and regular monitoring to track changes and better understand spatial and temporal distribution patterns and dynamics and associated threats such as those posed by competing macroalgae species due to eutrophication (Neckles et al., 2012; Li et al., 2019). As demonstrated in Chapter 3, ultra-high multispectral UAV imagery can provide detailed information on seagrass habitats at species level. Such information can be highly relevant to the assessment of the spatial distribution and species dynamics at small scales. However, while UAVs facilitate regular monitoring due to their user-friendly portability and integral software and may be highly practical for managing a seagrass-macroalgae environment to some degree, they cannot practicably cover very large areas, often restricted to up to 250 km² coverage area and still require regular visits to the field site. This knowledge of spatiotemporal dynamics of seagrass habitats at larger site-scales is required for effective seagrass management and conservation. As discussed in Chapter 4, airborne hyperspectral imagery in turn can fill this gap, covering larger areas in comparison to UAV flights, with local site coverage of up to 2,300 ha (LNNR), but may not be costeffective for monitoring programmes.

Satellite imagery has been at the forefront of optical remote sensing technology for several decades, not least for the cost-effective development of continuous, large-scale habitat maps for monitoring seagrass ecosystems (Veettil et al., 2020). Depending on the detail required for mapping seagrass environments, lower spatial resolution satellite imagery may be suitable and can be acquired free of charge at low-medium spatial resolution (e.g., Sentinel (20m), Landsat (30m)), whereas higher spatial resolution imagery is available commercially (e.g., PlanetScope, WorldView 2/3 (1.8 - 3.7m)) (ESA, 2024; Apollo Mapping, 2024). Whilst commercially available imagery may generate more accurate maps of seagrass environments, previous studies tend to present only single image analyses; time series are cost-prohibitive, so outputs cannot credibly be used for monitoring purposes (e.g., Wabnitz et al., 2008; Pu & Bell, 2017; Wilson et al., 2022). Freely available satellite imagery is clearly more cost-effective and may be assembled into time series, hence has received more attention from the scientific community for seagrass monitoring applications (Hossain

et al., 2015). However, given the lower spatial resolutions involved, these studies are often confined to assessing seagrass cover at relatively coarse levels, to successfully map seasonal (Zoffoli et al., 2020; Fauzan et al., 2021), annual and decadal variation in seagrass cover and extent (Gullström et al., 2006; Zoffoli et al., 2021). For example, Fernandes et al. (2022), used Landsat imagery data to demonstrate large-scale regional change in seagrass cover over three decades, and found that the seagrass cover expanded over the mapped area in Adelaide, South Australia. This study utilised Support Vector Machine (SVM) classifier which yielded an Overall Accuracy (OA) between 83% and 95% of classified maps. In contrast, Ha et al. (2021), demonstrated decadal decline in seagrass cover by 50% from 1990-2019 in the Tauranga harbour, New Zealand, by comparing machine learning models including Random Forest, Support Vector Machine and CatBoost to evaluate their performance for seagrass habitat change detection, with all classifiers yielding an OA accuracy > 93%. Although similar time series analyses for seagrass habitat monitoring have also been tested using Sentinel-2 imagery (Zoffoli et al., 2020), its timespan is shorter, so decadal change analyses are not yet possible. However, higher spatial resolutions (10m for visible and near infrared bands) are shown to be beneficial for more detailed habitat mapping at taxonomic level (Roelfsema et al., 2014).

Lower spatial resolution imagery can prove challenging when mapping and monitoring large complex seagrass environments (Roelfsema, et al., 2013), due to for example, lack of detail in benthic features at taxonomic level, and the differentiation especially between those with similar spectral reflectance (i.e., seagrass and macroalgae), and limitations in capturing small-scale changes, which may be relevant for tracking habitat conditions in dynamic rapidly ecosystem (Kaufman & Bell, 2022). Despite the successful applications of lower-medium spatial resolution imagery, these have been mostly applied in homogenous seagrass environments for coarse habitat mapping e.g., (Topouzelis et al., 2018; Leblanc et al., 2021). Where studies have utilised Sentinel-2 imagery to map seagrass-macroalgae environments, these have most often been applied in seagrass habitats that were distinctly segregated from macroalgae cover (Hogrefe et al., 2014; Traganos et al., 2018).

To accurately map and monitor complex large-scale seagrass-macroalgae environments, cost-effective higher spatial resolution imagery is required (Légaré et al., 2022). While Unoccupied Aerial Vehicle (UAVs) and airborne hyperspectral imagery provide significant promise for various applications, the practicality of their

implementation is constrained by the scale of operations and associated costs, as demonstrated in Chapter 3 and 4. Until recently, satellites did not provide data with sufficiently high spatial resolution. The emergence of new generations of satellites with higher spatial, spectral, and temporal resolutions is changing this landscape, offering advantages such as lower costs, constellation -based operation and their potential for cost-effective monitoring programmes (Kopacz et al., 2020). Planet Lab's PlanetScope multispectral CubeSats (also smallsats) constellation, is at the forefront of this new wave of technology for earth observations. PlanetScope offers multispectral (up to 8 spectral bands) imagery data at a spatial resolution of 3m and covers the entire globe daily (Planet, 2022). Although primarily commercial, the company's commitment to open data access makes this available for research and non-commercial purposes at lower costs and often available at discounted options for non-profit organisations (Planet Labs, 2024). This makes PlanetScope a viable source for potential seagrass monitoring programmes (Schill et al., 2021), if robust analytical methods can be developed. High temporal resolution is likely to benefit temperate intertidal seagrass mapping, due to the increased probability of acquiring cloud-free images and the likelihood of capturing exposed seagrass at low tide, avoiding negative effects of water and turbidity. Furthermore, higher spatial resolution than many other lower-cost satellites may allow accurate large-scale mapping and monitoring of complex seagrass-macroalgae environments (Wicaksono & Lazuardi, 2018). Although the utilisation of PlanetScope data for seagrass mapping is still in its early stages, some studies have demonstrated its potential for complex seagrass mapping in tropical and Mediterranean submerged seagrass-macroalgae environments (Traganos & Reinartz, 2018; Wicaksono & Lazuardi, 2018) and intertidal areas (Légaré et al., 2022; Ha et al., 2023). With ongoing improvements of PlanetScope imagery such as increasing number of spectral bands and radiometric resolution, it may make mapping and monitoring of complex intertidal seagrass-macroalgae habitats possible in the near future. However, this potential is yet to be explored. Assessing the feasibility of reliable change detection analyses for PlanetScope is an important next step towards proving its potential for management applications. This Chapter evaluates a time series of PlanetScope Imagery, developing change detection methods for mapping and monitoring of complex-intertidal seagrass environments, for the first time.

The overall aim of this Chapter was to develop habitat change detection methods for PlanetScope SuperDove imagery and evaluate its potential for seagrass monitoring.

The objectives where: 1) to create an accurate time series of habitat maps at 6-class level using a Random Forest classifier (the most accurate classification combination demonstrated in Chapters 4); 2) to assess the potential for ecologically relevant change detection in the resulting classified habitat maps; 3) to discuss the potential of PlanetScope for management and monitoring programmes.

5.2. Methods and Materials

5.2.1. Ground-truth data

The study area covered the intertidal flats at Lindisfarne in their entirety (approx. 2,300 ha). Similarly, to Chapter 4, training and validation data was collected for the Causeway area only, as these were primarily generated using the three UAV classified habitat maps produced in Chapter 3; 347 random points were created across the three maps. Six habitat classes as defined in Chapter 4 were considered, including: sparse SG, mod-dense SG, macroalgae, SG/MA mixed, bare ground/shells (bare ground here after); and water. First, the UAV maps were aligned to the PlanetScope imagery. To allow the creation of regions of interest (ROIs/pixels) for generating training data, 3mx3m quadrats created from PlanetScope pixel areas, were generated in ENVI v.5.7. (Figure 5.1a). These quadrats were then used to estimate the percentage cover of seagrass, macroalgae and bare ground derived from the classified UAV maps and following the defined benthic classes in Chapter 4 including, sparse SG, mod-dense SG, macroalgae, SG/MA mixed, bare ground) were assigned to each PlanetScope pixel (Figure 5.1b). To account for potential water in the images, the class 'water' was created by assigning pixels to this category where water was available in the imagery (e.g., water streams). To increase the number of training data points and due to the limited representativeness of the entire Causeway area, additional samples from quadrat sampling, used in Chapter 4, were added to the training data. Here, the 1m x 1m quadrat geo locations were aligned onto the PlanetScope pixels, and benthic categories were assigned to respective PlanetScope pixel. Overall, 791 training pixels were created, whereby the number of training pixels varied across classes resulting in unbalanced sampling data (Table 5.1).

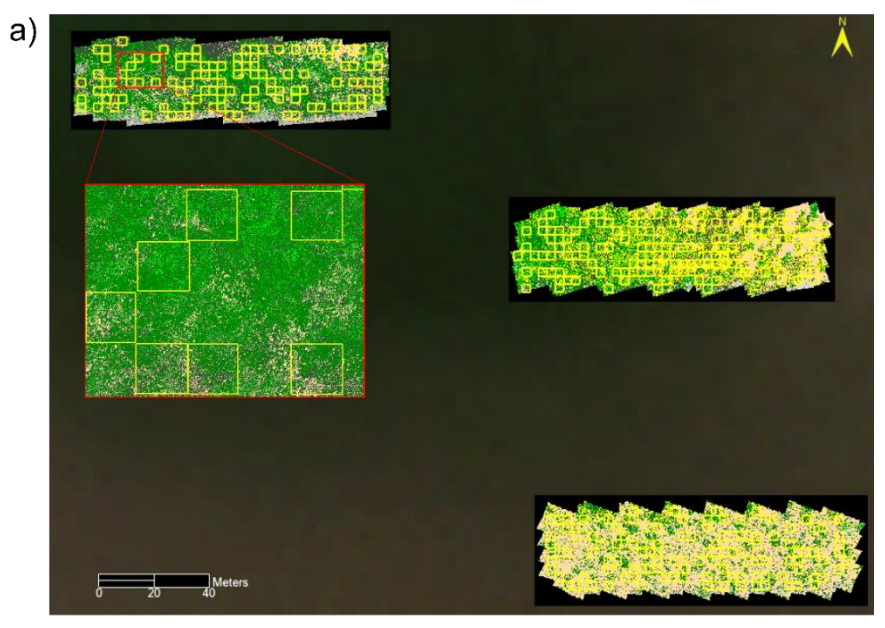




Figure 5.1. a) Random 3m pixel quadrat samples used to create b) UAV derived training data.

Table 5.1. Number of training pixels for created habitat classes.

| Habitat classes | #of training pixels |
|-----------------|---------------------|
| sparse SG | 109 |
| mod-dense SG | 205 |
| macroalgae | 120 |
| SG/MA mixed | 172 |
| bare ground | 80 |
| water | 105 |
| Total | 791 |

5.2.2. Image data acquisition

PlanetScope is a satellite constellation operated by Planet Labs Inc., a private Earth imaging company (Planet Labs, 2024). First launched in April 2016, Planet Labs have continued to deploy additional satellites and improve their constellations. Currently, Planet offers imagery from three PlanetScope satellite constellations (DoveClassic, Dove-R, and SuperDove), with differing sensor characteristics. All three sensors are available at between 3m and 4.2m, spatial resolution, and they differ in spectral resolution and length of operation (Planet, 2022) (Table 5.2). This study used their SuperDove imagery, due its higher spectral resolution and the likelihood that operations will continue, making it potentially viable for future monitoring programmes.

Table 5.2. Available PlanetScope satellite imagery data and the respective spectral resolution for each sensor.

| | DoveClassic | Dove R | SuperDove |
|------------------------|---|---|--|
| Data availability | July 2014 – April 2022 | March 2019 – April 2022 | March 2020 – present |
| Spectral resolution | Blue: 455-515nm Green: 500-590nm Red: 590-670nm NIR: 780-860nm | Blue: 464-517nm Green: 547-585nm Red: 650-682nm NIR: 846-888nm | Coastal Blue: 431-452nm Blue: 465-515nm Green I: 513-549nm Green: 547-583nm Yellow: 600-620nm Red: 650-680nm RedEdge: 697-713nm NIR: 845-885nm |

The seasonal study used four SuperDove images acquired in the year 2021 in the months of April, May, August, and October (Figure 5.2). The study of interannual variability acquired SuperDove images for the years 2020, 2021, 2022 and 2023, between July and September, as close in time as possible to quadrat and UAV surveys and seagrass peak biomass (August 2021) (Figure 5.3). All scenes were selected based on low cloud coverage and low at which the intertidal area was exposed (Table 5.3).

Table 5.3. Information acquisition of imagery used in this study including tidal stage and the approximate hours before or after low tide.

| | Date | Time | Tidal stages | Approx. hours before/after low tide |
|----------|------------------------------|----------|-----------------------------|-------------------------------------|
| Annual | 17 th Sep 2020 | 11:21:01 | Low (09:13) High (15:37) | 2.5 hrs |
| | 14 th Aug 2021 | 10:25:42 | Low (13:24) High (19:55) | 3 hrs |
| | 18 th July 2022 | 10:17:14 | Low (13:02) High (19:36) | 2.5 hrs |
| | 4 th Sep 2022 | 11:00:58 | Low (12:24) High (18:50) | 1.5 hr |
| Seasonal | 19 April 2021 | 10:27:35 | Low (13:50) High (20:38) | 3.5 hrs |
| | 31 st May 2021 | 10:26:26 | Low (13:12) High (19:55) | 2.5 hrs |
| | 14 th August 2021 | 10:25:42 | Low (13:24) High (19:50) | 3 hrs |
| | 21st Oct 2021 | 10:39:28 | Low (09:45) (High 16:10) | 1 hr |



Figure 5.2. PlanetScope's SuperDove imagery scenes utilised for seasonal time series analysis in 2021, including the months April, May, August, and October. Imageries are presented using RGB bands.

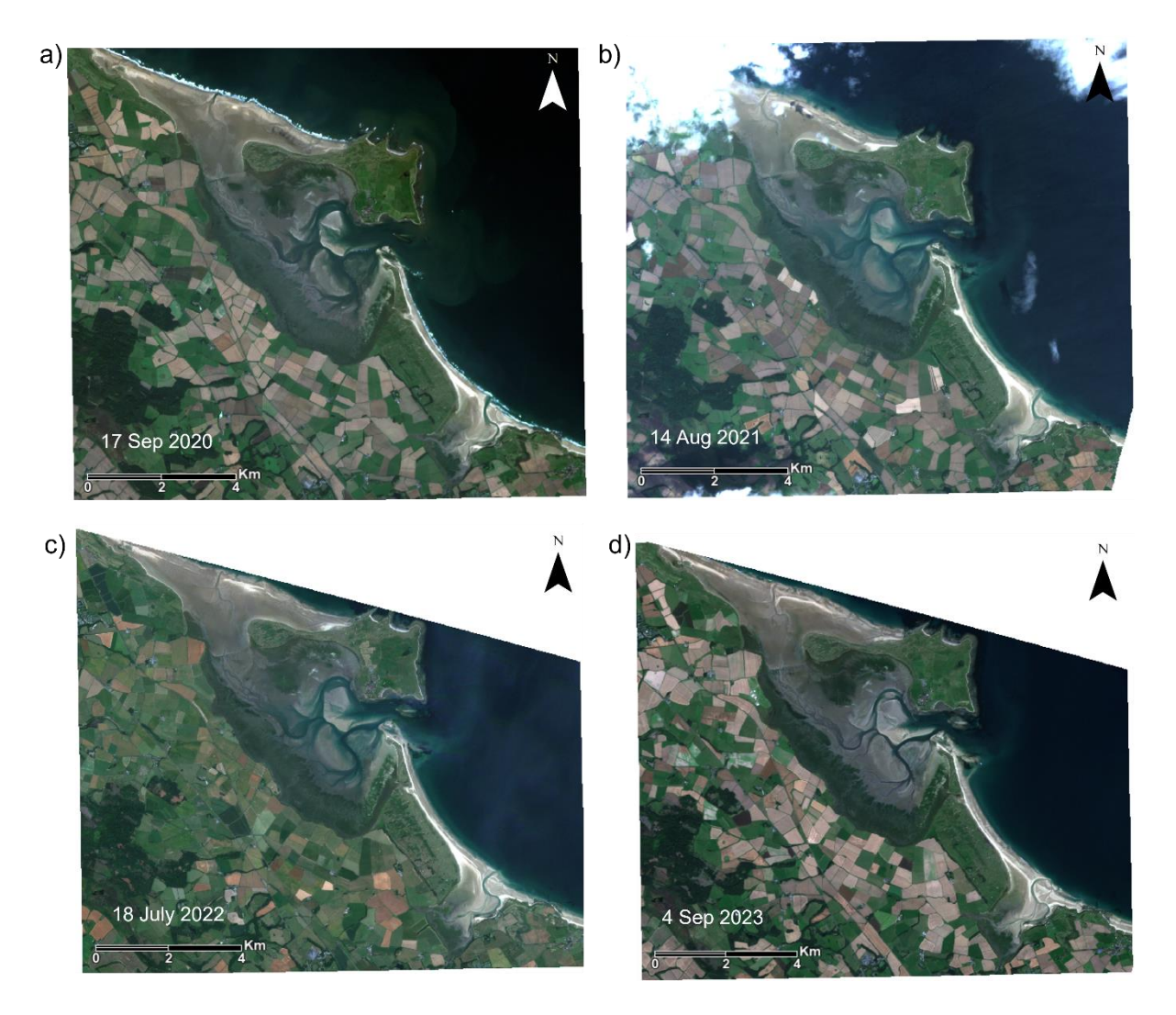


Figure 5.3. PlanetScope's SuperDove imagery scenes utilised for annual time series analyses. Imagery dates for the years including 2020, 2021, 2022 and 2023 were chosen based on availability as close as possible to ground truth surveys and seagrass peak biomass in August. Imageries are presented using RGB bands.

5.2.3. PlanetScope pre-processing

The SuperDove (PSB.SD) 3B Analytic Ortho Scene Product has an accurate geolocation with a positional accuracy of less than 10m, cartographic projection (UTM) with data processed to surface reflectance and is readily available for download from Planet Explorer platform (Planet Labs, 2023). While the ground sampling distance of the PSB.SD data is approximately 3.7m - 4.2m, the data is resampled to 3m x 3m and available in a 16-bit GeoTIFF format.

Prior to distributing the data as surface reflectance products, Planet Labs conduct multiple pre-processing stages including, radiometric calibration, geometric calibration and atmospheric correction (Planet, 2022).

To ensure comparability between imagery scenes and assess whether haze or other atmospheric interference was still present in images, the consistency of spectral reflectance was assessed prior to performing classification analysis. Four areas at which the least change in spectral reflectance was expected throughout the year and seasons were chosen for this analysis. These areas included, a white roof top, a main road, a sandy white beach near the coast to account for higher atmospheric haze and an area covered in grass near the coast.

5.2.4. Classifier and accuracy assessment

Here, multitemporal change detection involves the identification of differences in characteristics of remotely sensed imagery data over time. The post-classification change detection enables the comparison of the classified habitat maps to identify changes in benthic cover, specifically seagrass, macroalgae and SG/MA mixed in this study. For reasons explained in Chapter 4, the Random Forest (RF) classifier was also applied in this Chapter. Furthermore, the RF classifier has been successfully used for seagrass change detection studies where Overall Accuracies exceeded 80% (Ha et al., 2020; Benmokhtar et al., 2023).

To avoid the separate training of each image, which would require training data for each time point, the classification model was trained on one image (14th Aug 2021). Afterwards, the trained model was applied across all other images to create classified habitat maps. The PlanetScope imagery taken by SuperDove on 14th August 2021 was trained using RF and ENVI Modeler (ENV v. 5.7) until a stable OOB-score was reached in the process, using the out-of-bag approach, the accuracy assessment was performed, and a confusion matrix was created to assess benthic class misclassification (see Chapter 4 for detailed explanation).

Classified habitat maps are utilised to calculate and report seasonal and annual areal change detection through the time series. Differences for the entire areas, including LNNR, and Causeway, Fenham Flats and Budle Bay separately, for each vegetation class are calculated to assess cover change. The number of pixels classified for each class were calculated in percent cover and km².

5.3. Results

5.3.1. Spectral reflectance

Analysis of spectral signatures indicated the largest separability between water and all other benthic classes (J-M: 2.0). Similarly, high separability across the spectrum were found between bare ground and all the vegetation classes (mod-dense SG, sparse SG, macroalgae, and SG/MA mixed) (J-M: 1.7-1.9) (Table 5.4). All vegetation classes indicated a peak spectral reflectance between 447nm and 620nm and a steep increase from 650nm to 885nm (Figure 5.4). Among the vegetation classes, the largest separability was found between macroalgae and the SG classes (mod-dense SG and sparse SG, respectively; J-M: 1.4) (Table 5.4). While this separation was found across the spectrum between sparse SG and macroalgae, the major separation between mod-dense SG started at 447nm and was largest at 885nm in the near infrared band (Figure 5.4). Sparse SG also showed a moderate separation across the spectrum with mod-dense SG and SG/MA mixed. The least separability was found between SG/MA mixed and macroalgae (J-M: 0.5) (Table 5.4), with no indication of separation of spectral curves across the spectrum. Low separation was also found between SG/MA mixed and mod-dense SG (J-M: 1.1). Here, the greatest separability was from 457nm to 885nm. (Figure 5.4).

Table 5.4. Results of Jeffries – Matusita (J-M) index, indicating spectral pair separability of benthic habitat classes.

| Benthic pair classes | | | J-M value |
|----------------------|---|--------------|-----------|
| SG/MA mixed | - | macroalgae | 0.5 |
| SG/MA mixed | - | mod-dense SG | 1.1 |
| sparse SG | - | SG/MA mixed | 1.2 |
| sparse SG | - | mod-dense SG | 1.3 |
| sparse SG | - | macroalgae | 1.4 |
| macroalgae | - | mod-dense SG | 1.4 |
| bare ground | - | SG/MA mixed | 1.7 |
| bare ground | - | macroalgae | 1.8 |
| bare ground | - | sparse SG | 1.8 |
| bare ground | - | mod-dense SG | 1.9 |
| water | - | SG/MA mixed | 2.0 |
| water | - | mod-dense SG | 2.0 |
| water | - | sparse SG | 2.0 |
| water | - | macroalgae | 2.0 |

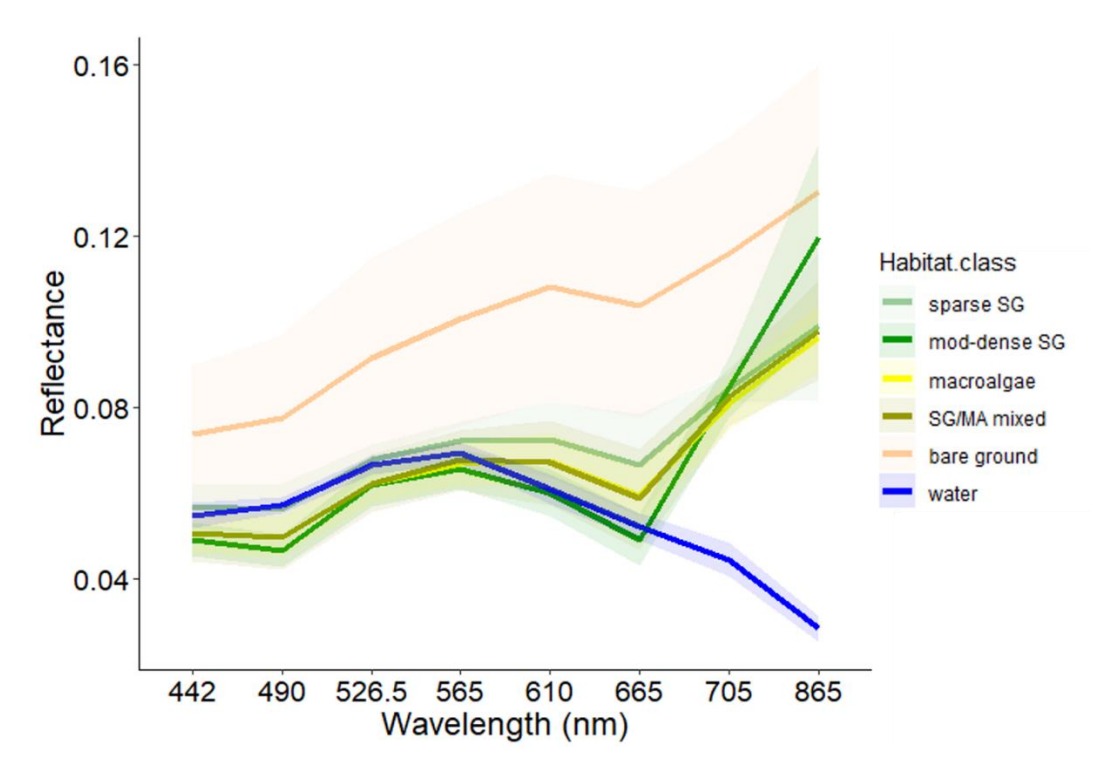


Figure 5.4. Spectral reflectance curves of benthic class training data. The shaded area represents ± standard deviation.

When assessing spectral reflectance of the roof, road, grass, and sand area to check seasonal and annual majority of reflectance curves indicated reasonable consistency, except for the annual roof imageries comparisons (Figure 5.5). Here the year 2023 indicated significant differences in spectral reflectance in comparison to all other years. This may possibly be due to for example, accumulation of dirt or filamentous vegetation/algae, or replacement or repainting of roof. Some variability between years and months in spectral reflectance were also found for the sand images. This variability may be for example, due to whether the sand area was dry or wet.

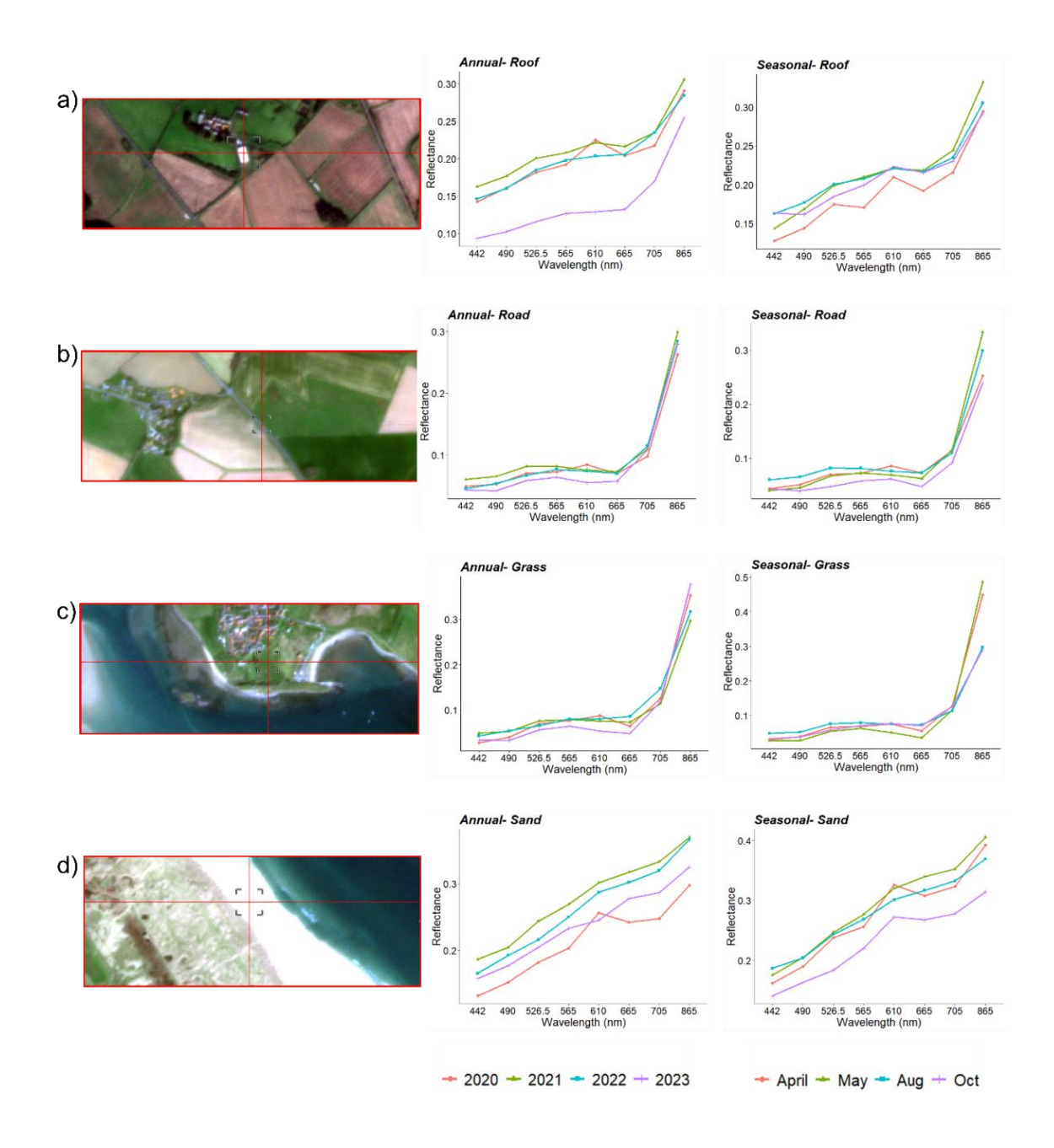


Figure 5.5. Areas chosen to assess the consistency in spectral reflectance across time series imagery. a) a white roof top; b) main road; c) sandy beach area; and d) vegetation area.

5.3.2. Accuracy assessment and habitat classification

Results of the trained random forest classifier indicated an Overall Accuracy (OA) of 94% with an OOB score of 72% when using parameters of 200 ntree; 9 max_depth of trees and 3 mtry features (Table 5.5). The highest benthic class accuracy was found for the classes water and bare ground (Precision: 100%), followed by the benthic class SG/MA mixed (Precision: 97.3%; Recall: 84%), which showed a very low percentage of pixel misclassification with mod-dense SG and macroalgae (1.3 %) (Figure 5.6). The

habitat classes macroalgae and mod-dense SG indicated the same class accuracy (Precision: 91.3%; Recall: 97% and 98% respectively). Both macroalgae and mod-dense SG were mostly misclassified as sparse SG (3.1% and 5.2%, respectively) and SG/MA mixed (3.9% and 2.6%, respectively). Among all vegetation classes, sparse SG showed the lowest class accuracy (Precision: 85.3%; Recall: 85%), which was mostly incorrectly classified as SG/MA mixed (Figure 5.6; Table 5.5). Using this trained model, seasonal and interannual classified habitat maps could be successfully created (Figure 5.7; Figure 5.9).

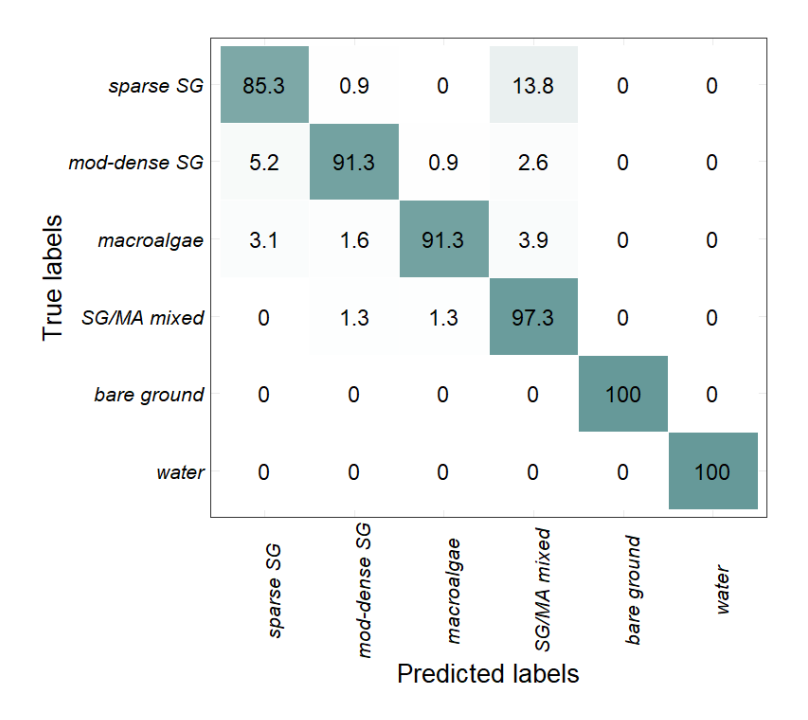


Figure 5.6. Confusion matrix output of the Random Forest (RF) classification method showing the correctly classified pixels (green diagonal values) and misclassification between true labels and predicted labels. Values represent the percent (%) numbers of pixels.

Table 5.5. Accuracy results of the Random Forest classification for the train imagery 14th August 2021.

| Habitat class | Precision | Recall | F1-score |
|--|--|-------------------------------------|-------------------------------------|
| sparse SG mod-dense SG macroalgae SG/MA mixed bare ground water | 0.85 0.91 0.91 0.97 1.0 1.0 | 0.85 0.98 0.97 0.84 1.0 | 0.85 0.94 0.93 0.90 1.0 |
| Overall Accuracy = | 0.94 | | |

5.3.3. Habitat change detection

When assessing the classified seasonal and interannual habitat maps, results indicated large variation in the distribution and cover of all vegetation classes across the time series and between the different areas across the LNNR (Causeway, Fenham Flats and Budle Bay, respectively) (Figure 5.7; Figure 5.9).

The seasonal change detection assessment revealed an initially low cover 0.01 km² of seagrass in April, a slight increase change in cover by May (0.05%) and the largest increase cover change between May and August (15%), with seagrass cover reaching 2.9 km² across the site. This cover then declined by 11% to 0.9 km² by October. Results appear promising, as they align with expected seasonal trends. In August, the largest cover of Seagrass was found for Fenham Flats (2.2 km²) with an increase cover change of 17%, followed by the Causeway area (0.4 km; 23%) and Budle Bay (1.3%) (Figure 5.8a; Figure 5.11). The habitat classes SG/MA mixed and macroalgae indicate opposing patterns in the months before and after August. April shows dominant SG/MA mixed cover (5.2 km²) across all three intertidal areas. While macroalgae was found to be lower in cover, it was notably distributed around the inner edges of the intertidal area in April (Figure 5.8b; Figure 5.11). However, cover declined substantially in May by 14% for SG/MA mixed and 4% for macroalgae, in all three areas, but increased by up to 5% in August during peak seagrass biomass season, with a cover of 3.2km2 and 1.1 km², respectively (Figure 5.8b, c; Figure 5.11). Notably, here, the Causeway showed the largest increase in SG/MA mixed by 5% and with a cover of 0.9 km², whereas Fenham Flats contained the largest increase in macroalgae cover (by 5%) of 0.6 km² area covered (Figure 5.8b; Figure 5.11). In October, the LNNR was dominated by macroalgae, and SG/MA mixed across all areas (2.6 km² and 6.6 km², respectively), whereas seagrass declined to 1 km² in total cover. Here, Fenham Flats showed the highest increase in SG/MA mixed cover (19%) with a total cover of 4.1 km², the Causeway area showed similar increase cover of macroalgae and SG/MA mixed (8% and 6%, respectively) and Budle Bay had the lowest cover for both classes (0.2%-1.2%). In comparison to Causeway area and Fenham Flats, Budle Bay indicated very low change cover across all benthic classes (< 1.3%). Although benthic classes within Budle Bay remained stable in cover across the season, notably the vegetation class SG/MA mixed was found to be more than double in cover, in comparison to all other benthic classes across all investigated months (Figure 5.8b, c; Figure 5.11). Overall,

the entire LNNR area experienced an increasing trend in all observed vegetation classes across the season in the year 2021 (Table 5.6).

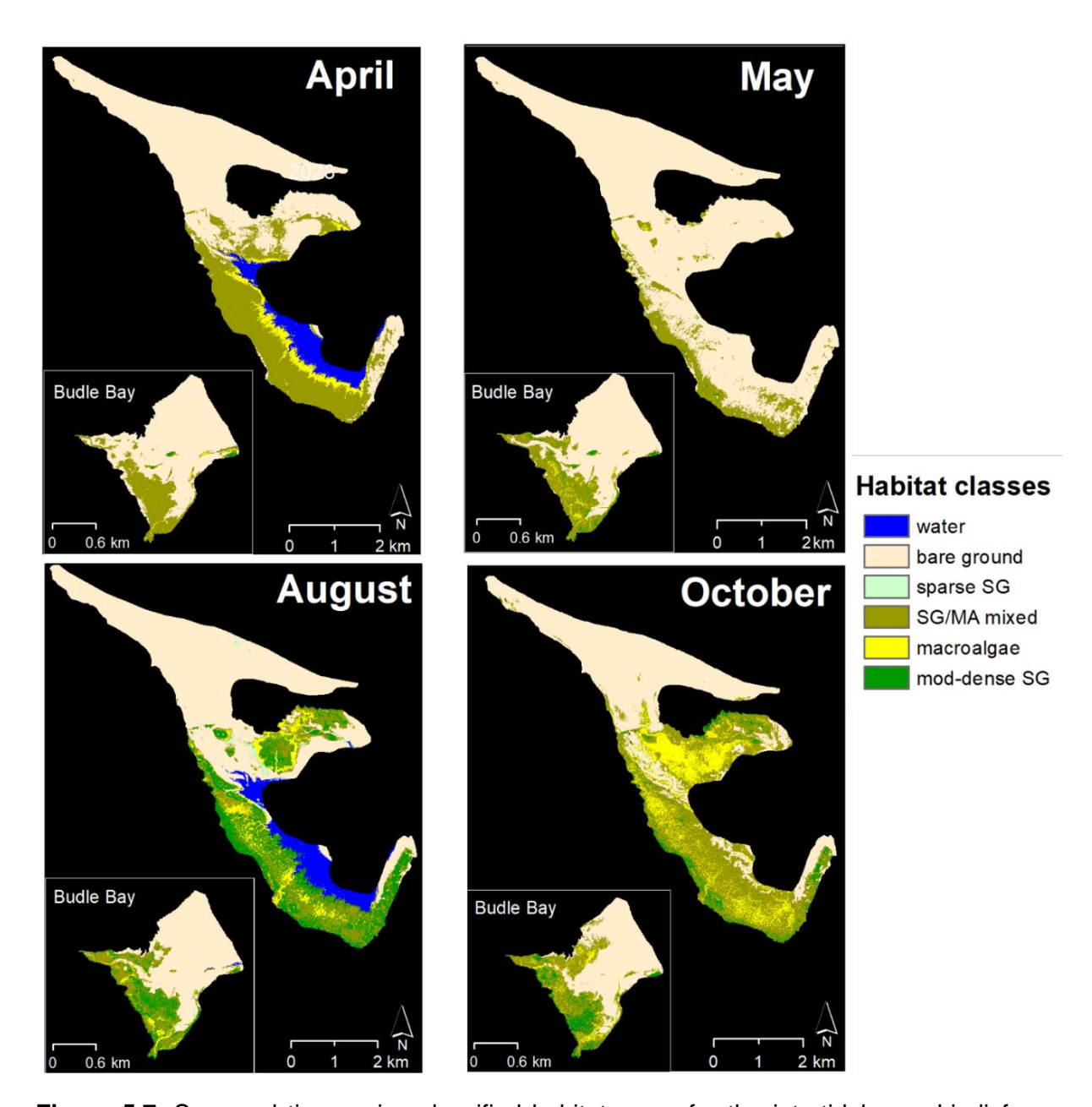


Figure 5.7. Seasonal time-series classified habitat maps for the intertidal area Lindisfarne National Nature Reserve (LNNR), using Random Forest classification method.

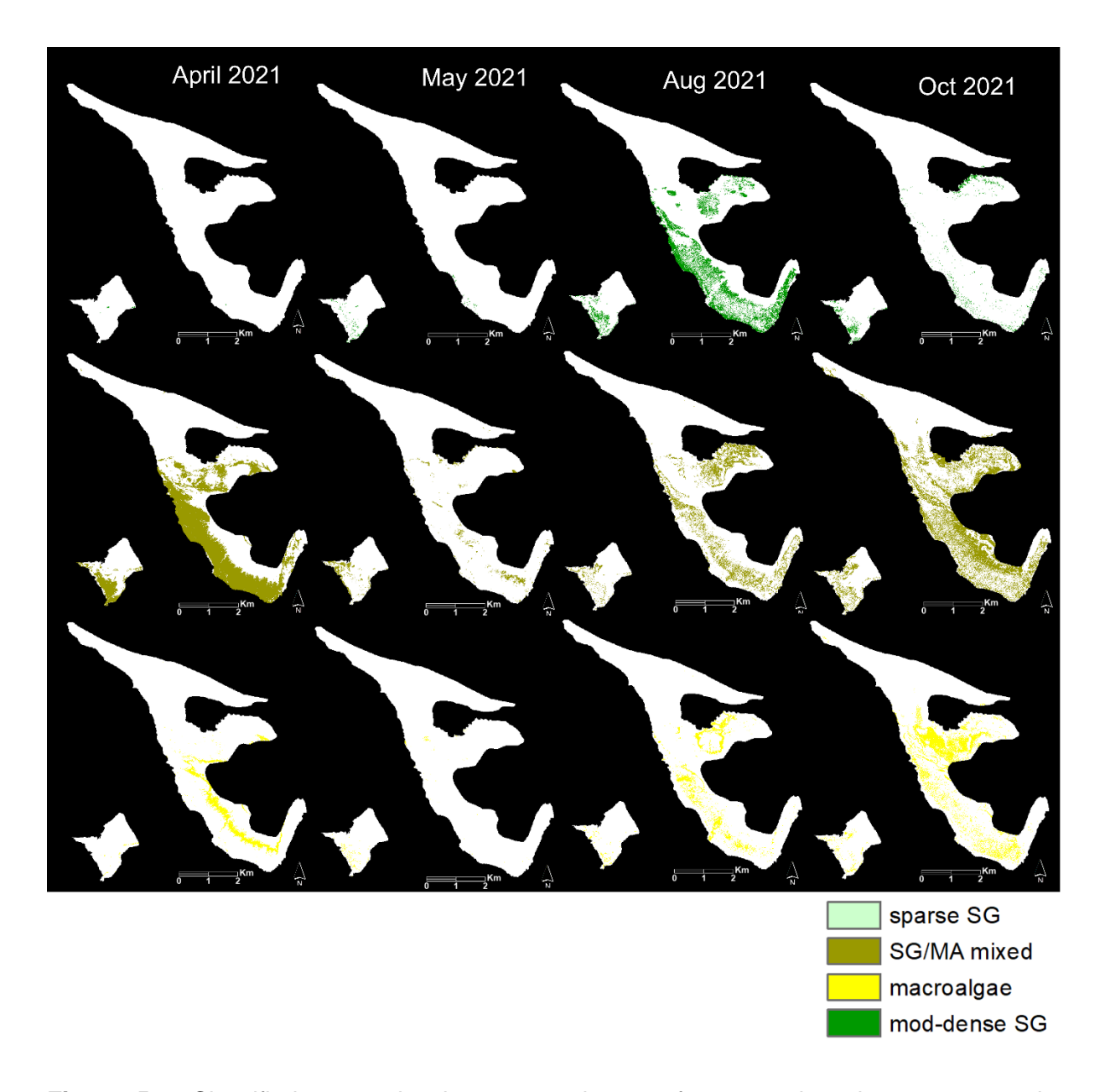


Figure 5.8. Classified maps showing seasonal cover for vegetation classes separately, including seagrass (sparse SG and mod-dense SG), macroalgae and SG/MA mixed distributions in the intertidal LNNR area.

The 2020 image in the interannual time series was analysed first revealing the largest cover as SG/MA mixed (6.9 km²) followed by seagrass (mod-dense SG: 1.8 km²; sparse SG: 0.01km²) and macroalgae (1km²) (Figure 5.10; Table 5.11). The following year, 2021, the LNNR saw a significant drop in SG/MA mixed cover by 19% with a decline of areal coverage by (3.2 km²) and an increase of seagrass by 7% (2.9 km²). Here, the largest decline in SG/MA mixed was found for Fenham Flats (by 19%), followed by Causeway (8%) and Budle Bay (0.03%) (Figure 5.10; Figure 5.11). Fenham Flats also appeared to support the largest increase in seagrass cover (2.2)

km²) while the Causeway and Budle Bay experienced slight declines in seagrass cover (by 2% and 1%, respectively). Opposing results were generated for the year 2022 in the LNNR area with a notable drop in seagrass cover by 8% with an aerial coverage of 1.4 km². The largest decline was seen at Fenham Flats (7.3%), with a smaller decrease observed in the Causeway and Budle Bay areas (3%) (Figure 5.10a; Figure 5.11). The year 2023 again marked an increase in seagrass cover by 21% and a decline in SG/MA mixed by 8% in comparison to the year 2022, with Fenham Flats and Causeway area indicating the largest change (20% and 8% increases in cover, respectively). Except for 2021, which showed very low macroalgae cover across all areas, change in macroalgae remained relatively consistent and low, ranging between 1-2% change in cover (Figure 5.10a, c; Figure 5.11). While sparse SG and macroalgae cover maintained low and consistent coverage across the time series and the areas. notably, SG/MA mixed and mod-dense SG showed higher dynamics with opposite trends in coverage for most investigated years. However, this pattern was not observed for Budle Bay, which showed consistent cover across the time series for all benthic classes (Table 5.10; Table 5.6). Here, also, higher cover in SG/MA mixed was found across all years in comparison to all other vegetation classes. Overall, the LNNR experienced a significant increase in seagrass, a slight increase in macroalgae and a significant decline in SG/MA mixed over the observed time series (Table 5.6).

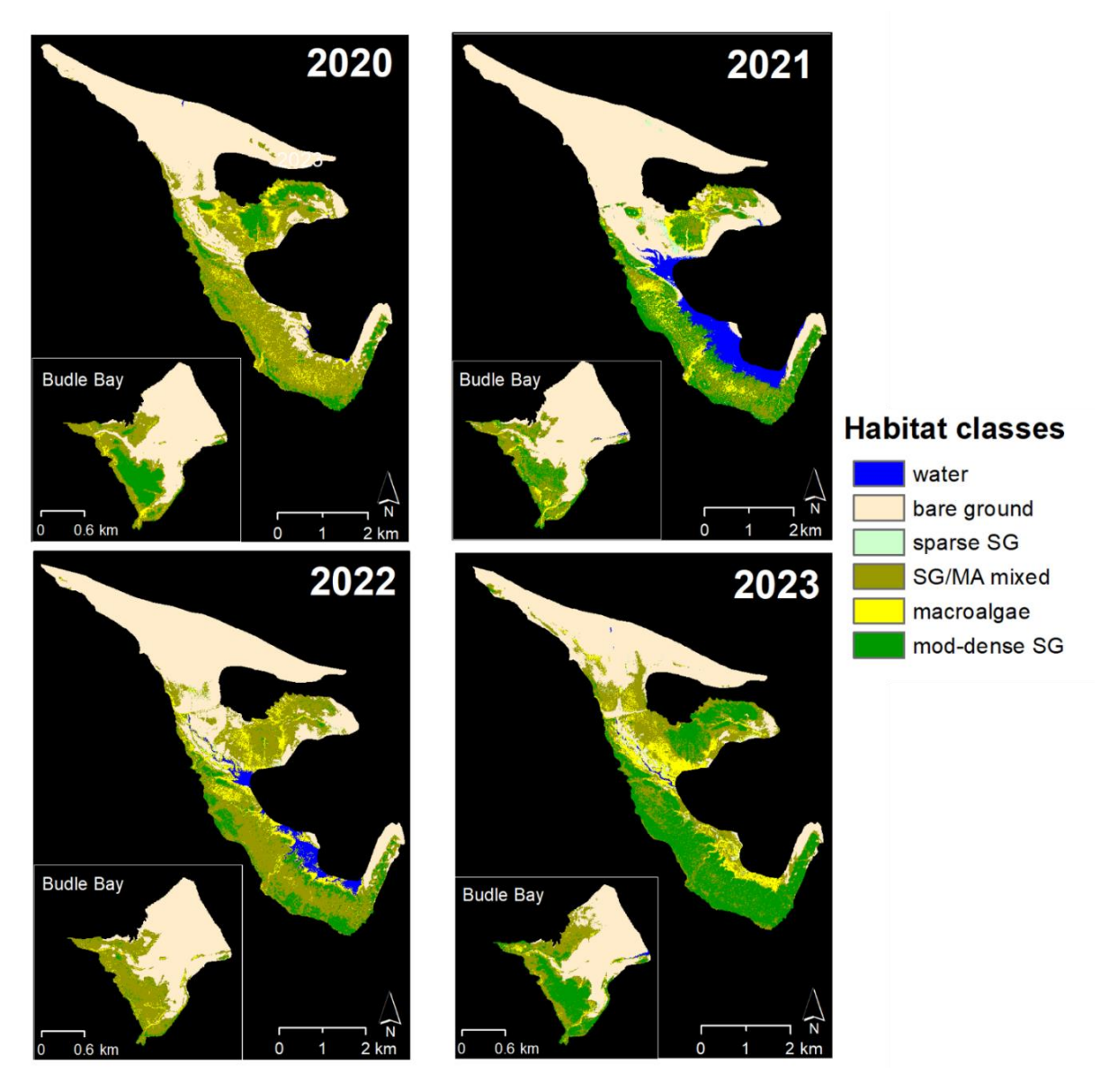


Figure 5.9. Interannual time-series classified habitat maps of the intertidal area Lindisfarne National Nature Reserve (LNNR), using Random Forest classification method.

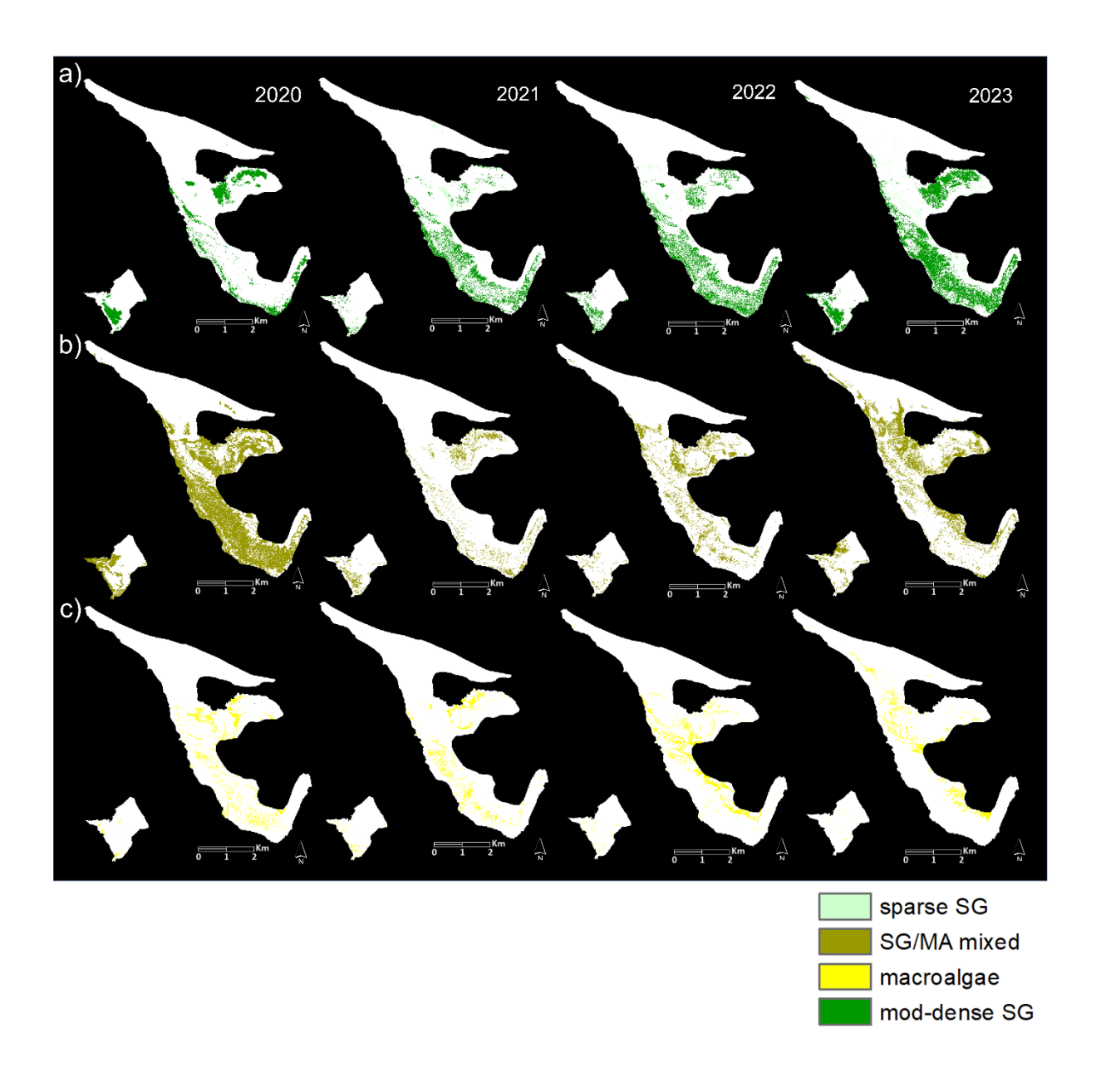


Figure 5.10. Classified maps showing interannual cover for vegetation classes separately in seagrass (sparse SG and mod-dense SG), macroalgae and SG/MA mixed distributions in the intertidal LNNR area.

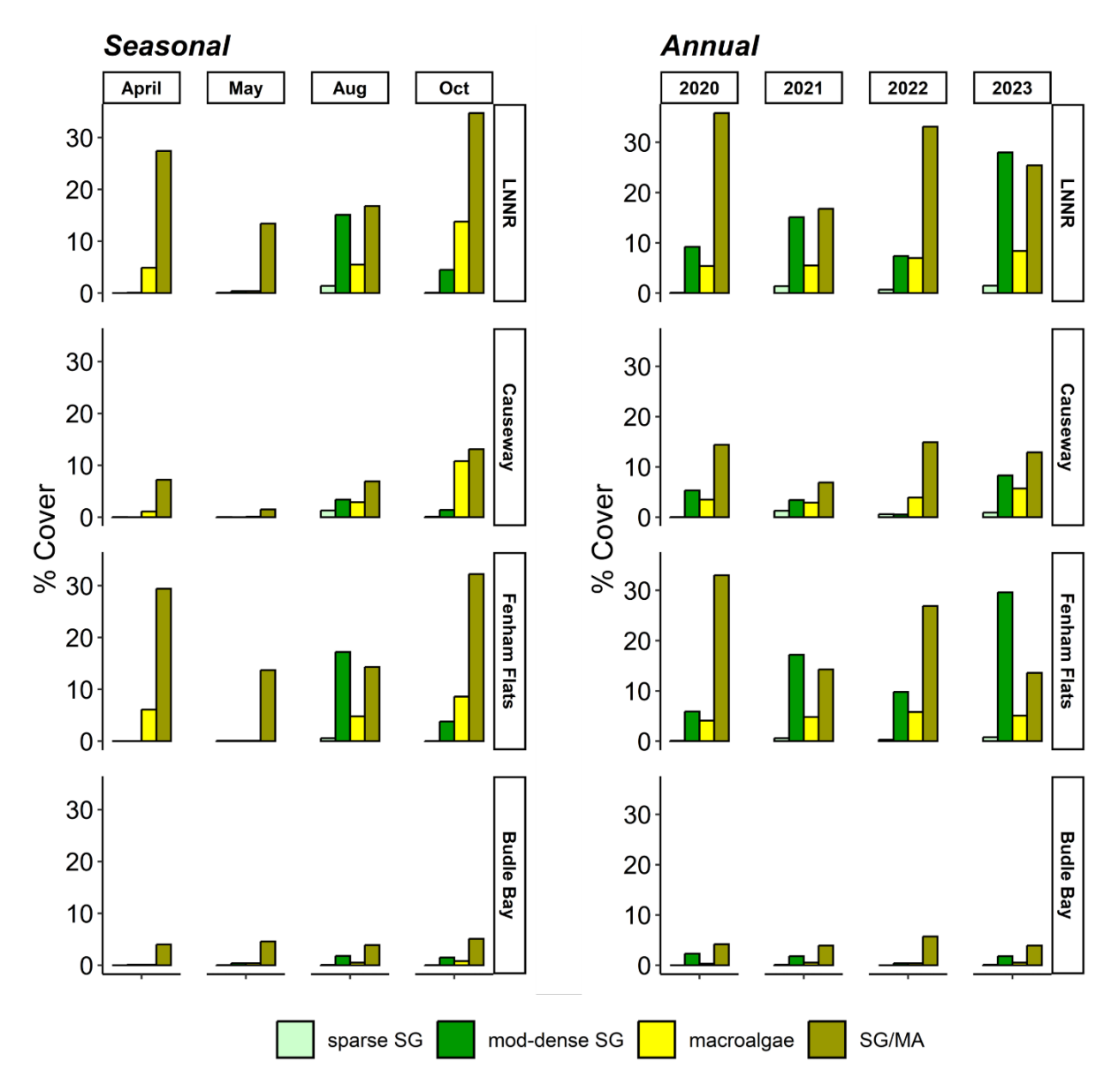


Figure 5.11. Seasonal and interannual percent change in habitat class cover for LNNR, as well as for the different investigated areas (Causeway, Fenham Flats, and Budle Bay, respectively) separately.

Table 5.6. Seasonal and interannual total habitat class cover (km²) change for the investigated LNNR and different areas separately including Causeway, Fenham Flats and Budle Bay.

| | | Seasonal | | | Annual | | | | |
|-----------------|--------------|----------|--------|--------|---------|------------|-------|-------|-------|
| | | April | May | August | October | 2020 | 2021 | 2022 | 2023 |
| LNNR | | | | | | | | | |
| | water | 1.4 | 0.0001 | 1.4 | 0.02 | 0.04 | 1.4 | 0.7 | 0.1 |
| | bare ground | 11.5 | 16.4 | 10.3 | 8.9 | 9.5 | 10.3 | 9.2 | 7.0 |
| | sparse SG | 0.004 | 0.01 | 0.3 | 0.02 | 0.01 | 0.3 | 0.1 | 0.3 |
| | Sg/MA mixed | 5.2 | 2.6 | 3.2 | 6.6 | 6.9 | 3.2 | 6.3 | 4.8 |
| | macroalgae | 0.9 | 0.1 | 1.1 | 2.6 | 1.0 | 1.1 | 1.3 | 1.6 |
| | mod-dense SG | 0.01 | 0.1 | 2.9 | 0.9 | 1.8 | 2.9 | 1.4 | 5.3 |
| Causeway | | | | | | | | | |
| | water | 0.2 | 0.0 | 0.2 | 0.01 | 0.003 | 0.2 | 0.1 | 0.03 |
| | bare ground | 2.8 | 3.8 | 2.0 | 0.7 | 1.0 | 2.0 | 1.3 | 0.4 |
| | sparse SG | 0.003 | 0.001 | 0.2 | 0.01 | 0.004 | 0.2 | 0.1 | 0.1 |
| | Sg/MA mixed | 0.9 | 0.2 | 0.9 | 1.7 | 1.8 | 0.9 | 1.9 | 1.7 |
| | macroalgae | 0.1 | 0.02 | 0.4 | 1.4 | 0.4 | 0.4 | 0.5 | 0.7 |
| | mod-dense SG | 0.0001 | 0.0003 | 0.4 | 0.2 | 0.7 | 0.4 | 0.1 | 1.1 |
| Fenham Flats | | | | | | | | | |
| i iats | water | 1.2 | 0.0001 | 1.2 | 0.001 | 0.03 | 1.2 | 0.5 | 0.03 |
| | bare ground | 0.9 | 4.9 | 0.7 | 1.0 | 1.1 | 0.7 | 0.6 | 0.4 |
| | sparse SG | 0.0009 | 0.01 | 0.1 | 0.01 | 0.01 | 0.1 | 0.0 | 0.1 |
| | Sg/MA mixed | 3.8 | 1.8 | 1.8 | 4.1 | 4.2 | 1.8 | 3.5 | 1.7 |
| | macroalgae | 0.8 | 0.01 | 0.6 | 1.1 | 0.5 | 0.6 | 0.7 | 0.6 |
| | mod-dense SG | 0.001 | 0.01 | 2.2 | 0.5 | 8.0 | 2.2 | 1.3 | 3.8 |
| Budle Bay | | | | | | | | | |
| | water | 0.001 | 0.0 | 0.004 | 0.01 | 0.000 1 | 0.004 | 0.001 | 0.004 |
| | bare ground | 1.6 | 1.4 | 1.3 | 1.2 | 1.3 | 1.3 | 1.3 | 1.3 |
| | sparse SG | 0.0001 | 0.004 | 0.0 | 0.002 | 0.000 1 | 0.01 | 0.003 | 0.01 |
| | Sg/MA mixed | 0.5 | 0.6 | 0.5 | 0.7 | 0.5 | 0.5 | 0.7 | 0.5 |
| | macroalgae | 0.02 | 0.1 | 0.1 | 0.1 | 0.04 | 0.1 | 0.1 | 0.1 |
| | mod-dense SG | 0.01 | 0.1 | 0.2 | 0.2 | 0.3 | 0.2 | 0.1 | 0.2 |

5.4. Discussion

5.4.1. Habitat classification

The main objective of this Chapter was to evaluate the potential of PlanetScope imagery for mapping seasonal and interannual change of a complex intertidal-seagrass environment. This study showed that 6-class habitat maps could be created successfully at 94% Overall Accuracy (OA) using Random Forest classifier to map and

detect seasonal and interannual change across the intertidal mudflat areas. While these results compare to some previous studies that have utilised high resolution satellite imagery and Random Forest (RF) classifiers, some differences are apparent. For instance, Benmokhtar et al. (2021) used a SPOT 7 imagery that consist of a 1.5m spatial resolution and 4-band spectral resolution to map a *Zostera noltei* and algae environment yielding a similar Overall Accuracy to this study of 95%. Another study by Forsey et al. (2020) conducted in a subtidal homogenous seagrass environment indicated similar high accuracy results of 97.6% using RF and very high spatial imagery (0.5m; 9-spectral bands). In contrast, Traganos & Reinartz (2018) that utilised Planet's RapidEye (5m; 5-bands) and mapped a submerged multispecies seagrass environment using RF and achieved an OA between 73.5% and 82% across the time series.

Accuracies of other studies that used lower spatial resolution imagery such as Sentinel were varied, most achieving lower OA accuracy than this study, but unexpectedly, some achieving similar results. For example, Ha et al. (2020) used a Sentinel-2 imagery to map a temperate intertidal sparse and dense seagrass habitat in New Zealand and achieved an OA of 87%, while Fauzan et al. (2021), that mapped tropical seagrass cover in Indonesia reported an OA of 93%. However, given the varying complexity, often less complex than this study, comparisons remain challenging. As demonstrated in Chapter 4, accuracy levels generally increase with less habitat complexity or number of habitat classes. A study performed by Benmokhtar et al. (2023), that mapped a complex *Zoster noltei* environment, using Sentinel-2 and RF and Object Based Image Analysis (OBIA) in the coastal region of Morocco, a segarss environment similar to this study including seagrass, algae, and mixed algae and seagrass classes, reported OA ranging between 89% and 94%, indicating the potential of lower spatial resolution imagery to accurately map complex intertidal seagrass areas.

While some misclassification was observed among vegetation classes, these were expected due to similar spectral signature especially between vegetation classes as demonstrated in Chapter 4 with the higher 7-class map. However, considering only vegetation classes the lowest misclassification and largest separability that was found between macroalgae, and mod-dense seagrass may indicate the great potential for mapping and identifying distinct areas for macroalgae cover, highly relevant for management implications as discussed in Chapter 4.

Class accuracy errors and misclassifications may also arise from the ground-truth approach that was used. For example, the UAV classified habitat maps that were used to generate training data already contain inaccuracies (see Chapter 3), which may be amplified in subsequent uses. Quadrat samples used as ground-data may also contribute to misclassification errors, especially due to the mismatch in spatial resolution between the PlanetScope imagery (3m) and quadrat sizes (1m), as information within the pixel may not be fully represented in the quadrat. To address these issues, a ground-truth design that captures all the information within a PlanetScope pixel i.e., 3m quadrats, which then can also be utilised to validate against the UAV classified habitat map could have potentially improved accuracies.

Training a transferable model that can be applied to multiple data sets over time should have significant advantages for management and monitoring. It should prove cost-effective, as unneeded ground-truth data for each time-step is not required, saving field costs, time and computational resources. However, although we present promising results here, the real feasibility of this has not yet been tested. Dynamic and complex environments such as the intertidal area studied can vary in appearance (hence spectral signatures) in different months and seasons (Bargain et al., 2013) posing challenges for transferability. For example, although all UAV images for ground-truthing were acquired at low tide, residual water may vary according to the stage of drainage, which could lead to varying spectral characteristics between images of dryer and wetter areas over different dates.

5.4.2. Change detection, ecology, and implications for management

In ideal environmental conditions, and with absence of external threats such as macroalgae overgrowth, Zostera spp. typically starts propagating in April/May with a gradual growth rate during warmer months and maximum growth in August (Azcárate-García et al., 2022). However, such common and distinct patterns were not observed in the early months of the season in this study. Instead, the seasonal patterns showed a high cover of SG/MA mixed class, suggesting the proliferation of macroalgae across the LNNR region, and in turn making it challenging to detect seagrass and to draw conclusions about its growth and distribution patterns, as observed especially for the month of April.

Seagrass and macroalgae growth patterns can be influenced by numerous environmental factors such as light availability, temperature (Deng et al., 2012; Hammer et al., 2018; Moore & Wetzel, 2000; Wong et al., 2020), physical disturbance (e.g., storms), or nutrient availability (Lee et al., 2003; Bourque et al., 2015). Next to high nutrient levels, the proliferation of algae can especially be stimulated by increased temperatures, which are often related to algal blooms (Green-Gavrielidis & Thornber, 2022). For example, in the UK, the end of March 2021 was marked by unusual record temperatures (Figure 5.12), which may have led to algal proliferation in the area, thus may explain the observed high cover of SG/MA mixed habitat class in April 2021. These extreme high temperatures were then followed by unusually low cold temperatures across the UK during the same months of April (Figure 5.12). This surge in cold temperatures in turn, may have led to subsequent low growth in seagrass and potential damage or die-off of SG/MA mixed in the Causeway and Fenham Flats area in May. However, the observed maintained cover in Budle Bay may be related to microclimatic effects which allowed the maintenance of higher temperatures, due to its location within a bay and less exposure.

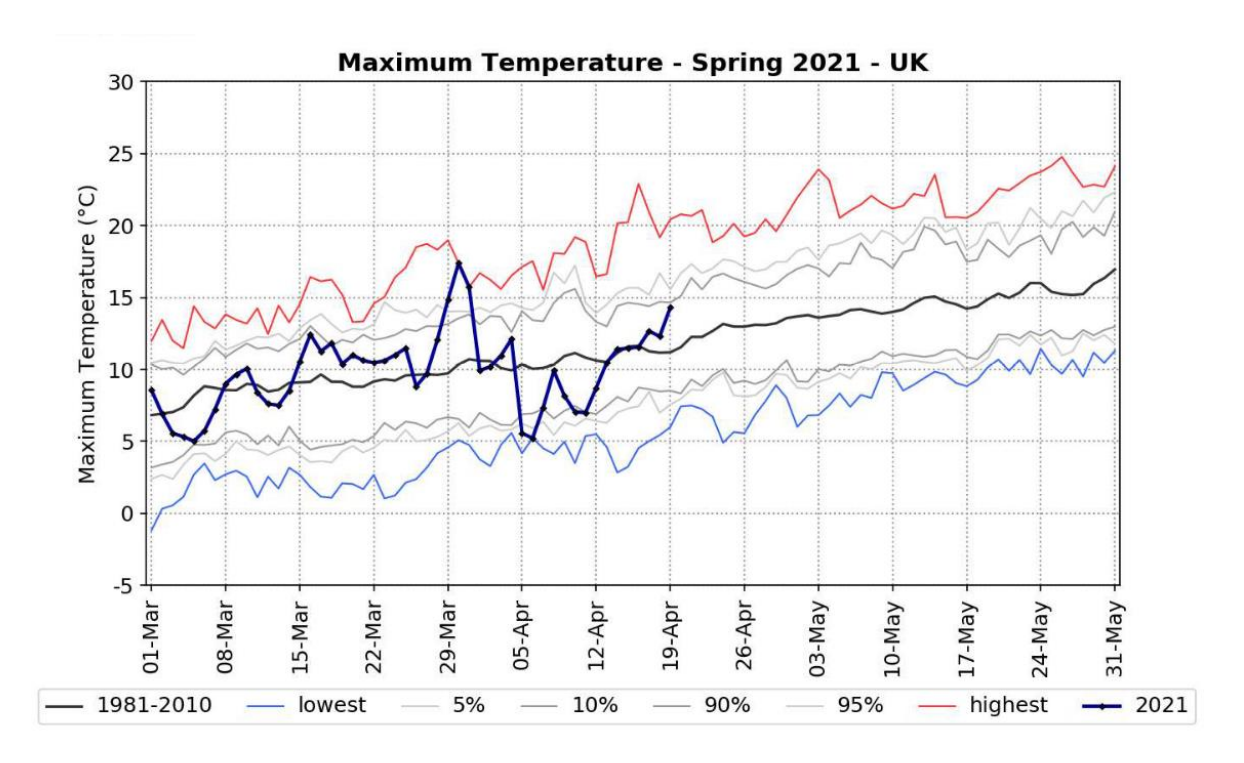


Figure 5.12. Time series of average UK daily maximum temperatures for spring 2021. (Source: Met Office, 2021: Contains public sector information licensed under the Open Government Licence v3.0.)

The extensive seagrass cover during peak biomass in August, may suggest that the observed low cover early in the season may not have had an impact on seagrass growth and biomass. Another explanation for this distributional pattern may be related to misclassification error. It is plausible that seagrass may have been very low in cover. Given the large cover of bare ground within the sparse SG benthic class, this class may have been misclassified as bare ground. The seagrass die-off in October was distinctly apparent in the field site with observed sharp decline in seagrass and simultaneous increase in algae and SG/MA mixed. However, given the high cover of SG/MA mixed which may mask seagrass cover, it is questionable how much seagrass may possibly still be present in the area, as often healthy seagrass can be found below opportunistic algal mats. Thus, while a positive interannual directional trend in seagrass cover was observed, it is guestionable whether the lower covers of seagrass prior 2023 are actual true values, as healthy seagrass may have been covered by macroalgae, represented through the benthic class SG/MA mixed. As such, the variation in seagrass cover could be associated with the varying dates of image acquisition. For example, it is possible that higher nutrient levels in specific years and months such as 2020 and 2022, may have led to an algal proliferation. The large increase in seagrass cover in 2023, especially for Causeway and Fenham Flats, may indicate a positive trend in the expansion of seagrass. However, when visually comparing between 2022 and 2023, it appears that the areas may have expanded earlier, but were covered by algae in the previous year.

Large-scale mapping and monitoring of seasonal and interannual change to understand the distribution patterns and dynamics between seagrass and macroalgae cover over time is critical for seagrass inventory. For example, short term stress and disturbance may influence seasonal growth patterns, productivity structure and stability of seagrass populations (Soissons et al., 2018). In combination with causative drivers, e.g., water quality and temperature data sets, time-series maps could be utilised to track the underlying causes of changes to better understand occurring declines for example, during peak biomass.

Despite the high variation in seasonal and interannual patterns, the maps can be utilised to effectively assess dynamics in small to large-scale patterns of seagrass and macroalgae cover. Here, information and visual assessment of patch sizes and configurations of seagrass and macroalgae across different areas, seasons and years can be extracted to support decision-making. Maps of this level of accuracy could

assist in prioritising areas for conservation and management implications/interventions and effective operationalisation. For example, where areas of consistent macroalgae cover over time was observed, e.g., Budle Bay, necessary measures such as routine removal of algae, particularly early in the season, may potentially improve seagrass growth over the season. Moreover, the produced maps could support compliance monitoring as an effective communication tool, to identify necessary measures to be taken.

To better understand the underlying causes of seasonal and annual changes in macroalgae and seagrass cover, the integration of produced maps with comprehensive ancillary data may provide more insights into causative effects. Shortand long-term changes in cover may for example be better explained utilising: (1) Water quality data including nutrient levels which can affect seagrass and macroalgal growth (Moore & Wetzel, 1999; Han et al., 2016); (2) Hydrodynamic data, such as tidal flows and wave actions that may affect nutrient distribution and macroalgae dispersion and limit seagrass growth (Sakamaki et al., 2006; La Nafie et al., 2012); (3) Water temperature can influence algal growth and data of temperature variations therefore help to understand seasonal and annual variability in growth patterns (Green-Gavrielidis & Thornber, 2022); (4) Anthropogenic data such as agricultural practices, locations of agricultural fields and areas of urban development may help identify sources of pollution that can contribute to pollutant and nutrient loads through runoff; (5) Finally, precipitation and storm events may increase nutrient flow and thus macroalgal proliferation (Chang et al., 2023). Integrating these ancillary data in generated habitat maps using geospatial analysis and modelling approaches may aid in identifying the sources of drivers of macroalgal growth and seagrass decline. A secondary benefit of integrating such ancillary data will be to improve decision-making and management strategies through targeted interventions. For example, where agricultural runoff is identified as a major driver of macroalgae growth management action could focus on these sites. Finally, maps that show the sources, causes, and drivers of algal growth and seagrass decline can improve communication with stakeholders, policymakers, and the public, delivering more informed, strategic, and successful management practice.

5.4.3. Limitations, challenges, and recommendations

Despite the successful use of PlanetScope imagery for mapping and monitoring a complex intertidal seagrass-macroalgae environment, limitations and challenges exist and need to be considered if the technology and methods presented here are to be used in a robust monitoring programme. However, PlanetScope is revolutionising the realm of miniature satellites, bringing many advantages for monitoring over traditional satellites. New methods are required to support this. The use of smaller satellites, such as the PlanetScope CubeSats, can allow more frequent updates and improvements of sensors over shorter periods and are more cost-effective for rapid development of the technology and associated applications such as monitoring. However, frequent updates with improved sensors results in changes in imagery data characteristics (e.g., improved radiometric resolution), which can make multi temporal comparisons challenging, hampering the utilisation of early launched satellites. Data continuity and consistency is critical for long-term monitoring programmes, as often historic data are highly valuable to understand and elucidate trends in seagrass and macroalgae cover. It is possible to resample, for example the spectral resolution of newer sensor imagery (e.g., SuperDove; 8 spectral bands) to satellite imagery from earlier sensors (e.g., Dove Classic: 4 spectral bands) which would enable historic mapping and monitoring from years earlier than 2020 when using PlanetScope data. However, this approach requires careful consideration as other disparities in sensor specifications between satellite constellations exist, such as different band widths and their placements and ground sampling distance, which can influence data quality thus making mapping results incomparable (Frazier & Hemingway, 2021).

Collectively, the constellation of many small satellites provides a high frequency of revisits to specific locations. This higher temporal resolution may especially benefit monitoring intertidal temperate seagrass environments, where areas prone to cloud coverage and/or where seagrass habitats are not frequently exposed at low tide to capture this time span. However, due to the narrow sensor swaths that PlanetScope satellites offer, larger areas of interest such the LNNR often cannot be captured in one single path. The stitching of imagery from multiple satellites or passes within the constellation into one single scene may be required. This can result in varying viewing angles, differing illumination across merged imagery scenes, and reduced numbers of usable images, all of which can present problems for analysis, which also restricted the selection and number of imagery acquisition in this study. This could make the

utilisation of the platform challenging for monitoring programmes, due to unreliability and potentially inconsistent data availability (Frazier & Hemingway, 2021).

Developing a classification model on one image then using it to predict on images taken at different times can be very useful if no ground-truth data is available. However, in a spectrally complex environment such as the intertidal, spectral reflectance of benthic classes may vary between images in a time series dependent on tidal stage and weather condition. To ensure that the classification model accounts for such temporal changes and variations, it is recommended to have ground-truth data for each time step to validate the model's performance and map accuracy most accurately.

Although the methodology used in this study is user-friendly due to the application of an existing classifier that enables rapid and accurate habitat mapping, often geospatial analysts may be required to perform the analysis at an increasing expense, and while image acquisition can be cost-effective, specialist knowledge and associated hardware and software can also be expensive. While PlanetScope imagery can be accessible free of charge for research work, the acquisition of data for long-term monitoring may require more sophisticated agreements and additional payments (Planet Labs, 2024). However, successful examples exist. PlanetScope was used to good effect for ecosystem monitoring by the Allen Coral Atlas (allencoralatlas.org/), that aims at mapping and monitoring coral reefs across the globe and includes proximate seagrass habitats, restricted to tropical regions.

5.4.4. Conclusion

This chapter presented the first assessment of the potential of PlanetScope imagery for multitemporal seasonal and interannual change detection in a complex intertidal seagrass-macroalgae environment. Maps produced enabled the examination of spatiotemporal distribution and dynamics between seagrass and macroalgae cover. Insights gained from the analysis of change detection maps provides critical information between seagrass-and macroalgae dynamics that could be used for effective management decision-making to combat macroalgae threat in the region. The user-friendly approach achieved by the transferable single random forest model across time series shows promise, offering a potentially effective, low input method for rapid large-scale mapping and monitoring of the intertidal area. Despite some limitations, the results of this study provide the ground-work and crucial steps in understanding the

possibilities and limitations of PlanetScope imagery for seagrass large-scale mapping and monitoring in an intertidal seagrass-macroalgae environment.

Chapter 6: Thesis overview, limitations, and future directions

This thesis has evaluated the application of optical remote sensing methods to map and monitor a complex, intertidal seagrass-macroalgae environment. Three platform and sensor combinations with varying spectral, spatial, and temporal resolutions were utilised to create habitat maps to inform potential monitoring and management of a temperate intertidal seagrass environment. This study assesses strengths and weaknesses across scales, from methods used to produce fine-scale habitat maps at lower spatial coverage to less detailed maps at larger coverage. This study also delineates spatial patterns and dynamics of seagrass and macroalgae in a temperate intertidal area for management and conservation purposes. As the first comprehensive study utilising multiscale optical remote sensing to map and monitor a complex temperate intertidal seagrass-macroalgae environment in the UK, this approach provides novel insights into the implementation of these methods for effective management and conservation of seagrass habitats. Given the ongoing threats that seagrass habitats are facing globally (Unsworth et al., 2022), the urgent need for effective management to protect and reduce their decline (Green et al., 2021; Jones & Unsworth, 2016), and the rapidly evolving cost-effective optical remote sensing technologies and their success in mapping seagrass habitats (Hossain et al., 2015; Veettil et al., 2020), the thesis provides timely and valuable contribution to this field of research. This final chapter presents an overview of the thesis and key findings; critically assesses the implications of the results for intertidal seagrass management; and discusses the wider implications of study, its limitations, and future directions.

6.1. Key findings

In recent years, seagrass habitats have received increasing interest and attention globally, by researchers, policymakers, and the public. In particular, their significant role as 'blue carbon ecosystems' is increasingly recognised and highlights the need for their protection to combat climate change (McLeod et al., 2011; UN-WCMC, 2020). The applications of optical remote sensing technologies for seagrass habitat mapping have increased in parallel (Pham et al., 2019; Hossain et al., 2015). This study advances this field of research by filling the gap in knowledge of the application of

optical remote sensing methods in temperate intertidal seagrass environments. Key technical findings of the thesis are as follows:

- Chapter 3 utilised a high-resolution multispectral imagery acquired through UAV and demonstrated successful fine-scale habitat mapping in a high level heterogeneous and mixed species intertidal seagrass-macroalgae environment, including the discrimination between seagrass species (Zostera noltii and Zostera marina) and opportunistic macroalgae. Using the maximum likelihood classifier, map accuracies ranged between 84% and 91% across three discrete areas, including Zostera noltii dominated, Zostera marina dominated and macroalgae dominated transects. Findings highlight the distinct benefit of the additional red edge and near infrared bands that significantly contributed to the separation between vegetation classes. However, this platform is constrained to small area mapping and cannot elucidate large-scale patterns or dynamics.
- Thus, recognising the need for larger area coverage, methods for the analysis of airborne CASI hyperspectral imagery were developed in Chapter 4 and proved effective in mapping the entire intertidal seagrass area of the LNNR. Maps with varying numbers of habitat classes (5-class, 6-class, 7-class, respectively) were produced using a Random Forest (RF) classifier. Findings indicated accuracies ranging between 76% and 97%, OA increasing with lower numbers of habitat classes. To identify whether benefits identified required hyperspectral data or could be simplified based on findings in Chapter 3, hyperspectral bands were reduced from 23 bands to 5 and 8-spectral bands. Similar accuracy levels were achieved, reemphasising the importance of red bands and highlighting potential redundancy in the hyperspectral sensor for intertidal seagrass mapping. While multispectral sensors may be sufficient to map intertidal seagrass-macroalgae environments, the scale of data collection offered by the aircraft platform enabled the assessment of ecology and spatial patterns of seagrass and macroalgae distribution across a large site (approx. 2,300 ha). However, utilisation of airborne platforms for monitoring is constrained by high associated costs, especially where more frequent imagery is required to map and monitor competitive dynamics between seagrass and macroalgae cover over time.

• Aiming for lower costs and acknowledging the need to acquire more frequent imagery, multispectral satellite data from PlanetScope SuperDove was utilised to map the intertidal seagrass environment and test the potential for seasonal and interannual monitoring. Using a Random Forest classifier, a 6-class habitat map was successfully produced at high accuracy (OA 94%). The model developed, supported the creation of timeseries habitat maps. This permits the rapid production of large-scale area habitat maps and could form the basis for a highly practical method for coastal managers to effectively assess intertidal seagrass ecosystem changes and trends. Seasonal and interannual habitat maps could be utilised to reveal complex spatiotemporal seagrass and macroalgae distribution patterns and their dynamics with significant benefits for management.

 Table 6.1: Summary of specifications of different platforms and sensors for monitoring an intertidal seagrass environment.

| | Quadrat sampling | Multispectral UAV | Airborne Hyperspectral (CASI) | Satellite multispectral (PlanetScope) |
|---------------------------------------|---|---|--|---|
| Platform | Photo Camera | UAV | Airborne | Satellite |
| Sensor specifications | Spatial: 0.1cm Spectral: RGB Temporal: on demand | Spatial: 0.5 cm Spectral:5-bands Temporal: on demand | Spatial: 1m Spectral: 29-bands Temporal: on demand | Spatial: 3m Spectral:8-bands Temporal: daily |
| Spatial Coverage | Limited, small-scale (1m²) | Limited, small-scale (e.g., discrete areas such as transects) | Limited, local coverage (e.g., LNNR) | Local, regional, and national coverage |
| Application | Limited sampling numbers (e.g., 30 quadrats each section in LNNR) | Detailed small-scale habitat mapping | Large-scale habitat mapping | Large-scale spatiotemporal habitat mapping |
| Classification Method | Visual assessment of photographs | Maximum-Likelihood Classifier | Random Forest | Random Forest |
| Accuracies | - | Overall Accuracies: 80-90% | Overall Accuracies: 76% - 97% | Overall Accuracies: 94% |
| Acquired information and key findings | Percent cover of benthic substrate | Detailed information on seagrass species (Zostera noltii and Zostera marina) and macroalgae; benefit of additional red edge and near infrared bands for vegetation separation | Spatial distribution patterns of seagrass and macroalgae; similar accuracy levels to 23 - bands acquired with 5-8 bands spectral bands | Seasonal and temporal spatial distribution patterns of seagrass and macroalgae; time series maps could be utilised to reveal dynamics between seagrass and macroalgae |
| Limitations | Limited number of samples across the area; cannot capture accurate large-scale patterns | Limited area coverage; cannot capture large-scale patterns | Limited to single imagery acquisition: cost intensive; not viable for monitoring programmes | Restricted by imagery selection due to cloud cover; spatial resolution may be insufficient to capture accurate spatial patterns |

| Skills requirements | Data analysis | Operational skills; data processing and analysis | Operational skills; data processing and analysis | Data processing and analysis |
|---------------------------|--------------------------|---|---|------------------------------|
| Costs for LNNR (~2300 ha) | Quadrat frame, GNSS RTK: | UAV license, DJI Multispectral UAV, GNSS RTK, Software (Pix4D): | Flying licence, Platform (plane), sensor, software: | Single imagery: |
| | ~ £ 30.00 | ~ £ 7,500.00 | ~ 52,200.00 | ~ 70.00 |

6.2. Implications for management

The implications of remote sensing for coastal habitat management are significant and are often promoted as part of a toolbox to help managers to assess the ecological patterns and change to prevent ecosystem decline. Maps are also often important communication tools to help managers for decision-making and of conservation areas (McCarthy et al., 2017; Pettorelli et al., 2014). While the application of optical remote sensing technologies to seagrass habitats are well covered in the literature (Hossain et al., 2015) (Chapter 2, Table 2.2), the benefits must be operationalised for the management of seagrass decline. Methods are often analytically complex, and less intensive approaches are required by busy management organisations. Barriers to operationalisation may be due primarily to remote sensing technologies being challenging to integrate into monitoring programmes, constraints associated with limited budgets, accessibility of the required data, technical expertise, and data processing challenges.

To facilitate the utilisation of optical remote sensing for seagrass habitat mapping and monitoring and ensure cost-effectiveness for management, careful planning is required, and the analytical complexities must be addressed. The type of optical remote sensing technology and method to be used will primarily depend on the management aims and objectives of required information of the seagrass environment. These may range across different needs and interests, for example whether information is required at seagrass species level, or for large scale habitat dynamics and threats such as macroalgae overgrowth — successful approaches to which have been demonstrated in chapters presented in this thesis. Management objectives will dictate the required spatial, spectral, and temporal resolution imagery data to map, monitor and manage seagrass environments, but promising methods have now been identified across various scales.

6.2.1. Applications of multiscale mapping for management and costeffectiveness

As demonstrated, seagrass habitat maps can be produced using imagery from multiple platforms to acquire habitat information based on differing sensor specifications. Each platform comes with strengths and weaknesses regarding resolution and spatial

coverage, and trade-offs are required based on the habitat information required and associated costs (Table 6.1). For example, while UAV imagery may enable fine-scale habitat mapping, it lacks the required spatial coverage to assess large-scale habitat patterns, whereas satellite platforms can provide this at the cost of lower spatial resolution. To maximise the utilisation of available optical remote sensing data resources, the leveraging of strengths and weaknesses through combination of data from different platforms may provide more cost-effective approaches for the management and conservation of habitats (Carpenter et al. 2022; Bergamo et al. 2023).

UAV imagery will be most appropriate when 1) the fine-scale ecology of seagrass and macroalgae is required, for example to monitor and assess species composition by performing several flight transects across the site as demonstrated in Chapter 3; 2) where detailed information is required in inaccessible areas, for example, dangerous mudflat areas where sites are inaccessible on foot; 3) to monitor the success of restoration projects by assessing for example, seagrass plant growth and biomass (Ridge and Johnston, 2020); 4) to overcome challenging and exhaustive quadrat sampling across the field site, where UAV derived habitat maps could be utilised as training data for large-scale habitat mapping such as for PlanetScope imagery (as methodology used in Chapter 5), which has lower spatial resolution but provides larger coverage to assess large-scale distributional patterns.

Where information at species level is not required, lower spatial resolution imagery with larger coverage area will be more appropriate. This is required to inform our understanding of the ecology of seagrass and macroalgae, elucidating large-scale patterns and dynamics, as demonstrated in Chapter 4 and Chapter 5 by utilising Airborne Hyperspectral data and Satellite PlanetScope Satellite data. While the CASI hyperspectral imagery with its high spatial resolution at 1m was a highly valuable resource for mapping small-scale patch dynamics of seagrass and macroalgae, it may not be cost-effective due to costs associated with using an aeroplane platform and the expensive CASI sensor. However, this study demonstrated that the high number of spectral bands is not required to achieve similarly accurate maps, so costs could be reduced somewhat by utilising consumer grade multispectral sensors that retain red edge and near infrared bands, instead of a hyperspectral sensor. Where such high spatial resolution may not be required for mapping seagrass and macroalgae, high resolution multispectral satellite imagery such as PlanetScope (3m) then provides

more cost-effective options for monitoring programmes. Satellite approaches enable the more frequent acquisition of imagery to capture temporal dynamics between seagrass and macroalgae. Furthermore, satellite imagery such as PlanetScope could be utilised to assess the health of seagrass habitats to identify existing and newly identified seagrass areas, or areas of significant change. These can then be explored in more detail by using UAV imagery.

When conducting a multiscale mapping approach combining or fusing imagery data with differing spatial and spectral resolution, it is essential to consider factors that may influence the accuracy of mapped seagrass and macroalgae cover (e.g., the loss of detailed information with decreasing spatial and spectral resolution).

6.3. Wider implications

Although the maps created are specific to the management of intertidal seagrass habitats in Lindisfarne National Nature Reserve (LNNR), UK, the approaches and methodologies used in this thesis are applicable to seagrass habitats in other temperate regions and provide valuable information to inform their management. Intertidal seagrass habitats occur in other temperate regions such as, USA, New Zealand and wider Europe (France, Spain, Portugal, Sweden etc). Although some studies that have used optical remote sensing in these regions are available, this study fills the gap identified for intertidal seagrass environments (Chapter 2, Table 2.2.). The majority of methods tested in this study have been applied in a complex intertidal seagrass-macroalgae environment for the first time. This progresses our understanding of the applications of optical remote sensing technology and methods from clear tropical waters to temperate intertidal seagrass habitats and moves beyond the mapping and monitoring of homogenous seagrass habitats to identification of species within complex intertidal seagrass-macroalgae habitats, allowing us to address challenges, such as eutrophication, that seagrass environments are facing across coastal regions (Burkholder et al., 2007).

This study may provide a framework for the use of optical remote sensing by existing projects and organisations, supporting efforts in coastal habitat management and conservation within the UK, of seagrass systems and beyond. For example:

• The EU funded project, EU LIFE Wader (2024), aims to improve the water quality and ecological conditions of different habitats across the

Northumberland Coast, UK. Moreover, they aim to improve management to improve the health (condition) of protected site features in the study area, such as mudflats and seagrass. The methodologies produced in this thesis could especially support their ongoing efforts in mitigating macroalgae growth in the LNNR. For example, methods underpinning maps in Chapter 4 and 5, may provide a powerful tool to map macroalgae patches and support prioritisation of macroalgae removal.

- Projects funded by diverse stakeholders across the EU and UK such as, Stronger Shores (2024), Restoration of Seagrass for Ocean Wealth UK (ReSOWUK, 2024) and Restoring Meadow, Marsh and Reef (ReMeMaRe, 2024) aim to restore seagrass meadows across the UK. Here, the methods used to produce large-scale maps (Chapter 4 and 5) could be utilised to identify habitat suitability for potential seagrass restoration areas (e.g., bare ground areas) (Bertelli et al., 2022; Dalby et al., 2023). The multispectral UAV methodologies developed in Chapter 3 could support high level change detection and monitoring of seagrass restoration programmes (Ventura et al., 2022), where they may help quantify success and enable the detection of early threats, such as algal growth.
- The DEFRA (Department for Environment Food and Rural Affairs) programme, marine National Capital Ecosystem Assessment (mNCEA, 2024) aims to evaluate the health and functioning of marine ecosystems, including the assessment of biodiversity, ecosystem services and the overall condition of marine environment. Tools developed in this thesis could assist in the assessment of ecosystem services (Andrew et al., 2014; Hossain & Hashim, 2019) and support condition monitoring through: 1) utilising baseline habitat maps produced in Chapter 4 and 5, to assess the initial state of the seagrass environment; 2) Change detection to assess habitat condition over time and to identify trends in seagrass increase or decline (Chapter 5).
- To improve the accuracy of seagrass and macroalgae mapping in intertidal areas and to increase effective management practices, a citizen science project could be integrated in management planning. For example, as part of Natural

England's' community engagement plan to raise awareness on the natural environment in the region. Such engagement could involve the collection of seasonal and annual ground-truth data through quadrat photographs, or the collection of high-resolution imagery data conducted for example, by UAV flying hobbyists. Ultimately, data collected could be used for spatiotemporal map validations. However, it is important that safety measures in such a challenging environment are considered in designing a 'citizen science' project. Moreover, to minimise the impact on seagrass disturbance, numbers of volunteers allowed onto the field site must be carefully considered and regulated.

• Finally, habitat maps generated are of fundamental use in applied ecology (Pettorelli et al., 2014). They can provide information for ecological research, answering specific seagrass ecology questions. For example, the maps created in Chapter 4 and 5 could be used: in combination with species distribution models to better understand seagrass and macroalgae distribution patterns (Beca-Carretero et al., 2020) and their potential drivers, when combined with other sources of data (e.g., nutrients) (Han et al., 2016); or estimate seagrass properties such as leaf area, or make biomass and carbon storage estimates crucial for climate change research (Simpson et al., 2022; Sousa et al., 2019).

Overall, remote sensing technologies operating at multiple scales can provide a holistic overview of ecosystems for management and conservation purposes (McCarthy et al., 2017; Rose et al., 2015). This study develops a foundation for multi-level remote sensing in intertidal seagrass habitat mapping, monitoring, and management. It can provide tools to better understand seagrass declines, which can be related to threats, as well as monitoring the success of restoration efforts for intertidal seagrass habitats across the UK and beyond. Funded by NERC and Natural England, the statutory nature conservation body, this work has always had end-user support, and additional organisations and projects have shown interest in the outputs to date. Further collaborative work proposed indicates the value and impact of this study to intertidal seagrass management and conservation organisations. Applications of the approach beyond seagrass habitats are also possible.

6.4. Limitations and future directions

The study was subject to several limitations, primarily associated with the time constraints of data collection and analysis, as a function of carrying out the research over the duration of a Ph.D. These may have impacted results in the following ways: (1) The low number of ground-truth samples resulted in unbalanced training class samples, which may have impacted accuracies, and potentially challenge the reliability of map results; (2) The data collection confined to the Causeway area, may limit the generalisation of findings across the full extent of the field site, particularly undermining results in areas such as Fenham Flats and Budle Bay; (3) The focus of the study in one specific intertidal area, with, for example, specific sediment characteristics, may potentially limit the validity of results in other geographic regions. A study design that incorporates these constraints may enable a higher degree of transferability to other intertidal seagrass environments.

The inherent nature of the intertidal area retaining water at low tides, and the appearance of sun glint may both have impacted spectral responses, potentially resulting in higher misclassifications and reduced reliability of classified habitat maps. While this could theoretically be mitigated by increasing the time for water to drain after low tide, this was often restricted by topography, unfavourable weather conditions (e.g., UAV sensitive to rain and wind), the need to leave before the incoming tide made the area unsafe for working, or satellite imagery acquisition occurring at sub-optimal times shortly before high water.

Given the high complexity of area investigated, with two species of seagrass and multiple macroalgae co-occurring, varying sediment types, hyperspectral and satellite resolutions of 1m and 3m, respectively (Chapter 4 and 5), may have been insufficient to separate similar habitat classes spectrally. The acquisition of satellite imagery with higher spatial resolution would enable the assessment and validation for improved accurate habitat mapping. The availability of satellite imagery over intertidal areas is inherently constrained, e.g., data is collected out with tides, rendering many images unsuitable for intertidal monitoring. These temporal limitations potentially hamper detection of fast growing macroalgae; this inability to capture these inter-specific dynamics inhibits accurate monitoring of seagrass cover. Higher frequency of mapping may enable the delineation of more accurate seagrass information and the finer description of dynamic interactions with macroalgae. Furthermore, as discussed in

Chapter 4 and 5, the integration of environmental, climatic, hydrodynamic, and anthropogenic data into generated maps should be considered, to analyse and evaluate spatiotemporal patterns, causes and drivers of macroalgal growth and seagrass decline. This will help design management interventions to effectively mitigate macroalgae growth and seagrass decline.

One future direction for this study entails the development of more cost-effective analysis, specifically the integration of freely available software and programming languages. The cost of software utilised in this study for data processing and analyses, including for example, ArcGIS and ENVI, may limit the accessibility for coastal managers often restricted by limited budgets. To address this limitation, open-source software such QGIS and programming languages including R and Python may provide more cost-effective options (Rocchini et al. 2017). To enhance the practicality and efficiency of data retrieval and analysis, cloud-based platforms such as Google Earth Engine may provide another option for geospatial analyses, including for optical remote sensing applications (Traganos et al., 2018; Amani et al., 2020;). Ultimately, the automation of data processing and image analysis could lead to the creation of an intertidal seagrass habitat mapping toolbox (Bremner et al., 2023) usable without expert input, which would contribute to management efforts. Here, the integration of Deep Learning (DL) methods and Object-Based-Image Analysis (OBIA) could potentially lead to more accurate and robust classification (e.g., Hobley et al., 2021). Evaluating and selecting the most appropriate and accurate classification methods, will consequently minimise error propagation when leveraging multiscale data.

6.5. Concluding remarks

In conclusion, this thesis has demonstrated the potential of cost-effective and relatively user-friendly production of habitat mapping and monitoring of a complex intertidal temperate seagrass-macroalgae environment using both consumer grade and cutting-edge optical remote sensing technology. The utilisation of different platforms, sensors with high resolution imagery coupled with machine learning classifiers and field-based validation, enabled the successful extraction of detailed information to better understand patterns of distribution and the dynamics between seagrass and macroalgae. Overall, this study has enabled a holistic evaluation of optical remote sensing technology to advance our understanding of the possibilities, geospatial intricacies, and limitations for applications in the investigated environment. However,

it is important to acknowledge the inherent challenges of the field site, including data limitations, uncertainties in methods applied and the need for improved validation, methodologies, and collaboration with stakeholders to enhance reliability and applicability of seagrass habitat mapping and monitoring for conservation efforts.

With rapidly advancing and emerging remote sensing technologies and increasing threats faced by seagrass habitats, the findings of this study not only contribute to filling critical research gaps, but also provide a foundation for future research and development of improved methods to enhance our understanding of applications of optical remote sensing across multiple scales in temperate intertidal seagrass environments, their practicality and operational considerations. This is a significant step towards their integration into effective monitoring programmes, greatly benefiting management and conservation efforts to prevent observed declines in this important habitat.

Appendix A: Table including the 33 Channels (spectral bands) and central wavelength \pm FWHM (Full Width at Half Maximum) of the CASI hyperspectral sensor.

| Channel # | Central Wavelength +/- Full Width at Half Maximum (FWHM) /nm |
|------------|--|
| Channel 1 | 394.918nm +/- 14.203nm |
| Channel 2 | 442.246nm +/- 14.195nm |
| Channel 3 | 487.186nm +/- 14.188nm |
| Channel 4 | 513.195nm +/- 11.821nm |
| Channel 5 | 554.561nm +/- 15.362nm |
| Channel 6 | 577.012nm +/- 7.089nm |
| Channel 7 | 595.915nm +/- 9.451nm |
| Channel 8 | 611.273nm +/- 5.907nm |
| Channel 9 | 624.267nm +/- 7.087nm |
| Channel 10 | 643.166nm +/- 9.449nm |
| Channel 11 | 663.244nm +/- 5.905nm |
| Channel 12 | 676.236nm +/- 7.086nm |
| Channel 13 | 686.865nm +/- 3.543nm |
| Channel 14 | 693.951nm +/- 3.543nm |
| Channel 15 | 702.218nm +/- 4.724nm |
| Channel 16 | 712.846nm +/- 5.905nm |
| Channel 17 | 727.018nm +/- 5.905nm |
| Channel 18 | 736.465nm +/- 3.543nm |
| Channel 19 | 745.913nm +/- 5.905nm |
| Channel 20 | 752.998nm +/- 1.181nm |
| Channel 21 | 755.360nm +/- 1.181nm |
| Channel 22 | 757.722nm +/- 1.181nm |
| Channel 23 | 760.084nm +/- 1.181nm |
| Channel 24 | 762.446nm +/- 1.181nm |
| Channel 25 | 764.807nm +/- 1.181nm |
| Channel 26 | 767.169nm +/- 1.181nm |
| Channel 27 | 769.531nm +/- 1.181nm |
| Channel 28 | 771.893nm +/- 1.181nm |
| Channel 29 | 774.255nm +/- 1.181nm |
| Channel 30 | 799.055nm +/- 14.172nm |
| Channel 31 | 852.204nm +/- 12.993nm |
| Channel 32 | 879.372nm +/- 11.813nm |
| Channel 33 | 1008.190nm +/- 15.372nm |
| Channel 33 | 1008.190nm +/- 15.372nm |

References

Ackleson, S. G., & Klemas, V. (1987). A comparison of Landsat TM to MSS imagery for detecting submerged aquatic vegetation in Lower Chesapeake Bay. *Remote Sensing of Environment*, 22, 235–248.

Ackerman, J.D., (2006). Sexual Reproduction of Seagrasses: Pollination in the Marine Context. In: Larkum A.W.D., Orth R.J., Duarte C.M (Eds), Seagrasses: Biology, Ecology, and Conservation (pp. 89–109). Springer, Dordrect, the Netherlands.

Agisoft. (2021). Agisoft Metashape User Manual. In *Agisoft Metashape* (Issue September, p. 160). https://www.agisoft.com/pdf/metashape-pro_1_5_en.pdf

Amani, M., Ghorbanian, A., Ahmadi, S. A., Kakooei, M., Moghimi, A., Mirmazloumi, S. M., Moghaddam, S. H. A., Mahdavi, S., Ghahremanloo, M., Parsian, S., Wu, Q., & Brisco, B. (2020). Google Earth Engine Cloud Computing Platform for Remote Sensing Big Data Applications: A Comprehensive Review. *IEEE Journal of Selected Topics in Applied Earth Observations and Remote Sensing*, 13, 5326–5350.

Andrew, M. E., Wulder, M. A., & Nelson, T. A. (2014). Potential contributions of remote sensing to ecosystem service assessments. *Progress in Physical Geography*, *38*(3), 328–353.

Apollo Mapping (2024). Accessed: 12/11/2023 https://apollomapping.com/

Armitage, R. P., Alberto Ramirez, F., Mark Danson, F., & Ogunbadewa, E. Y. (2013). Probability of cloud-free observation conditions across Great Britain estimated using MODIS cloud mask. *Remote Sensing Letters*, *4*(5), 427–435.

Astuty, I. S., & Wicaksono, P. (2019). Seagrass species composition and above-ground carbon stock mapping in Parang Island using Planetscope image. *SPIE*, 1131103.

Azcárate-García, T., Beca-Carretero, P., Cara, C. L., Villamayor, B., Cosnett, E., Bermejo, R., Hernández, I., Brun, F. G., & Stengel, D. B. (2022). Seasonal plant development and meadow structure of Irish and southern Spanish seagrass populations. *Aguatic Botany*, *183*, 103569.

Baden, S., Gullström, M., Lundén, B., Pihl, L., & Rosenberg, R. (2003). Vanishing Seagrass (Zostera marina, L.) in Swedish Coastal Waters. *AMBIO: A Journal of the Human Environment*, 32(5), 374.

Bargain, A., Robin, M., Le Men, E., Huete, A., & Barillé, L. (2012). Spectral response of the seagrass Zostera noltii with different sediment backgrounds. *Aquatic Botany*, 98, 45–56.

Bargain, A., Robin, M., Méléder, V., Rosa, P., Le Menn, E., Harin, N., & Barillé, L. (2013). Seasonal spectral variation of Zostera noltii and its influence on pigment-based Vegetation Indices. *Journal of Experimental Marine Biology and Ecology*, *446*, 86–94.

Barillé, L., Robin, M., Harin, N., Bargain, A., & Launeau, P. (2010). Increase in seagrass distribution at Bourgneuf Bay (France) detected by spatial remote sensing. *Aquatic Botany*, *92*, 185–194.

Beaumont, N. J., Austen, M. C., Mangi, S. C., & Townsend, M. (2008). Economic valuation for the conservation of marine biodiversity. *Marine Pollution Bulletin*, *56*, 386–396.

Beca-Carretero, P., Varela, S., & Stengel, D. B. (2020). A novel method combining species distribution models, remote sensing, and field surveys for detecting and mapping subtidal seagrass meadows. *Aquatic Conservation: Marine and Freshwater Ecosystems*, *30*, 1098–1110.

Belgiu, M., & Drăgu, L. (2016). Random forest in remote sensing: A review of applications and future directions. *ISPRS Journal of Photogrammetry and Remote Sensing*, 114, 24–31.

Bell, S. S., & Hall, M. O. (1997). Drift macroalgal abundance in seagrass beds: Investigating large-scale associations with physical and biotic attributes. *Marine Ecology Progress Series*, *147*, 277–283.

Benmokhtar, S., Robin, M., Maanan, M., & Bazairi, H. (2021). Mapping and quantification of the dwarf eelgrass zostera noltei using a random forest algorithm on a SPOT 7 satellite image. *ISPRS International Journal of Geo-Information*, 10, 313.

Benmokhtar, S., Robin, M., Maanan, M., Boutoumit, S., Badaoui, B., & Bazairi, H. (2023). Monitoring the Spatial and Interannual Dynamic of Zostera noltei. *Wetlands*, *43*(43).

Bergamo, T. F., de Lima, R. S., Kull, T., Ward, R. D., Sepp, K., & Villoslada, M. (2023). From UAV to PlanetScope: Upscaling fractional cover of an invasive species Rosa rugosa. *Journal of Environmental Management*, 336, 117693.

Bergsma, E. W. J., & Almar, R. (2020). Coastal coverage of ESA' Sentinel 2 mission. *Advances in Space Research*, *65*, 2636–2644.

Bertelli, C. M., Stokes, H. J., Bull, J. C., & Unsworth, R. K. F. (2022). The use of habitat suitability modelling for seagrass: A review. *Frontiers in Marine Science*, *9*, 997831.

Bertelli, C. M., & Unsworth, R. K. F. (2014). Protecting the hand that feeds us: Seagrass (Zostera marina) serves as commercial juvenile fish habitat. *Marine Pollution Bulletin*, 83, 425–429.

Blaschke, T. (2010). Object based image analysis for remote sensing. *ISPRS Journal of Photogrammetry and Remote Sensing*, *65*, 2–16.

Borum, J., Duarte, C., Krause-Jensen, D., & Greve, T. M. (2004). European seagrasses: an introduction to monitoring and management. *The M&MS Project Date*, 1–95.

Bourque, A. S., Kenworthy, W. J., & Fourqurean, J. W. (2015). Impacts of physical disturbance on ecosystem structure in subtropical seagrass meadows. *Marine Ecology Progress Series*, *540*, 27–41.

Breiman, L. (1996). Bagging predictors. Machine Learning, 24, 123-140.

Breiman, L. (2001). Random Forest. *Machine Learning*, 45, 5–32.

Breininger, D. R., Breininger, R. D., & Hall, C. R. (2017). Effects of surrounding land use and water depth on seagrass dynamics relative to a catastrophic algal bloom. *Conservation Biology*, *31*(1), 67–75.

Bremner, J., Petus, C., Dolphin, T., Hawes, J., Beguet, B., & Devlin, M. J. (2023). A Seagrass Mapping Toolbox for South Pacific Environments. *Remote Sensing*, *15*, 834.

Bull, J. C., Kenyon, E. J., & Cook, K. J. (2012). Wasting disease regulates long-term population dynamics in a threatened seagrass. *Oecologia*, *169*, 135–142.

Bunker, F., & Green, B. (2019). Seagrass condition monitoring in Plymouth Sound and Estuaries SAC 2018. In *Natural England Commissioned Reports, Number 294.* (Issue May).

Burkholder, J. A. M., Tomasko, D. A., & Touchette, B. W. (2007). Seagrasses and eutrophication. *Journal of Experimental Marine Biology and Ecology*, *350*, 46–72.

Butcher, R. W. (1933). Zostera. Report on the Present Condition of Eel Grass on the Coasts of England, based on a Survey during August to October, 1933. *Fisheries Research Station, Alresford, Hampshire*, 49–64.

Carlson, D. F., Vivó-Pons, A., Treier, U. A., Mätzler, E., Meire, L., Sejr, M., & Krause-Jensen, D. (2023). Mapping intertidal macrophytes in fjords in Southwest Greenland using Sentinel-2 imagery. *Science of the Total Environment*, *865*, 161213.

Carpenter, S., Byfield, V., Felgate, S. L., Price, D. M., Andrade, V., Cobb, E., Strong, J., Lichtschlag, A., Brittain, H., Barry, C., Fitch, A., Young, A., Sanders, R., & Evans, C. (2022). Using Unoccupied Aerial Vehicles (UAVs) to Map Seagrass Cover from Sentinel-2 Imagery. *Remote Sensing*, *14*, 477.

Carr, J. A., D'Odorico, P., McGlathery, K. J., & Wiberg, P. L. (2012). Stability and resilience of seagrass meadows to seasonal and interannual dynamics and environmental stress. *Journal of Geophysical Research: Biogeosciences*, 117, G01007.

Casal, G., Kutser, T., Domínguez-Gómez, J. A., Sánchez-Carnero, N., & Freire, J. (2013). Assessment of the hyperspectral sensor CASI-2 for macroalgal discrimination on the Ría de Vigo coast (NW Spain) using field spectroscopy and modelled spectral libraries. *Continental Shelf Research*, *55*, 129–140.

Chan, J. C. W., & Paelinckx, D. (2008). Evaluation of Random Forest and Adaboost tree-based ensemble classification and spectral band selection for ecotope mapping using airborne hyperspectral imagery. *Remote Sensing of Environment*, *112*, 2999–3011.

Chand, S., & Bollard, B. (2021). Low altitude spatial assessment and monitoring of intertidal seagrass meadows beyond the visible spectrum using a remotely piloted aircraft system. *Estuarine, Coastal and Shelf Science*, *255*, 107299.

Chang, D., Li, S., & Lai, Z. (2023). Effects of extreme precipitation intensity and duration on the runoff and nutrient yields. *Journal of Hydrology*, 626, 130281.

Chen, J., & Sasaki, J. (2021). Mapping of Subtidal and Intertidal Seagrass Meadows via Application of the Feature Pyramid Network to Unmanned Aerial Vehicle Orthophotos. *Remote Sensing*, *13*, 4880.

Clarke, K., Hennessy, A., McGrath, A., Daly, R., Gaylard, S., Turner, A., Cameron, J., Lewis, M., & Fernandes, M. B. (2021). Using hyperspectral imagery to investigate large-scale seagrass cover and genus distribution in a temperate coast. *Scientific Reports*, *11*, 17173.

Collins, K. J., Suonpää, A. M., & Mallinson, J. J. (2010). The impacts of anchoring and mooring in seagrass, Studland Bay, Dorset, UK. *International Journal of the Society for Underwater Technology*, *29*(3), 117–123.

Cortes, C., & Vapnik, V. (1995). Support-Vector Networks. *Machine Learning*, 20, 273–297.

Costanza, R., D'Arge, R., de Groot, R., Farber, S., Grasso, M., Hannon, B., Limburg, K., Naeem, S., O'Neill, R. V., Paruelo, J., Raskin, R. G., Sutton, P., & van den Belt, M. (1997). The value of the world's ecosystem services and natural capital. *Nature*, *387*.

Dalby, O., Pucino, N., Tan, Y. M., Jackson, E. L., Macreadie, P. I., Coleman, R. A., Young, M. A., Ierodiaconou, D., & Sherman, C. D. H. (2023). Identifying spatio-temporal trends in seagrass meadows to inform future restoration. *Restoration Ecology*, *31*(3), 1–13.

Pham, T., Xia, J., Thang Ha, N., Tien Bui, D., Nhu Le, N., & Tekeuchi, W. (2019). A review of remote sensing approaches for monitoring blue carbon ecosystems: Mangroves, sea grasses and salt marshes during 2010–2018. *Sensors*, *19*, 1933.

Davies, B. F. R., Gernez, P., Oiry, S., Rosa, P., Zoffoli, M. L., & Barill, L. (2023). Multiand hyperspectral classification of soft-bottom intertidal vegetation using a spectral library for coastal biodiversity remote sensing. *Remote Sensing of Environment*, 290, 113554.

Davis, B. C., & Fourqurean, J. W. (2001). Competition between the tropical alga, Halimeda incrassata, and the seagrass, Thalassia testudinum. *Aquatic Botany*, *71*(3), 217–232.

Dekker, A., Brando, V., Anstee, J., Fyfe, S., Malthus, T., & Karpouzli, E. (2006). Remote sensing of seagrass ecosystems: Use of spaceborne and airborne sensors. In: Larkum A.W.D., Orth R.J., Duarte C.M (Eds), Seagrasses: Biology, Ecology, and Conservation (pp. 347–359). Springer, Dordrect, the Netherlands.

Dekker, A. G., Brando, V. E., & Anstee, J. M. (2005). Retrospective seagrass change detection in a shallow coastal tidal Australian lake. *Remote Sensing of Environment*, 97, 415–433.

Den Hartog, C. (1989). Early records of wasting-disease-like damage patterns in eelgrass Zostera marina. *Diseases of Aquatic Organisms*, 7, 223–226.

den Hartog, C. (1994). Suffocation of a littoral Zostera bed by Enteromorpha radiata. *Aguatic Botany*, *47*, 21–28.

Deng, Y., Tang, X., Huang, B., & Ding, L. (2012). Effect of temperature and irradiance on the growth and reproduction of the green macroalga, Chaetomorpha valida (Cladophoraceae, Chlorophyta). *Journal of Applied Phycology*, *24*, 927–933.

Dierssen, H. M., Bostrom, K. J., Chlus, A., Hammerstrom, K., Thompson, D. R., & Lee, Z. (2019). Pushing the limits of seagrass remote sensing in the turbid waters of Elkhorn Slough, California. *Remote Sensing*, *11*, 1664.

Dietterich, T. G. (1999). Experimental comparison of three methods for constructing ensembles of decision trees: bagging, boosting, and randomization. *Machine Learning*, 40, 139–157.

do Amaral Camara Lima, M., Bergamo, T. F., Ward, R. D., & Joyce, C. B. (2023). A review of seagrass ecosystem services: providing nature-based solutions for a changing world. *Hydrobiologia*, 850, 2655–2670.

Doggett, M., & Northen, K. (2023). Studland Bay Marine Conservation Zone (MCZ): Subtidal Seagrass Monitoring Survey 2021.

Doukari, M., Batsaris, M., & Topouzelis, K. (2021). UASea: A data acquisition toolbox for improving marine habitat mapping. *Drones*, *5*, 73.

Duarte, C. M., & Chiscano, C. L. (1999). Seagrass biomass and production: A reassessment. *Aquatic Botany*, *65*, 159–174.

Duarte, C. M., Merino, M., Agawin, N. S. R., Uri, J., Fortes, M. D., Gallegos, M. E., Marbá, N., & Hemminga, M. A. (1998). Root production and belowground seagrass biomass. *Marine Ecology Progress Series*, *171*, 97–108.

Duffy, J. P., Pratt, L., Anderson, K., Land, P. E., & Shutler, J. D. (2018). Spatial assessment of intertidal seagrass meadows using optical imaging systems and a lightweight drone. *Estuarine, Coastal and Shelf Science*, *200*, 169–180.

EnMAP (2023). Environmental Mapping and Analysis Program. *Earth Observation Center EOC of DLR*. Accessed: 12/12/2023 https://www.enmap.org/

Environment Agency (2024). Accessed: 18/01/2023

https://www.gov.uk/government/organisations/environment-agency

ESA. (2024). European Space Agency. Accessed: 12/12/2023 https://www.esa.int/

EU LIFE Wader (2024). Accessed: 12/12/2023 https://tweedforum.org/our-work/life-wader/

Fauzan, M. A., Wicaksono, P., & Hartono. (2021). Characterizing Derawan seagrass cover change with time-series Sentinel-2 images. *Regional Studies in Marine Science*, 48, 102048.

Fernandes, M. B., Hennessy, A., Law, W. B., Daly, R., Gaylard, S., Lewis, M., & Clarke, K. (2022). Landsat historical records reveal large-scale dynamics and enduring recovery of seagrasses in an impacted seascape. *Science of the Total Environment*, *813*, 152646.

Firth, L. B., Foggo, A., Watts, T., Knights, A. M., & deAmicis, S. (2023). Invasive macroalgae in native seagrass beds: vectors of spread and impacts. *Annals of Botany*, 1–10.

Foody, G. M., Campbell, N. A., Trodd, N. M., & Wood, T. F. (1992). Derivation and applications of probabilistic measures of class membership from the maximum-likelihood classification. *Photogrammetric Engineering & Remote Sensing*, *58*(9), 1335–1341.

Forsey, D., Leblon, B., Larocque, A., Skinner, M., & Douglas, A. (2020). Eelgrass mapping in Atlantic Canada using worldview-2 imagery. *International Archives of the Photogrammetry, Remote Sensing and Spatial Information Sciences - ISPRS Archives*, *XLIII-B3-2*, 685–692.

Fourqurean, J. W., Duarte, C. M., Kennedy, H., Marbà, N., Holmer, M., Mateo, M. A., Apostolaki, E. T., Kendrick, G. A., Krause-Jensen, D., McGlathery, K. J., & Serrano, O. (2012). Seagrass ecosystems as a globally significant carbon stock. *Nature Geoscience*, *5*, 505–509.

Frazier, A. E., & Hemingway, B. L. (2021). A Technical Review of Planet Smallsat Data: Practical Considerations for Processing and Using PlanetScope Imagery. *Remote Sensing*, *13*, 3930.

Fyfe, S. K. (2003). Spatial and temporal variation in spectral reflectance: Are seagrass species spectrally distinct? *Limnology and Oceanography*, *48*, 464–479.

Gallant, E., LaRocque, A., Leblon, B., & Douglas, A. (2021). Eelgrass mapping with sentinel-2 and UAV data in Prince Edward Island (CANADA). *ISPRS Annals of the Photogrammetry, Remote Sensing and Spatial Information Sciences*, *5*(3), 125–132.

Gao, G., Beardall, J., Jin, P., Gao, L., Xie, S., & Gao, K. (2022). A review of existing and potential blue carbon contributions to climate change mitigation in the Anthropocene. *Journal of Applied Ecology*, *59*, 1686–1699.

Garono, R. J., Simenstad, C. A., Robinson, R., & Ripley, H. (2004). Using high spatial resolution hyperspectral imagery to map intertidal habitat structure in Hood Canal, Washington, U.S.A. *Canadian Journal of Remote Sensing*, *30*(1), 54–63.

Geomatics Hub (2024). Remote Sensing & Surveying in the Environment Agency. Defra Data Service Platform. https://environment.data.gov.uk/survey

Ghamisi, P., Plaza, J., Chen, Y., Li, J., & Plaza, A. J. (2017). Advanced Spectral Classifiers for Hyperspectral Images: A review. *IEEE Geoscience and Remote Sensing Magazine*, 8–32.

Gilbert, P. M., Kelly, V., Alexander, J., Codispoti, L. A., Boicourt, W. C., Trice, T. M., & Michael, B. (2008). In situ nutrient monitoring: A tool for capturing nutrient variability and the antecedent conditions that support algal blooms. *Harmful Algae*, *8*(1), 175–181.

Grech, A., Chartrand-Miller, K., Erftemeijer, P., Fonseca, M., McKenzie, L., Rasheed, M., Taylor, H., & Coles, R. (2012). A comparison of threats, vulnerabilities and management approaches in global seagrass bioregions. *Environmental Research Letters*, 7.

Green, A. E., Unsworth, R. K. F., Chadwick, M. A., & Jones, P. J. S. (2021). Historical Analysis Exposes Catastrophic Seagrass Loss for the United Kingdom. *Frontiers in Plant Science*, 12.

Green-Gavrielidis, L. A., & Thornber, C. S. (2022). Will Climate Change Enhance Algal Blooms? The Individual and Interactive Effects of Temperature and Rain on the Macroalgae Ulva. *Estuaries and Coasts*, *45*, 1688–1700.

Gullström, M., Lundén, B., Bodin, M., Kangwe, J., Öhman, M. C., Mtolera, M. S. P., & Björk, M. (2006). Assessment of changes in the seagrass-dominated submerged vegetation of tropical Chwaka Bay (Zanzibar) using satellite remote sensing. *Estuarine, Coastal and Shelf Science*, 67, 399–408.

Ha, N. T., Manley-Harris, M., Pham, T. D., & Hawes, I. (2020). A comparative assessment of ensemble-based machine learning and maximum likelihood methods for mapping seagrass using sentinel-2 imagery in Tauranga Harbor, New Zealand. *Remote Sensing*, *12*, 1–16.

Ha, N. T., Manley-Harris, M., Pham, T. D., & Hawes, I. (2021). Detecting Multi-Decadal Changes in Seagrass Cover in Tauranga Harbour, New Zealand, Using Landsat Imagery and Boosting Ensemble Classification Techniques. *ISPRS International Journal of Geo-Information*, 10, 371.

Ha, N. T., Nguyen, H. Q., Pham, T. D., Hoang, C. T., & Hawes, I. (2023). Superpixel for seagrass mapping: a novel method using PlanetScope imagery and machine learning in Tauranga harbour, New Zealand. *Environmental Earth Sciences*, 82(6), 1–19.

Hammer, K. J., Borum, J., Hasler-Sheetal, H., Shields, E. C., Sand-Jensen, K., & Moore, K. A. (2018). High temperatures cause reduced growth, plant death and metabolic changes in eelgrass Zostera marina. *Marine Ecology Progress Series*, *604*, 121–132.

Han, Q., & Liu, D. (2014). Macroalgae blooms and their effects on seagrass ecosystems. *Journal of Ocean University of China*, 13, 791–798.

Han, Q., Soissons, L. M., Bouma, T. J., van Katwijk, M. M., & Liu, D. (2016). Combined nutrient and macroalgae loads lead to response in seagrass indicator properties. *Marine Pollution Bulletin*, *106*, 174–182.

Haro, S., Jesus, B., Oiry, S., Papaspyrou, S., Lara, M., González, C. J., & Corzo, A. (2022). Microphytobenthos spatio-temporal dynamics across an intertidal gradient using Random Forest classification and Sentinel-2 imagery. *Science of the Total Environment*, 804, 149983 Contents.

Hartigan, J. A., & Wong, M. A. (1979). A K-Means Clustering Algorithm. *Journal of the Royal Statistical Society: Series C (Applied Statistics)*, *28*(1), 100–108.

Hauxwell, J., Cebrián, J., Furlong, C., & Valiela, I. (2001). Macroalgal canopies contribute to eelgrass (Zostera marina) decline in temperate estuarine ecosystems. *Ecology*, 82(4), 1007–1022.

Hemminga, M. A., & Duarte, C. M. (2000). Seagrass architectural features. In: Hemminga, M. A., & Duarte, C. M. (Eds). Seagrass Ecology (pp. 27–61). Cambridge University Press.

Hobley, B., Arosio, R., French, G., Bremner, J., Dolphin, T., & Mackiewicz, M. (2021). Semi-supervised segmentation for coastal monitoring seagrass using RPA imagery. *Remote Sensing*, *13*, 1741.

Hogrefe, K. R., Ward, D. H., Donnelly, T. F., & Dau, N. (2014). Establishing a baseline for regional scale monitoring of eelgrass (Zostera marina) habitat on the lower Alaska Peninsula. *Remote Sensing*, *6*(12), 12447–12477.

Holmquist, J. G. (1997). Disturbance and gap formation in a marine benthic mosaic: Influence of shifting macroalgal patches on seagrass structure and mobile invertebrates. *Marine Ecology Progress Series*, *158*, 121–130.

Holon, F., Boissery, P., Guilbert, A., Freschet, E., & Deter, J. (2015). The impact of 85 years of coastal development on shallow seagrass beds (Posidonia oceanica L. (Delile)) in South Eastern France: A slow but steady loss without recovery. *Estuarine, Coastal and Shelf Science*, *165*, 204e212.

Hossain, M. S., Bujang, J. S., Zakaria, M. H., & Hashim, M. (2015). The application of remote sensing to seagrass ecosystems: an overview and future research prospects. *International Journal of Remote Sensing*, *36*(1), 61–114.

Hossain, M. S., & Hashim, M. (2019). Potential of Earth Observation (EO) technologies for seagrass ecosystem service assessments. *International Journal of Applied Earth Observation and Geoinformation*, 77, 15–29.

Hughes, A. R., Williams, S. L., Duarte, C. M., Heck, K. L., & Waycott, M. (2009). Associations of concern: Declining seagrasses and threatened dependent species. *Frontiers in Ecology and the Environment*, 7.

Hwang, C., Chang, C. H., Kildea, T., Burch, M., & Fernandes, M. (2019). Effects of Epiphytes and Depth on Seagrass Spectral Profiles: Case Study of Gulf St. Vincent, South Australia. *International Journal of Environmental Research and Public Health*, *16*, 2701.

Ivajnšic, D., Orlando-Bonaca, M., Mavric, B., Lipej, L., Donša, D., Grujic, V. J., Trkov, D., & 1. (2022). Evaluating Seagrass Meadow Dynamics by Integrating Field-Based and Remote Sensing Techniques. *Plants*, *11*, 1196.

James, D., Collin, A., Houet, T., Mury, A., Gloria, H., & Le Poulain, N. (2020). Towards Better Mapping of Seagrass Meadows using UAV Multispectral and Topographic Data. *Journal of Coastal Research*, *95*, 1117–1121.

Jia, J., Wang, Y., Chen, J., Guo, R., Shu, R., & Wang, J. (2020). Status and application of advanced airborne hyperspectral imaging technology: A review. *Infrared Physics and Technology*, *104*, 103115.

Jones, B. L., Cullen-Unsworth, L. C., & Unsworth, R. K. F. (2018). Tracking nitrogen source using δ15 N reveals human and agricultural drivers of seagrass degradation across the British isles. *Frontiers in Plant Science*, *9*, 133.

Jones, B. L., & Unsworth, R. K. F. (2016). The perilous state of seagrass in the British Isles. *Royal Society Open Science*, *3*, 150596.

Kaldy, J. E. (2014). Effect of temperature and nutrient manipulations on eelgrass Zostera marina L. from the Pacific Northwest, USA. *Journal of Experimental Marine Biology and Ecology*, *453*, 108–115 Contents.

Kattenborn, T., Leitloff, J., Schiefer, F., & Hinz, S. (2021). Review on Convolutional Neural Networks (CNN) in vegetation remote sensing. *ISPRS Journal of Photogrammetry and Remote Sensing*, 173, 24–49.

Kaufman, K. A., & Bell, S. S. (2022). The Use of Imagery and GIS Techniques to Evaluate and Compare Seagrass Dynamics across Multiple Spatial and Temporal Scales. *Estuaries and Coasts*, *45*, 1028–1044.

Keshava, N., & Mustard, J. F. (2002). Spectral unmixing. *IEEE Signal Processing Magazine*, 19, 44–57.

Kim, K., Choi, J. K., Ryu, J. H., Jeong, H. J., Lee, K., Park, M. G., & Kim, K. Y. (2015). Observation of typhoon-induced seagrass die-off using remote sensing. *Estuarine, Coastal and Shelf Science*, *154*, 111–121.

Kim, Y. K., Kim, S. H., & Lee, K. S. (2015). Seasonal Growth Responses of the Seagrass Zostera marina under Severely Diminished Light Conditions. *Estuaries and Coasts*, *38*(558–568).

Knudby, A., Newman, C., Shaghude, Y., & Muhando, C. (2010). Simple and effective monitoring of historic changes in nearshore environments using the free archive of Landsat imagery. *International Journal of Applied Earth Observation and Geoinformation*, 12, 116–122.

Kohlus, J., Stelzer, K., Müller, G., & Smollich, S. (2020). Mapping seagrass (Zostera) by remote sensing in the Schleswig-Holstein Wadden Sea. *Estuarine, Coastal and Shelf Science*, 238, 106699.

Kopacz, J. R., Herschitz, R., & Roney, J. (2020). Small satellites an overview and assessment. *Acta Astronautica*, *170*, 93–105.

Kovacs, E., Roelfsema, C., Lyons, M., Zhao, S., & Phinn, S. (2018). Seagrass habitat mapping: How do landsat 8 OLI, sentinel-2, ZY-3A, and worldview-3 perform? *Remote Sensing Letters*, *9*(7), 686–695.

Kuhwald, K., Schneider von Deimling, J., Schubert, P., & Oppelt, N. (2022). How can Sentinel-2 contribute to seagrass mapping in shallow, turbid Baltic Sea waters? *Remote Sensing in Ecology and Conservation*, 8(3), 328–346.

La Nafie, Y. A., de los Santos, C. B., Brun, F. G., van Katwijk, M. M., & Bouma, T. J. (2012). Waves and high nutrient loads jointly decrease survival and separately affect morphological and biomechanical properties in the seagrass Zostera noltii. *Limnology and Oceanography*, *57*(6), 1664–1672.

Lathrop, R. G., Montesano, P., & Haag, S. (2006). A multi-scale segmentation approach to mapping seagrass habitats using airborne digital camera imagery. *Photogrammetric Engineering and Remote Sensing*, 72(6), 665–675.

Leblanc, M. L., LaRocque, A., Leblon, B., Hanson, A., & Humphries, M. M. (2021). Using Landsat Time-Series to Monitor and Inform Seagrass Dynamics: A Case Study

in the Tabusintac Estuary, New Brunswick, Canada. *Canadian Journal of Remote Sensing*, 47(1), 65–82.

Leblon, B., Larocque, A., Gallant, E., Clyne, K., & Douglas, A. (2022). Eelgrass Bed Mapping with Multispectral UAV Imagery in Atlantic Canada. *International Archives of the Photogrammetry, Remote Sensing and Spatial Information Sciences - ISPRS Archives*, *43*(B3-2022), 649–656.

Lee, C. B., Martin, L., Traganos, D., Antat, S., Baez, S. K., Cupidon, A., Faure, A., Harlay, J., Morgan, M., Mortimer, J. A., Reinartz, P., & Rowlands, G. (2023). Mapping the National Seagrass Extent in Seychelles Using PlanetScope NICFI Data. *Remote Sensing*, *15*, 4500.

Lee, K.H., Isenhart, T.M., Schultz, R. C. (2003). Seasonal Dynamics of the Seagrass Zostera marina on the South Coast of the Korean Peninsula. *Journal of the Korean Society of Oceanography*, 38(2), 68–79.

Légaré, B., Bélanger, S., Singh, R. K., Bernatchez, P., & Cusson, M. (2022). Remote Sensing of Coastal Vegetation Phenology in a Cold Temperate Intertidal System: Implications for Classification of Coastal Habitats. *Remote Sensing*, 3000.

Lengyel, S., Kobler, A., Kutnar, L., Framstad, E., Henry, P. Y., Babij, V., Gruber, B., Schmeller, D., & Henle, K. (2008). A review and a framework for the integration of biodiversity monitoring at the habitat level. *Biodiversity and Conservation*, *17*, 3341–3356.

Levings, C. D., North, M. S., Piercey, G. E., Jamieson, G., & Smiley, B. (1999). Mapping nearshore and intertidal marine habitats with remote sensing and GPS: the importance of spatial and temporal scales. *Oceans Conference Record (IEEE)*, 1249–1255.

Li, M., Lundquist, C. J., Pilditch, C. A., Rees, T. A. V., & Ellis, J. (2019). Implications of nutrient enrichment for the conservation and management of seagrass Zostera muelleri meadows. *Aquatic Conservation: Marine and Freshwater Ecosystems*, 29, 1484–1502.

Lønborg, C., Thomasberger, A., Stæhr, P. A. U., Stockmarr, A., Sengupta, S., Rasmussen, M. L., Nielsen, L. T., Hansen, L. B., & Timmermann, K. (2021). Submerged aquatic vegetation: Overview of monitoring techniques used for the

identification and determination of spatial distribution in European coastal waters. Integrated Environmental Assessment and Management, 00(00), 1–17.

Lundén, B., & Gullström, M. (2003). Satellite remote sensing for monitoring of vanishing seagrass in Swedish coastal waters. *Norsk Geografisk Tidsskrift- Norwegian Journal of Geography*, *57*(2), 121–124.

Lyons, M. B., Phinn, S. R., & Roelfsema, C. M. (2012). Long term land cover and seagrass mapping using Landsat and object-based image analysis from 1972 to 2010 in the coastal environment of South East Queensland, Australia. *ISPRS Journal of Photogrammetry and Remote Sensing*, 71, 34–46.

Lyons, M. B., Roelfsema, C. M., & Phinn, S. R. (2013). Towards understanding temporal and spatial dynamics of seagrass landscapes using time-series remote sensing. *Estuarine, Coastal and Shelf Science*, *120*, 42–53.

Lyons, M., Phinn, S., & Roelfsema, C. (2011). Integrating Quickbird multi-spectral satellite and field data: Mapping bathymetry, seagrass cover, seagrass species and change in Moreton Bay, Australia in 2004 and 2007. *Remote Sensing*, 3, 42–64.

Macleod, R. D., & Congalton, R. G. (1998). A quantitative comparison of change-detection algorithms for monitoring eelgrass from remotely sensed data. *Photogrammetric Engineering and Remote Sensing*, *64*(3), 207–216.

Maggiori, E., Tarabalka, Y., Charpiat, G., & Alliez, P. (2017). Convolutional Neural Networks for Large-Scale Remote-Sensing Image Classification. *IEEE Transactions on Geoscience and Remote Sensing*, *55*(2), 645–657.

Maier, G., Nimmo-Smith, R. J., Glegg, G. A., Tappin, A. D., & Worsfold, P. J. (2009). Estuarine eutrophication in the UK: current incidence and future trends. *Aquatic Conservation: Marine and Freshwater Ecosystems*, *19*, 43–56.

Martin, R., Ellis, J., Brabyn, L., & Campbell, M. (2020a). Change-mapping of estuarine intertidal seagrass (Zostera muelleri) using multispectral imagery flown by remotely piloted aircraft (RPA) at Wharekawa Harbour, New Zealand. *Estuarine, Coastal and Shelf Science*, *246*, 107046.

Massa, S. I., Arnaud-Haond, S., Pearson, G. A., & Serrão, E. A. (2009). Temperature tolerance and survival of intertidal populations of the seagrass Zostera noltii

(Hornemann) in Southern Europe (Ria Formosa, Portugal). *Hydrobiologia*, *619*, 195–201.

McCarthy, M. J., Colna, K. E., El-Mezayen, M. M., Laureano-Rosario, A. E., Méndez-Lázaro, P., Otis, D. B., Toro-Farmer, G., Vega-Rodriguez, M., & Muller-Karger, F. E. (2017). Satellite Remote Sensing for Coastal Management: A Review of Successful Applications. *Environmental Management*, *60*, 323–339.

McGlathery, K. J. (2001). Macroalgal blooms contribute to the decline of seagrass in nutrient-enriched coastal waters. *Journal of Phycology*, *37*, 453–456.

McKenzie, L. J., Nordlund, L. M., Jones, B. L., Cullen-Unsworth, L. C., Roelfsema, C., & Unsworth, R. K. F. (2020). The global distribution of seagrass meadows. *Environmental Research Letters*, *15*, 074041 Environmental.

McLeod, E., Chmura, G. L., Bouillon, S., Salm, R., Björk, M., Duarte, C. M., Lovelock, C. E., Schlesinger, W. H., & Silliman, B. R. (2011). A blueprint for blue carbon: Toward an improved understanding of the role of vegetated coastal habitats in sequestering CO2. *Frontiers in Ecology and the Environment*, *9*(10), 552–560.

Met Office, 2021. Extremes of temperature, March and April 2021. Accessed: 12/12/2023

https://www.metoffice.gov.uk/binaries/content/assets/metofficegovuk/pdf/weather/learn-about/uk-past-events/interesting/2021/2021 03 high temperatures.pdf

Minghelli, A., Vadakke-Chanat, S., Chami, M., Guillaume, M., & Peirache, M. (2021). Benefit of the Potential Future Hyperspectral Satellite Sensor (BIODIVERSITY) for Improving the Determination of Water Column and Seabed Features in Coastal Zones. *IEEE Journal of Selected Topics in Applied Earth Observations and Remote Sensing*, 14, 1222–1232.

mNCEA (2024). marine National Capital Ecosystem Assessment. Accessed: 12/12/2023 https://marinescience.blog.gov.uk/2022/04/13/introducing-the-marine-natural-capital-and-ecosystem-assessment-programme-mncea/

Moore, K. A. (2004). Influence of seagrasses on water quality in shallow regions of the lower Chesapeake Bay. *Journal of Coastal Research*, *45*, 162–178.

Moore, K. A., & Wetzel, R. L. (2000). Seasonal variations in eelgrass (Zostera marina L.) responses to nutrient enrichment and reduced light availability in experimental ecosystems. *Journal of Experimental Marine Biology and Ecology*, *244*, 1–28.

Mountrakis, G., Im, J., & Ogole, C. (2011). Support vector machines in remote sensing: A review. *ISPRS Journal of Photogrammetry and Remote Sensing*, 66, 247–259.

Mumby, P. J., Green, E., Edwards, a J., & Clark, C. D. (1999). The cost-effectiveness of remote sensing for tropical coastal resources assessment and management. *Journal of Environmental Management*, *55*, 157–166.

Myers, J. S., & Miller, R. L. (2005). Optical airborne remote sensing. In *Remote Sensing of Coastal Aquatic Environments* (pp. 51–67). https://doi.org/10.1007/1-4020-3100-9 3

Nagendra, H., Lucas, R., Honrado, J. P., Jongman, R. H. G., Tarantino, C., Adamo, M., & Mairota, P. (2013). Remote sensing for conservation monitoring: Assessing protected areas, habitat extent, habitat condition, species diversity, and threats. *Ecological Indicators*, 33, 45–59.

Nahirnick, N. K., Hunter, P., Costa, M., Schroeder, S., & Sharma, T. (2019a). Benefits and Challenges of UAS Imagery for Eelgrass (Zostera marina) Mapping in Small Estuaries of the Canadian West Coast. *Journal of Coastal Research*, *35*(3), 673–683.

Nahirnick, N. K., Reshitnyk, L., Campbell, M., Hessing-Lewis, M., Costa, M., Yakimishyn, J., & Lee, L. (2019b). Mapping with confidence; delineating seagrass habitats using Unoccupied Aerial Systems (UAS). *Remote Sensing in Ecology and Conservation*, *5*(2), 121–135.

Natural England (2024). Accessed: 12/12/2023 https://naturalengland-defra.opendata.arcgis.com/maps/e009f2adbc9b4028a34842b133c6636b/about

Neckles, H. A., Kopp, B. S., Peterson, B. J., & Pooler, P. S. (2012). Integrating Scales of Seagrass Monitoring to Meet Conservation Needs. *Estuaries and Coasts*, *35*, 23–46.

O'Gorman, P. A. (2015). Precipitation Extremes Under Climate Change. *Current Climate Change Reports*, *1*, 49–59.

O'Neill, J. D., & Costa, M. (2013). Mapping eelgrass (Zostera marina) in the Gulf Islands National Park Reserve of Canada using high spatial resolution satellite and airborne imagery. *Remote Sensing of Environment*, 133, 152–167.

O'Neill, J. D., Costa, M., & Sharma, T. (2011). Remote sensing of shallow coastal benthic substrates: In situ spectra and mapping of eelgrass (Zostera marina) in the Gulf Islands National Park Reserve of Canada. *Remote Sensing*, *3*, 975–1005.

Orth, R. J., Carruthers, T. J. B., Dennison, W. C., Duarte, C. M., Fourqurean, J. W., Heck JR., K. L., Hughes, R. A., Kendrick, G. A., Kenworthy, W. J., Olyarnik, S., Short, F. T., Waycott, M., & Williams, S. L. (2006). A Global Crisis for Seagrass Ecosystems. *BioScience*, *56*(12), 987–996.

Orth, R. J., Fishman, J. R., Wilcox, D. J., Moore, K. A., Beach, P., & Moore, A. (2002). Identification and Management of Fishing Gear Impacts in a Recovering Seagrass System in the Coastal Bays of the Delmarva Peninsula, USA. *Journal of Coastal Research*, 37, 111–129.

Over, J.-S. R., Ritchie, A. C., Kranenburg, C. J., Jenna A., B., Buscombe, D., Noble, T., Sherwood, C. R., Warrick, J. A., & Wernette, P. A. (2021). *Processing Coastal Imagery With Agisoft Metashape Professional Edition, Version 1 . 6 — Structure From Motion Workflow Documentation.*

Pal, M. (2005). Random forest classifier for remote sensing classification. *International Journal of Remote Sensing*, *26*(1), 217–222.

Pandey, P. C., Balzter, H., Srivastava, P. K., Petropoulos, G. P., & Bhattacharya, B. (2020). Future perspectives and challenges in hyperspectral remote sensing [Bookitem]. *Hyperspectral Remote Sensing: Theory and Applications*, 429–439.

Pereira, L. (2021). Macroalgae. Encyclopedia, 1, 177-188.

Pettorelli, N., Laurance, W. F., O'Brien, T. G., Wegmann, M., Nagendra, H., & Turner, W. (2014). Satellite remote sensing for applied ecologists: Opportunities and challenges. *Journal of Applied Ecology*, *51*, 839–848.

Phillips, R. C., & Menez, E. G. (1988). *Seagrasses*. Smithsonian contributions to the marine sciences. Number 34. Smithsonian Institution Press, Washington, D.C.

Phinn S., Roelfsema C., Kovacs E., Canto R., Lyons M., Saunders M., Maxwell P. (2018a). Mapping, Monitoring and Modelling Seagrass Using Remote Sensing

Techniques. In: Larkum A. W.D. Kendrick G. A., Ralph, Peter J. (Eds) Seagrasses of Australia: Structure, ecology and conservation. Pp 445- 490. Springer Nature Switzerland AG.

Phinn, S. R., Kovacs, E. M., Roelfsema, C. M., Canto, R. F., Collier, C. J., & McKenzie, L. J. (2018b). Assessing the potential for satellite image monitoring of seagrass thermal dynamics: for inter- and shallow sub-tidal seagrasses in the inshore Great Barrier Reef World Heritage Area, Australia. *International Journal of Digital Earth*, 11(8), 803–824.

Phinn, S., Roelfsema, C., Dekker, A., Brando, V., & Anstee, J. (2008). Mapping seagrass species, cover and biomass in shallow waters: An assessment of satellite multi-spectral and airborne hyper-spectral imaging systems in Moreton Bay (Australia). *Remote Sensing of Environment*, *112*, 3413–3425.

Pihl, L., Svenson, A., Moksnes, P. O., & Wennhage, H. (1999). Distribution of green algal mats throughout shallow soft bottoms of the Swedish Skagerrak archipelago in relation to nutrient sources and wave exposure. *Journal of Sea Research*, *41*, 281–294.

Planet (2022). Planet Imagery Product Specifications. Accessed: 12/02/2023

https://www.planet.com/products/satelliteimagery/files/Planet_Imagery_Product_Specs.pdf

Planet Labs (2024). Accessed: 12/02/2023 www.planet.com

Postlethwaite, V. R., McGowan, A. E., Kohfeld, K. E., Robinson, C. L. K., & Pellatt, M. G. (2018). Low blue carbon storage in eelgrass (Zostera marina) meadows on the Pacific Coast of Canada. *PLoS ONE*, *13*(6), e0198348.

Price, D. M., Felgate, S. L., Huvenne, V. A. I., Strong, J., Carpenter, S., Barry, C., Lichtschlag, A., Sanders, R., Carrias, A., Young, A., Andrade, V., Cobb, E., Le Bas, T., Brittain, H., & Evans, C. (2022). Quantifying the Intra-Habitat Variation of Seagrass Beds with Unoccupied Aerial Vehicles (UAVs). *Remote Sensing*, *14*, 480.

Prystay, T. S., Adams, G., Favaro, B., Gregory, R. S., & Le Bris, A. (2023). The reproducibility of remotely piloted aircraft systems to monitor seasonal variation in submerged seagrass and estuarine habitats. *Facets*, *8*, 1–22.

Pu, R., & Bell, S. (2017). Mapping seagrass coverage and spatial patterns with high spatial resolution IKONOS imagery. *International Journal of Applied Earth Observation and Geoinformation*, *54*, 145–158.

Pu, R., Bell, S., Meyer, C., Baggett, L., & Zhao, Y. (2012). Mapping and assessing seagrass along the western coast of Florida using Landsat TM and EO-1 ALI/Hyperion imagery. *Estuarine, Coastal and Shelf Science*, *115*, 234–245.

Quintano, C., Fernández-Manso, A., Shimabukuro, Y. E., & Pereira, G. (2012). Spectral unmixing. *International Journal of Remote Sensing*, *33*(17), 5307–5340.

ReMeMaRe. (2024). Restoring Meadow, Marsch and Reef.

Https://Ecsa.International/Reach/Restoring-Meadow-Marsh-and-Reef-Rememare.

Reshitnyk, L., Costa, M., Robinson, C., & Dearden, P. (2014). Evaluation of WorldView-2 and acoustic remote sensing for mapping benthic habitats in temperate coastal Pacific waters. *Remote Sensing of Environment*, *153*, 7–23.

ReSOWUK (2024). Restoration of Seagrass for Ocean Wealth UK. Accessed: 12/11/2023 https://resow.uk/

Richards, J. A. (1986). Remote Sensing Digital Image Analysis. In *Remote Sensing Digital Image Analysis* (4th ed.). Springer-Verlag Berlin Heidelberg.

Richards, J. A. (2013). Remote Sensing Digital Image Analysis. In *Remote Sensing Digital Image Analysis* (5th ed.). Springer-Verlag Berlin Heidelberg.

Richards, J. A. (2022). Remote Sensing Digital Image Analysis. In *Remote Sensing Digital Image Analysis* (6th ed.). Springer-Verlag Berlin Heidelberg.

Rocchini, D., Petras, V., Petrasova, A., Horning, N., Furtkevicova, L., Neteler, M., Leutner, B., & Wegmann, M. (2017). Open data and open source for remote sensing training in ecology. *Ecological Informatics*, *40*, 57–61.

Roelfsema, C., Kovacs, E. M., Saunders, M. I., Phinn, S., Lyons, M., & Maxwell, P. (2013). Challenges of remote sensing for quantifying changes in large complex seagrass environments. *Estuarine, Coastal and Shelf Science*, *133*, 161–171.

Roelfsema, C. M., Lyons, M., Kovacs, E. M., Maxwell, P., Saunders, M. I., Samper-Villarreal, J., & Phinn, S. R. (2014). Multi-temporal mapping of seagrass cover, species and biomass: A semi-automated object based image analysis approach. *Remote Sensing of Environment*, *150*, 172–187.

Roelfsema, C., Phinn, S., Jupiter, S., Comley, J., & Albert, S. (2013). Mapping coral reefs at reef to reef-system scales, 10s-1000s km2, using object-based image analysis. *International Journal of Remote Sensing*, *34*(18), 6367–6388.

Röhr, M. E., Holmer, M., Baum, J. K., Björk, M., Chin, D., Chalifour, L., Cimon, S., Cusson, M., Dahl, M., Deyanova, D., Duffy, J. E., Eklöf, J. S., Geyer, J. K., Griffin, J. N., Gullström, M., Hereu, C. M., Hori, M., Hovel, K. A., Hughes, A. R., ... Boström, C. (2018). Blue Carbon Storage Capacity of Temperate Eelgrass (Zostera marina) Meadows. *Global Biogeochemical Cycles*, *32*, 1457–1475.

Román, A., Tovar-Sánchez, A., Olivé, I., & Navarro, G. (2021). Using a UAV-Mounted Multispectral Camera for the Monitoring of Marine Macrophytes. *Frontiers in Marine Science*, *8*, 722698.

Rose, R. A., Byler, D., Eastman, J. R., Fleishman, E., Geller, G., Goetz, S., Guild, L., Hamilton, H., Hansen, M., Headley, R., Hewson, J., Horning, N., Kaplin, B. A., Laporte, N., Leidner, A., Leimgruber, P., Morisette, J., Musinsky, J., Pintea, L., ... Wilson, C. (2015). Ten ways remote sensing can contribute to conservation. *Conservation Biology*, *29*(2), 350–359.

Rossiter, T., Furey, T., McCarthy, T., & Stengel, D. B. (2020). UAV-mounted hyperspectral mapping of intertidal macroalgae. *Estuarine, Coastal and Shelf Science*, *242*, 106789.

Rowan, G. S. L., & Kalacska, M. (2021). A review of remote sensing of submerged aquatic vegetation for non-specialists. *Remote Sensing*, *13*, 623.

Sakamaki, T., Nishimura, O., Sudo R. (2006). Tidal time-scale variation in nutrient flux across the sediment-water interface of an estuarine tidal flat. *Estuarine, Coastal and Shelf Science*, 67, 653-663.

Schill, S. R., McNulty, V. P., Pollock, F. J., Lüthje, F., Li, J., Knapp, D. E., Kington, J. D., McDonald, T., Raber, G. T., Escovar-Fadul, X., & Asner, G. P. (2021). Regional high-resolution benthic habitat data from planet dove imagery for conservation decision-making and marine planning. *Remote Sensing*, *13*, 4215.

Schmidt, K. S., & Skidmore, A. K. (2003). Spectral discrimination of vegetation types in a coastal wetland. *Remote Sensing of Environment*, *85*, 92–108.

Scornet, E. (2017). Tuning parameters in random forests. *ESAIM: Proceedings and Surveys*, *60*, 144–162.

Sheykhmousa, M., Mahdianpari, M., Ghanbari, H., Mohammadimanesh, F., Ghamisi, P., & Homayouni, S. (2020). Support Vector Machine Versus Random Forest for Remote Sensing Image Classification: A Meta-Analysis and Systematic Review. *IEEE Journal of Selected Topics in Applied Earth Observations and Remote Sensing*, 13, 6308–6325.

Short, F., Carruthers, T., Dennison, W., & Waycott, M. (2007). Global seagrass distribution and diversity: A bioregional model. *Journal of Experimental Marine Biology and Ecology*, 350, 3–20.

Short, F. T., Coles, R., Fortes, M. D., Victor, S., Salik, M., Isnain, I., Andrew, J., & Seno, A. (2014). Monitoring in the Western Pacific region shows evidence of seagrass decline in line with global trends. *Marine Pollution Bulletin*, 83, 408–416.

Short, F. T., Koch, E. W., Creed, J. C., Magalhães, K. M., Fernandez, E., & Gaeckle, J. L. (2006). SeagrassNet monitoring across the Americas: Case studies of seagrass decline. *Marine Ecology*, *27*, 277–289.

Short, F. T., & Neckles, H. A. (1999). The effects of global climate change on seagrasses. *Aquatic Botany*, *63*, 169–196.

Simpson, J., Bruce, E., Davies, K. P., & Barber, P. (2022). A Blueprint for the Estimation of Seagrass Carbon Stock Using Remote Sensing-Enabled Proxies. *Remote Sensing*, *14*, 1–18.

Soissons, L. M., Haanstra, E. P., Van Katwijk, M. M., Asmus, R., Auby, I., Barillé, L., Brun, F. G., Cardoso, P. G., Desroy, N., Fournier, J., Ganthy, F., Garmendia, J. M., Godet, L., Grilo, T. F., Kadel, P., Ondiviela, B., Peralta, G., Puente, A., Recio, M., ... Bouma, T. J. (2018). Latitudinal patterns in european seagrass carbon reserves: Influence of seasonal fluctuations versus short-term stress and disturbance events. *Frontiers in Plant Science*, *9*, 1–12.

Sousa, A. I., da Silva, J. F., Azevedo, A., & Lillebø, A. I. (2019). Blue Carbon stock in Zostera noltei meadows at Ria de Aveiro coastal lagoon (Portugal) over a decade. *Scientific Reports*, *9*, 14387.

SSSI citation (1989). Site of Special Scientific Interest. SSSI citation-legal document Natural England. Accessed:12/ 11/2023

https://ukfossils.files.wordpress.com/2009/03/scremerston.pdf

Stafford, N. B., & Bell, S. S. (2006). Space competition between seagrass and Caulerpa prolifera (Forsskaal) Lamouroux following simulated disturbances in Lassing Park, FL. *Journal of Experimental Marine Biology and Ecology*, 333, 49–57.

Strachan, L. L., Lilley, R. J., & Hennige, S. J. (2022). A regional and international framework for evaluating seagrass management and conservation. *Marine Policy*, *146*, 105306.

Stronger Shores (2024). Accessed:12/ 11/2023 https://strongershores.com/

Svane, N., Lange, T., Egemose, S., Dalby, O., Thomasberger, A., & Flindt, M. R. (2022). Unoccupied aerial vehicle-assisted monitoring of benthic vegetation in the coastal zone enhances the quality of ecological data. *Progress in Physical Geography*, *46*(2), 232–249.

Tang, K. H. D., & Hadibarata, T. (2022). Seagrass Meadows under the Changing Climate: A Review of the Impacts of Climate Stressors. *Research in Ecology*, *4*(1), 27–36.

Thomson, J. A., Burkholder, D. A., Heithaus, M. R., Fourqurean, J. W., Fraser, M. W., Statton, J., & Kendrick, G. A. (2015). Extreme temperatures, foundation species, and abrupt ecosystem change: an example from an iconic seagrass ecosystem. *Global Change Biology*, *21*, 1463–1474.

Topouzelis, K., Makri, D., Stoupas, N., Papakonstantinou, A., & Katsanevakis, S. (2018). Seagrass mapping in Greek territorial waters using Landsat-8 satellite images. *International Journal of Applied Earth Observation and Geoinformation*, 67, 98–113.

Traganos, D., Aggarwal, B., Poursanidis, D., Topouzelis, K., Chrysoulakis, N., & Reinartz, P. (2018). Towards global-scale seagrass mapping and monitoring using Sentinel-2 on Google Earth Engine: The case study of the Aegean and Ionian Seas. *Remote Sensing*, *10*, 1227.

Traganos, D., & Reinartz, P. (2018). Interannual change detection of mediterranean seagrasses using RapidEye image time series. *Frontiers in Plant Science*, *9*, 96.

Uhl, F., Rasmussen, T. G., & Oppelt, N. (2022). Classification Ensembles for Beach Cast and Drifting Vegetation Mapping with Sentinel-2 and PlanetScope. *Geosciences*, 12, 15.

Uhrin, A. V., & Townsend, P. A. (2016). Improved seagrass mapping using linear spectral unmixing of aerial photographs. *Estuarine, Coastal and Shelf Science*, *171*, 11–22.

UNEP-WCMC. (2020). Out of Blue: The value of seagrasses to the environment and to people.

UNEP-WCMC, & Short, F. T. (2021). *Global distribution of seagrasses (version 7.1).* Seventh update to the data layer used in Green and Short (2003). Cambridge (UK): UN Environment World Conservation Monitoring Centre.

UNESC (2005). Applications of Satellite and Airborne Image Data to Coastal Management. Third Edition. Coastal region and small island papers 18, UNESCO, Paris. Vi+253pp. 15/01/2024 www.bilko.org/module7

Unsworth, R. K. F., Cullen-Unsworth, L. C., Jones, B. L. H., & Lilley, R. J. (2022). The planetary role of seagrass conservation. *Science*, 377, 609–613.

Unsworth, R. K. F., Nordlund, L. M., & Cullen-Unsworth, L. C. (2019). Seagrass meadows support global fisheries production. *Conservation Letters*, *12*, e12566. https://doi.org/10.1111/conl.12566

UN-WCMC (2020). Summary: Out of the Blue the Value of Seagrasses.

USGS (2023). Https://Www.Usgs.Gov/Faqs/What-Remote-Sensing-and-What-It-Used.

Vahtmäe, E., Kotta, J., Lõugas, L., & Kutser, T. (2021). Mapping spatial distribution, percent cover and biomass of benthic vegetation in optically complex coastal waters using hyperspectral CASI and multispectral Sentinel-2 sensors. *International Journal of Applied Earth Observation and Geoinformation*, 102, 102444.

Vahtmäe, E., Kutser, T., Kotta, J., Pärnoja, M., Möller, T., & Lennuk, L. (2012). Mapping Baltic Sea shallow water environments with airborne remote sensing. *Oceanology*, 52(6), 803–809.

Veettil, B. K., Ward, R. D., Lima, M. D. A. C., Stankovic, M., Hoai, P. N., & Quang, N. X. (2020). Opportunities for seagrass research derived from remote sensing: A review of current methods. *Ecological Indicators*, *117*, 106560.

Ventura, D., Bonifazi, A., Gravina, M. F., Belluscio, A., & Ardizzone, G. (2018). Mapping and classification of ecologically sensitive marine habitats using unmanned aerial vehicle (UAV) imagery and Object-Based Image Analysis (OBIA). *Remote Sensing*, 10, 1331.

Ventura, D., Mancini, G., Casoli, E., Pace, D. S., Lasinio, G. J., Belluscio, A., & Ardizzone, G. (2022). Seagrass restoration monitoring and shallow-water benthic habitat mapping through a photogrammetry-based protocol. *Journal of Environmental Management*, 304, 114262.

Vitousek, S., Buscombe, D., Vos, K., Barnard, P. L., Ritchie, A. C., & Warrick, J. A. (2023). The future of coastal monitoring through satellite remote sensing. *Cambridge Prisms: Coastal Futures*, 1(e10), 1–18.

Wabnitz, C. C., Andréfouët, S., Torres-Pulliza, D., Müller-Karger, F. E., & Kramer, P. A. (2008). Regional-scale seagrass habitat mapping in the Wider Caribbean region using Landsat sensors: Applications to conservation and ecology. *Remote Sensing of Environment*, 112, 3455–3467.

Wacker, A. G., & Landgrebe, D. A. (1972). Minimum Distance Classification in Remote Sensing. *LARS Technical Reports*.

Walker, S. E., Sheaves, M., & Waltham, N. J. (2023). Barriers to Using UAVs in Conservation and Environmental Management: A Systematic Review. *Environmental Management*.

Ward, D. H., Markon, C. J., & Douglas, D. C. (1997). Distribution and stability of eelgrass beds at Izembek Lagoon, Alaska. *Aquatic Botany*, *58*, 229–240.

Weismiller, R. A., Kristof, S. J., Scholtz, D. K., Anulta, P. E., & Momin, S. A. (1977). Change detection in coastal zone environments. *Photogrammetric Engineering and Remote Sensing*, *43*(12), 1533-1539.

Wicaksono, P., & Lazuardi, W. (2018). Assessment of PlanetScope images for benthic habitat and seagrass species mapping in a complex optically shallow water environment. *International Journal of Remote Sensing*, *39*(17), 5739–5765.

Wicaksono, P., Wulandari, S. A., Lazuardi, W., & Munir, M. (2021). Sentinel-2 images deliver possibilities for accurate and consistent multi-temporal benthic habitat maps in optically shallow water. *Remote Sensing Applications: Society and Environment*, 23, 100572.

Wilson, K. L., Skinner, M. A., & Lotze, H. K. (2019). Eelgrass (Zostera marina) and benthic habitat mapping in Atlantic Canada using high-resolution SPOT 6/7 satellite imagery. *Estuarine, Coastal and Shelf Science*, 226, 106292.

Wilson, K. L., Wong, M. C., & Devred, E. (2022). Comparing Sentinel-2 and WorldView-3 Imagery for Coastal Bottom Habitat Mapping in Atlantic Canada. *Remote Sensing*, *14*, 1254.

Wilson, K., Pressey, R. L., Newton, A., Burgman, M., Possingham, H., & Weston, C. (2005). Measuring and incorporating vulnerability into conservation planning. *Environmental Management*, *35*(5), 527–543.

Wong, M. C., Griffiths, G., & Vercaemer, B. (2020). Seasonal Response and Recovery of Eelgrass (Zostera marina) to Short-Term Reductions in Light Availability. *Estuaries and Coasts*, *43*, 120–134.

Yang, B., Hawthorne, T. L., Aoki, L., Beatty, D. S., Copeland, T., Domke, L. K., Eckert, G. L., Gomes, C. P., Graham, O. J., Harvell, C. D., Hovel, K. A., Hessing-Lewis, M., Harper, L., Mueller, R. S., Rappazzo, B., Reshitnyk, L., Stachowicz, J. J., Tomas, F., & Duffy, J. E. (2023). Low-Altitude UAV Imaging Accurately Quantifies Eelgrass Wasting Disease From Alaska to California. *Geophysical Research Letters*, *50*, e2022GL101985.

Yang, B., Hawthorne, T. L., Hessing-Lewis, M., Duffy, E. J., Reshitnyk, L. Y., Feinman, M., & Searson, H. (2020). Developing an introductory uav/drone mapping training program for seagrass monitoring and research. *Drones*, *4*(70).

Young, C. S., Peterson, B. J., & Gobler, C. J. (2018). The Bloom-Forming Macroalgae, Ulva, Outcompetes the Seagrass, Zostera marina, Under High CO2 Conditions. *Estuaries and Coasts*, *41*, 2340–2355.

Zeng, Y., Hao, D., Badgley, G., Damm, A., Rascher, U., Ryu, Y., Johnson, J., Krieger, V., Wu, S., Qiu, H., Liu, Y., Berry, J. A., & Chen, M. (2021). Estimating near-infrared reflectance of vegetation from hyperspectral data. *Remote Sensing of Environment*, 267, 112723.

Zimmerman, R. C. (2006). Light and Photosynthesis in Seagrass Meadows In: Larkum A.W.D., Orth R.J., Duarte C.M (Eds), Seagrass:Biology (pp. 303–321). Springer, Dordrect, the Netherlands.

Zoffoli, M. L., Gernez, P., Godet, L., Peters, S., Oiry, S., & Barillé, L. (2021). Decadal increase in the ecological status of a North-Atlantic intertidal seagrass meadow observed with multi-mission satellite time-series. *Ecological Indicators*, *130*, 108033.

Zoffoli, M. L., Gernez, P., Rosa, P., Le Bris, A., Brando, V. E., Barillé, A. L., Harin, N., Peters, S., Poser, K., Spaias, L., Peralta, G., & Barillé, L. (2020). Sentinel-2 remote sensing of Zostera noltei-dominated intertidal seagrass meadows. *Remote Sensing of Environment*, 251, 112020.

Zou, Y. F., Chen, K. Y., & Lin, H. J. (2021). Significance of belowground production to the long-term carbon sequestration of intertidal seagrass beds. *Science of the Total Environment*, 800, 149579.